7. SITE 761[1]

Shipboard Scientific Party[2]

HOLE 761A

Date occupied: 19 July 1988

Date departed: 19 July 1988

Time on hole: 6 hr, 45 min

Position: 16°44.23′S, 115°32.10′E

Bottom felt (rig floor; m, drill pipe measurement): 2179.3

Distance between rig floor and sea level (m): 11.4

Water depth (drill pipe measurement from sea level; m): 2188.80

Penetration (m): 9.5

Number of cores (including cores with no recovery): 1

Total length of cored section (m): 9.50

Total core recovered (m): 9.92

Core recovery (%): 104

HOLE 761B

Date occupied: 19 July 1988

Date departed: 21 July 1988

Time on hole: 1 day, 23 hr

Position: 16°44.23′S, 115°32.10′E

Bottom felt (rig floor; m, drill pipe measurement): 2179.3

Distance between rig floor and sea level (m): 11.4

Water depth (drill pipe measurement from sea level; m): 2167.9

Total depth (rig floor; m): 2466.00

Penetration (m): 286.70

Number of cores (including cores with no recovery): 33

Total length of cored section (m): 286.70

Total core recovered (m): 199.08

Core recovery (%): 69

Oldest sediment cored:
Depth (mbsf): 286.70
Nature: carbonate wackestone and packstone (shallow water carbonates)
Age: Rhaetian
Measured velocity (km/s): 5.014

HOLE 761C

Date occupied: 21 July 1988

Date departed: 25 July 1988

Time on hole: 3 days, 17 hr

Position: 16°44.23′S, 115°32.10′E

Bottom felt (rig floor; m, drill pipe measurement): 2179.9

Distance between rig floor and sea level (m): 11.4

Water depth (drill pipe measurement from sea level; m): 2167.9

Total depth (rig floor; m): 2616.00

Penetration (m): 436.70

Number of cores (including cores with no recovery): 33

Total length of cored section (m): 436.70

Total core recovered (m): 72.24

Core recovery (%): 16

Oldest sediment cored:
Depth (mbsf): 436.70
Nature: sand, silt, and laminated silty claystone
Age: Norian
Measured velocity (km/s): 1.688

Principal results: Site 761 is located on the central part of Wombat Plateau, approximately 20 km north of Site 760. The site was selected because seismic facies suggested a section younger than that at Site 760, expected to be Jurassic through Neogene in age.

We penetrated 437 m of Quaternary through Norian sediments in two holes drilled at Site 761. An upper 175.9-m-thick interval of Quaternary through early Paleocene foraminifer nannofossil ooze overlies a late Maestrichtian nannofossil chalk. Chert horizons were encountered in the lower Eocene. A nearly complete pelagic Paleocene section and Cretaceous/Tertiary boundary were recovered. The upper Cretaceous is represented by 22.8 m (175.9–198.7 mbsf) of white upper Maestrichtian nannofossil chalk, 41.3 m (198.7–240.0 mbsf) of pale brown lower–middle Albian to upper Maestrichtian nannofossil chalk with foraminifers and inoceramid shells. The lower Cretaceous is represented by (1) 15.4 m (240.0–255.4 mbsf in Hole 761C) of yellowish-brown Valanginian–upper Berriasian calcisphere nannofossil chalk with bentonite layers (derived from volcanic ash?) and (2) a very condensed 4.1-m-thick section (255.4–259.5 mbsf) of poorly dated (early Neocomian–Tithonian?) yellowish brown to dark brown ferruginous sandstone with abundant belemnites and *Inoceramus* fragments.

Below a major unconformity we recovered 78.8 m (259.5–338.3 mbsf) of white shallow-water limestone of Rhaetian age with *Triasina hantkeni* and megalodont shells, apparently a carbonate platform deposit. This limestone grades downhole into 61.0 m (338.3–399.3 mbsf) of very dark gray to black marine limestone rhythmically alternating with calcareous claystones, also of Rhaetian age. Below these are 23.1 m (399.3–422.4 mbsf) of dark, laminated calcareous claystones, alternating with crinoidal limestones of Rhaetian age, possibly a transgressive open-shelf deposit. At the base of the hole we penetrated 14.3 m of black Norian siltstones and claystones with coal, deposited in a paralic (lagoonal, deltaic, or floodplain) environment.

Because of severe bridging problems a full set of logs could not be run in Hole 761C. However, a valuable set of logs was obtained through the pipe in a single run of the gamma-ray geochemical combination tool, and the seismic stratigraphy tool was run in the open hole between 260 and 125 mbsf.

Stratigraphic highlights of the Wombat Plateau transect of Sites 759, 760, and 761 include a:

1. 20-m.y.-long record of late Triassic history documented by a composite section of almost 600 m; the section includes an important paralic to marginal-marine lower Carnian to Norian

[1] Haq, B. U., von Rad, U., et al., 1990. *Proc. ODP, Init. Repts.*, 122: College Station, TX (Ocean Drilling Program).

[2] Shipboard Scientific Party is as given in the list of Participants preceding the contents.

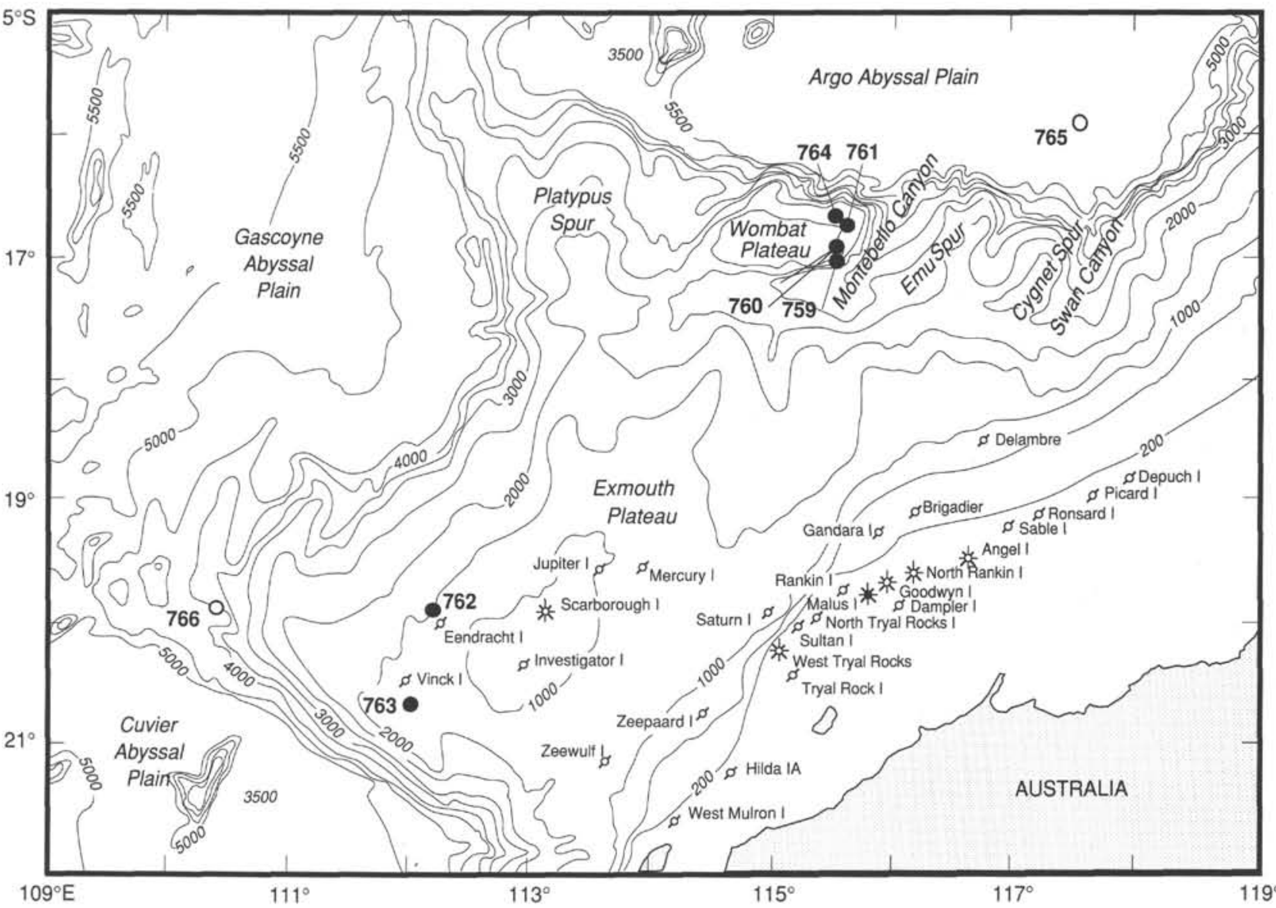

Figure 1. Bathymetric map of Exmouth Plateau showing locations of ODP sites (closed circles = Leg 122 sites, open circles = Leg 123 sites) and commercial wells. Leg 122 Sites 759 and 760 are at the position of proposed Site EP10A (shown by a single closed cirle). Site 761 corresponds to EP9E. Bathymetry is shown in meters (Exon, unpubl. data).

interval representing an early rift environment and containing the oldest nannoflora yet discovered either onshore or offshore, and a possibly complete marine Rhaetian section with ostracodes, foraminifers, nannofossils, and palynomorphs that might be unique in the southern hemisphere;

2. condensed hemipelagic lower Cretaceous section with belemnites;
3. probably complete Cretaceous/Tertiary boundary;
4. nearly complete Paleocene section that will be very valuable for magnetostratigraphy, stable isotopes, and plankton stratigraphy (including radiolarians).

BACKGROUND AND OBJECTIVES

Background

Site 761 (proposed Site EP9E) is located on the central Wombat Plateau, updip and approximately 20 km north of Site 760 (Fig. 1). This site, together with Sites 759 and 760 and proposed Site EP9F (Site 764, at the northern edge of the Plateau), forms a complete transect of sites covering the entire width of the Wombat Plateau. The background material for Sites 759 and 760 (see "Background and Objectives," Sites 759 and 760 chapters, this volume) thus serves as background for this site. Site 761 was selected because drilling at Site 760 revealed that an angular unconformity (prominent on seismic records at that site) separates the upper Cretaceous sediments from the Norian (upper Triassic), and that the Rhaetian, Jurassic, and lower Cretaceous succession has been removed by erosion. The seismic records in the vicinity of Site 761 suggested that at least part of this missing section was present in the central Wombat Plateau.

Objectives

The objectives of Site 761 are similar to those of the other sites of the Wombat transect (see "Background and Objectives," Sites 759 and 760 chapters): to reconstruct the early breakup and post-breakup history of the Wombat Plateau, to document depositional sequences, and to refine chronostratigraphy.

OPERATIONS

Hole 761A

The transit between Sites 760 and 761 (20 km apart) was made in 4 hours, including a brief site survey. Beacon SN 407 (14.5 kHz) was dropped at 0315 hr (local time, or LT) 19 July 1988, near 16°44.23'S, 115°32.10'E. The ship was positioned, and a 9-7/8-in. APC/XCB (advanced-piston-coring/extended-core-barrel) bit was selected.

Drilling this hole was of special interest because a new core-bit design was to be tried. Most APC/XCB bits were only available in the 11-7/16-in. size. The new bit, a 9-7/8-in. APC/XCB bit, had no moving parts but instead used fixed cutters composed of tungsten-carbide steel and polycrystalline synthetic diamonds.

The water depth (as determined by precision depth recorder, or PDR) was 2184 m, and the bit was positioned at 2179 m. However, a full core barrel was recovered, indicating that the bit had been below the mudline when the core was shot.

Hole 761B

The bit was raised to 2174 m for the second shot and a 4.2-m-long core was recovered, indicating that the seafloor was 2179.3 m below the dual-elevator stool (DES). Ten APC cores were obtained with over 100% recovery (Table 1, Fig. 2) before a pullout of 95,000 pounds was reached and piston coring was terminated. The first XCB core advanced the bit only 6 m during 70 min rotating time (Fig. 3). The barrel was pulled to determine if the cutter had been damaged. No damage was apparent, but only 1 m of penetration was made in 50 min of rotating time with the next core. Instead of grinding on an abnormally hard formation while risking damage to the XCB system, a center mill was run with the intent of breaking through the hard material. Five m of hole was made in 100 min before the bit broke through to softer material.

The next XCB run made 7.5 m of penetration in 55 min, encountering several very hard layers (later examination of the cores showed these to be chert). The center mill was run again at 109.2 mbsf, below which 13.5 m were drilled in 60 min. No additional mill runs were required, although minor chert layers were recovered in the remainder of the hole.

Between 122.7 and 217.7 mbsf recovery was excellent, with 78.7 m of core recovered in a firm ooze/chalk lithology (with minor chert). Not only was the percent recovery high (83%), but the average rate of penetration was only 14 min/core.

At 227 mbsf, the rate of recovery began to decline steadily (Fig. 2) for no apparent reason. The sediments at this depth, although somewhat firmer, were essentially the same as above; typically we observe improved recovery in firmer material. The penetration rate became highly erratic (Figs. 3 and 4) Cores 122-761B-25X and -26X took only 4 and 7 min to drill, respectively, but -28X required 130 min and the XCB shoe was worn to destruction. For Core 122-761B-29X, the XCB shoe was replaced with a natural diamond shoe. The rotating time was 66 min for 9.5 m of advancement, and it was necessary to jar the XCB barrel free of the bottom-hole assembly (BHA).

When the core barrel reached the deck we found that half the crown of the diamond cutter had been broken off. The break was fresh, which suggested that it occurred while jarring the barrel free. Core 122-761B-31X (273 mbsf) contained only a few cobbles of limestone; only 0.38 m of limestone were recovered in Core 122-761B-32X, and its core liner had collapsed and pump pressure was higher than normal. Collective evidence suggested a worn-out bit and possible downhole equipment problems. The hole was filled with 10 PPB (pounds/barrel) of mud and the drill string was recovered.

When the bit reached the surface we found that it was almost completely worn out. The LFV (lockable-flapper valve) was choked with sand and was in an open position. Four of the 6 bit jets were plugged and many of the inserts were freshly broken. The lack of fluid flow across the face of the bit (resulting from the plugged jets) had unquestionably caused the destruction of the inserts and low core recovery.

Hole 761C

Deeper-penetration coring was necessary to complete the scientific objectives at the site. The ship was offset 20 m north, and a Security MB4F bit was selected for coring. The BHA consisted of the 9-7/8-in. bit, mechanical bit release, head sub, control length drill collar, long top sub, seven 8-1/4-in. drill collars, cross over (XO), one 7-1/4-in. drill collar, and two stands of 5-1/2-in. drill pipe.

Core 122-761C-1C was drilled to 160.2 mbsf with the Atride center bit. Two cores were then taken in an attempt to recover a continuous Cretaceous/Tertiary (K/T) boundary sequence. Recovery was 70% for the interval, and a continuous (or nearly continuous) boundary was recovered. The hole was drilled to 230 mbsf at which point coring commenced.

With the exception of Core 122-761C-5R, the recovery rate for the remainder of the hole was very poor (32%; Fig. 5) despite taking 5-m-long cores (Figs. 6 and 7). The only apparent reason for the poor recovery was that the formation was alternately hard and soft. At 427.2 mbsf the scientific objectives of the hole had been achieved, coring was terminated, and preparation for logging began (see "Downhole Measurements," this chapter, for a summary of logging operations).

JOIDES Resolution was under way to the next site at 0200 hr (LT), 25 July 1988.

LITHOSTRATIGRAPHY

A 430-m-thick succession of Quaternary through upper Triassic sediments was recovered at Site 761. The Cretaceous through Quaternary portion of the sequence plus a short Rhaetian interval was cored in Hole 761B (to 286.7 mbsf). The Cretaceous and upper Triassic part of the section was cored at Site 761C, after washing through most of the interval between 0.0 and 230.0 mbsf. The Cretaceous/Tertiary boundary interval was re-cored at Hole 761C, from a depth of 160.2–179.2 mbsf. The poorly recovered bottom interval of Hole 761B (230.0–286.7 mbsf) was also re-cored in Hole 761C to provide an overlapping record.

The sedimentary succession was subdivided into six lithologic units (Table 2, Fig. 8) on the basis of visual core, smear slide, and thin-section descriptions. Throughout most of Hole 761B (cored using the APC/XCB), disturbance was slight to moderate and recovery was good (except for the hard interval of chert 95.0–123.0 mbsf, and the section below 233.0 mbsf). In Hole 761C, disturbance was intense and limestone recovery between 258.0 and 337.2 mbsf was minimal (less than 8%). Discrepancies of 1–15 m exist between Holes 761B and 761C regarding the sub-bottom depths of unit boundaries and key intervals, despite the mere 20 m between the holes. In part, these discrepancies result from the uncertainty in assigning the positions of recovered intervals within the 9.5-m core lengths. We evaluated each of these discrepancies and selected the sub-bottom depth value that (on the basis of core recovery) was most likely to be correct. These depth values are italicized in Table 2.

Unit I (0–175.9 mbsf)

Interval 122-761B-1H-1, 0 cm, to -21X-4, 122 cm, and Interval 122-761C-1C-1, 0 cm, to -3R-3, 70 cm.

Unit I consists of Quaternary through Paleocene, white to light-colored nannofossil ooze with foraminifers, nannofossil chalk, and chert. This unit is subdivided into 4 subunits on the basis of composition and degree of diagenesis.

Subunit IA (0–62.7 mbsf)

Interval 122-761B-1H-1, 0 cm, to -8H-1, 150 cm.

Subunit IA predominantly consists of nannofossil ooze with foraminifers, foraminifer nannofossil ooze, and minor nannofossil ooze. Nannofossils include coccoliths and a sub-

Table 1. Coring summary, Site 761.

Core no.	Date (July 1988)	Time (local)	Depth (mbsf)	Cored (m)	Recovered (m)	Recovery (%)
122-761A-						
1H	19	1000		9.5	9.92	104.4
Coring totals				9.5	9.92	104.4
122-761B-						
1H	19	1045	0.0–4.2	4.2	4.19	99.8
2H	19	1135	4.2–13.7	9.5	9.71	102.2
3H	19	1200	13.7–23.2	9.5	9.95	104.7
4H	19	1300	23.2–32.7	9.5	9.99	105.2
5H	19	1508	32.7–42.2	9.5	9.93	104.5
6H	19	1542	42.4–51.7	9.5	10.16	106.9
7H	19	1615	51.7–61.2	9.5	10.01	105.4
8H	19	1645	61.2–70.7	9.5	10.16	106.9
9H	19	1730	70.7–80.2	9.5	9.91	104.3
10H	19	1810	80.2–89.7	9.5	9.96	104.8
11X	19	2130	89.7–95.7	6.0	4.69	78.2
12X	19	2325	95.7–96.7	1.0	0.00	0.0
13C	20	0210	96.7–101.7	(Wash and drill—5.0 m)		
14X	20	0330	101.7–109.2	7.5	5.86	78.1
15C	20	0540	109.2–122.7	(Wash and dirll—13.5 m)		
16X	20	0645	122.7–132.2	9.5	6.44	67.8
17X	20	0730	132.2–141.7	9.5	9.73	102.4
18X	20	0815	141.7–151.2	9.5	9.52	100.2
19X	20	0900	151.2–160.7	9.5	6.75	71.1
20X	20	0945	160.7–170.2	9.5	8.27	87.1
21X	20	1035	170.2–179.7	9.5	8.87	93.4
22X	20	1110	179.7–189.2	9.5	8.29	87.3
23X	20	1135	189.2–198.7	9.5	7.42	78.1
24X	20	1245	198.7–208.2	9.5	6.23	65.6
25X	20	1330	208.2–217.7	9.5	7.15	75.3
26X	20	1410	217.7–227.2	9.5	2.72	28.6
27X	20	1615	227.2–236.7	9.5	5.28	55.6
28X	20	1900	236.7–244.7	8.0	0.23	2.9
29X	20	2125	244.7–254.2	9.5	2.41	25.4
30X	20	2235	254.2–263.7	9.5	3.66	38.5
31X	20	2345	263.7–273.2	9.5	0.35	3.7
32X	21	0225	273.2–282.7	9.5	0.38	4.0
33X	21	0420	282.7–286.7	4.0	0.86	21.5
Coring totals				286.7	199.08	69.4
Wash and drill = 18.5 m						
122-761C-						
1C	21	1640	0.0–160.2	(Wash and drill—160.2 m)		
2R	21	1855	160.2–169.7	9.5	5.33	56.1
3R	21	1940	169.7–179.2	9.5	7.89	83.1
4C	21	2140	179.2–230.0	(Wash and drill—50.8 m)		
5R	21	2225	230.0–235.0	5.0	3.69	73.8
6R	21	2305	235.0–240.0	5.0	0.92	18.4
7R	21	2345	240.0–245.0	5.0	2.35	47.0
8R	22	0030	245.0–250.0	5.0	2.05	41.0
9R	22	0105	250.0–255.0	5.0	1.86	37.2
10R	22	0230	255.0–259.5	4.5	2.05	45.6
11R	22	0315	259.5–264.5	5.0	0.02	0.4
12R	22	0400	264.5–269.5	5.0	0.76	15.2
13R	22	0440	269.5–274.5	5.0	0.20	4.0
14R	22	0520	274.5–279.5	5.0	0.31	6.2
15R	22	0615	279.5–284.5	5.0	0.51	10.2
16R	22	0710	284.5–289.5	5.0	0.66	13.2
17R	22	0800	289.5–294.5	5.0	0.20	4.0
18R	22	0900	294.5–304.0	9.5	1.27	13.4
19R	22	0950	304.0–313.5	9.5	0.52	5.5
20R	22	1040	313.5–323.0	9.5	0.24	2.5
21R	22	1120	323.0–332.5	9.5	0.12	1.3
22R	22	1240	332.5–337.2	4.7	0.58	12.3
23R	22	1545	337.2–346.7	9.5	5.75	60.5
24R	22	2020	346.7–356.2	9.5	3.92	41.3
25R	23	0214	356.2–365.7	9.5	1.36	14.3
26R	23	0525	365.7–375.2	9.5	9.38	98.7
27R	23	0655	375.2–384.7	9.5	1.07	11.3
28R	23	0815	384.7–389.2	4.5	1.01	22.4
29R	23	0940	389.2–398.7	9.5	1.63	17.2
30R	23	1105	398.7–408.2	9.5	2.77	29.2
31R	23	1325	408.2–417.7	9.5	6.67	70.2
32R	23	1620	417.7–427.2	9.5	4.54	47.8
33R	23	1715	427.2–436.7	9.5	2.51	26.4
Coring totals				225.7	72.14	32.0
Wash and drill = 211.0 m						

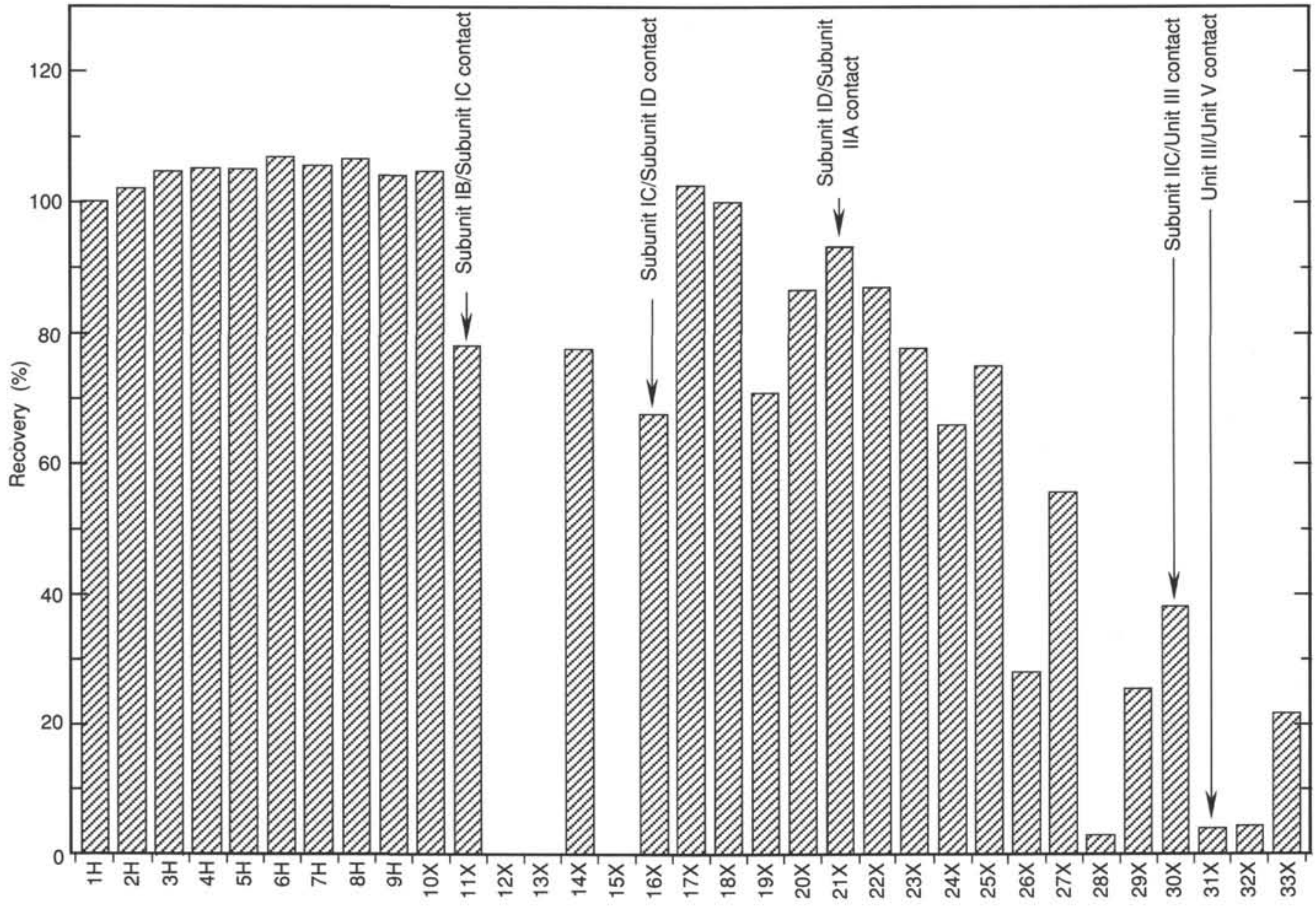

Figure 2. Core number versus recovery (%) for Hole 761B (APC/XCB).

stantial amount of discoasterids. Foraminifer abundance varies from 4%–5% to as much as 35%–40%. Clay is rare and is present in amounts up to 5% in Core 122-761B-6H and Section 122-761B-8H-1.

Oozes are predominantly structureless. Color mottling either results from bioturbation or, more commonly, from drilling disturbance. Dominant colors are white (2.5Y 8/2, 5Y 8/1, 10YR 8/1, 10YR 8/2, 5Y 8/2, and 10Y 8/1), slightly greenish, light gray (N7, 5Y 7/1, 5Y 7/2, 10YR 7/2, and 2.5Y 7/2), gray (5Y 6/1), and light greenish gray (10Y 7/1 and 10Y 8/1). From the sediment-water interface to approximately 1.0 mbsf the oxidized seafloor sediments are pink (5YR 8/3 and 5YR 8/4), mottled light gray (10Y 7/1), and light greenish gray (10Y 6/4). In the lower part of the unit, colors darken imperceptibly and include very pale brown hues (10YR 8/3, 10YR 8/4, 10YR 7/3, and 10YR 7/4), light brownish gray (10YR 6/2), and light yellowish brown (10YR 6/4) tints.

Rhythmic color banding of whites, browns, and grays alternate over 10–30-cm-intervals, and are well developed in Core 122-761B-3H. Whiter lithologies are pure nannofossil ooze, whereas darker sediments are richer in foraminifers.

The lower boundary of Subunit IA is gradational and is represented by a decrease in the foraminifer content in Core 122-761B-8H. This compositional change almost coincides with a middle Eocene to upper Oligocene hiatus in Section 122-761B-8H-1. The age of Subunit IA is late Oligocene through Quaternary. Two other hiatuses, one in the middle-upper Miocene and another from upper Miocene to upper Pliocene, are present in Core 122-761B-4H.

Subunit IB (62.7–90.5 mbsf)

Interval 122-761B-8H-1, 150 cm, to -11X-1, 75 cm.

Subunit IB consists of nannofossil ooze, extensively bioturbated and color-mottled, with minor banding. The color is white (10YR 8/2), mottled gray or homogenous, and becomes very pale brown (10YR 8/3) at the bottom of the subunit. Foraminifers are generally absent, and where present do not exceed 3%–5%. The age of Subunit IB is Middle Eocene. The lower boundary of Subunit IB corresponds to the uppermost occurrence of chert, at Interval 122-761B-11X-1, 75 cm.

Subunit IC (90.5–122.7 mbsf)

Interval 122-761B-11X-1, 75 cm, to -16X-1, 0 cm.

Subunit IC consists of nannofossil ooze interbedded with porcellanitic chert. The relative proportion of ooze and chert is unknown because this interval was poorly recovered. A 3-m-thick horizon of chert was inferred to occur at a depth of 95.7 mbsf because at this depth the drilling rate slowed to approximately 1.5 m/hour. Only small chips and a few cobbles of this interval were recovered. We assume that a large portion of the unrecovered intervals in this subunit consist of chert or chert-rich horizons, although this was not substantiated by well-log results.

The recovered silicified rock is vitreous olive yellow (2.5Y 6/6), brownish yellow (10YR 6/8), and yellow brown (10YR 5/6) opal-CT porcellanite replacing radiolarian foraminiferal chalk.

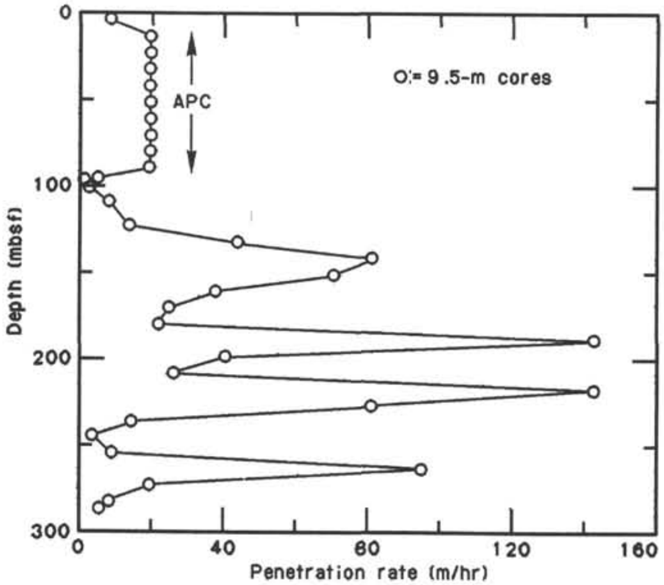

Figure 3. Penetration rate (m per hr) versus depth (mbsf) for Hole 761B (APC/XCB).

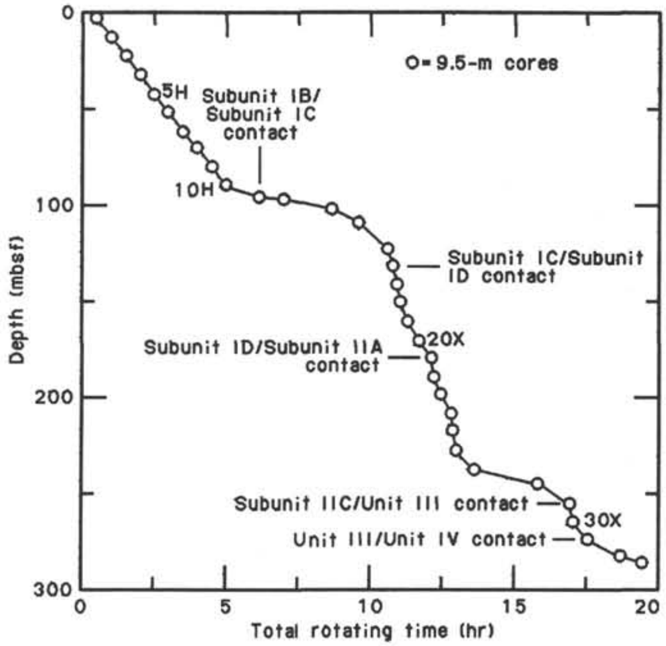

Figure 4. Total rotating time (hr) versus depth (mbsf) for Hole 761B (APC/XCB).

The interbedded ooze consists of nannofossil ooze and nannofossil ooze with foraminifers. Foraminifers occur in amounts from 5%–15%. Clay is locally present and may total as much as 10%. The color is very pale brown (10YR 8/3) grading with depth to pale yellow (5Y 8/3) and white (10YR 8/2).

The lower boundary of the subunit was placed at the uppermost occurrence of massive chalk (at the top of Core 122-761B-16X). There are very minor occurrences of chalk in Core 122-761B-14X, indicative of initial cementation.

The age of Subunit IC is middle Eocene. The interval corresponding to the upper Paleocene and early Eocene (Core 122-761B-15X) was not recovered.

Subunit ID (122.7–175.9 mbsf)

Interval 122-761B-16X-1, 0 cm, to -21X-4, 122 cm, and Interval 122-761C-2R, 0 cm, to -3R-3, 70 cm.

Subunit ID consists of massive nannofossil chalk with foraminifers (10%–20%), variably structureless and homogeneous or bioturbated and mottled. Drilling disturbance is moderate to intense, with drilling biscuits developed throughout the subunit. Colors range from dominant white (5YR 8/1, 10YR 8/1, and 10YR 8/2) to local very pale brown (10YR 8/3 and 10YR 8/4). Patches of ooze and silicified zones are present in the upper part of the subunit (Core 122-761B-16X). At the bottom of the subunit, zeolite (probably clinoptilolite) is present in amounts of 5%–10% (Cores 122-761B-20X and -21X). Clinoptilolite is formed authigenically (during diagenesis) from silica-rich pore solutions. The clay content is 5%–10% in Cores 122-761B-20X and -21X, as the color darkens from predominantly white to light gray (5Y 7/2 and 5Y 7/1).

The lower boundary of Unit I was placed at the lithologic change from light gray (5Y 7/2 and 5Y 7/1), clay-rich chalk of early Paleocene age to the white (10YR 8/1) late Maestrichtian nannofossil chalk. In Hole 761B, the K/T boundary is a drilling contact and the change in color and lithology is sharp. This interval was re-cored in Hole 761C (Core 122-761C-3R) and the section there is more complete, although it also was disturbed (Fig. 9). Late Maestrichtian white (10YR 8/1) nannofossil chalk with foraminifers, containing grayish brown (2.5Y 5/2) chert nodules at the top, is overlain by a layer of bioturbated and mottled very pale brown (10YR 7/3) chalk, also Late Maestrichtian in age. A drilling contact marks the transition to the overlying lower Paleocene strata, which consist of bioturbated and mottled clay-rich nannofossil chalk with foraminifers. This interval is dark greenish gray (10YR 5/2), becoming light greenish gray (10Y 7/0) 16 cm above the boundary. The age of the subunit is early Paleocene (Danian) to late Paleocene.

Unit II (175.9–255.4 mbsf)

Interval 122-761B-21X-4, 122 cm, to -30-1, 0 cm, and Interval 122-761C-3R-3, 70 cm, to -10R-1, 40 cm.

Unit II consists of Cretaceous white to light-colored nannofossil chalk with foraminifers. This unit is divided into 3 subunits on the basis of composition and biota. Recovery was good (average = 60%) and drilling disturbance was moderate.

Subunit IIA (175.9–198.7 mbsf)

Interval 122-761B-21X-4, 122 cm, to -24X-1, 0 cm, and Interval 122-761C-3R-3, 70 cm, to -3R-6, 135 cm.

Subunit IIA consists of white (10YR 8/1 and 10YR 8/2), locally yellowish white (2.5Y 7/8) and greenish white (2.5Y 7/0) nannofossil chalk, extensively bioturbated and faintly banded in some intervals. Foraminifer content does not exceed 10%, but amounts of 5%–6% are most common. Clay is present in trace amounts, up to 3%–4%, and detrital mica is usually less than 2%. Yellowish brown (10YR 6/6) radiolarian porcellanite chert nodules are present, but rare.

The lower boundary of Subunit IIA is gradational and is marked by an increase in the foraminifer content. This increase coincides with the uppermost occurrence of *Inoceramus* shell debris in the section.

The age of Subunit IIA is Late Maestrichtian.

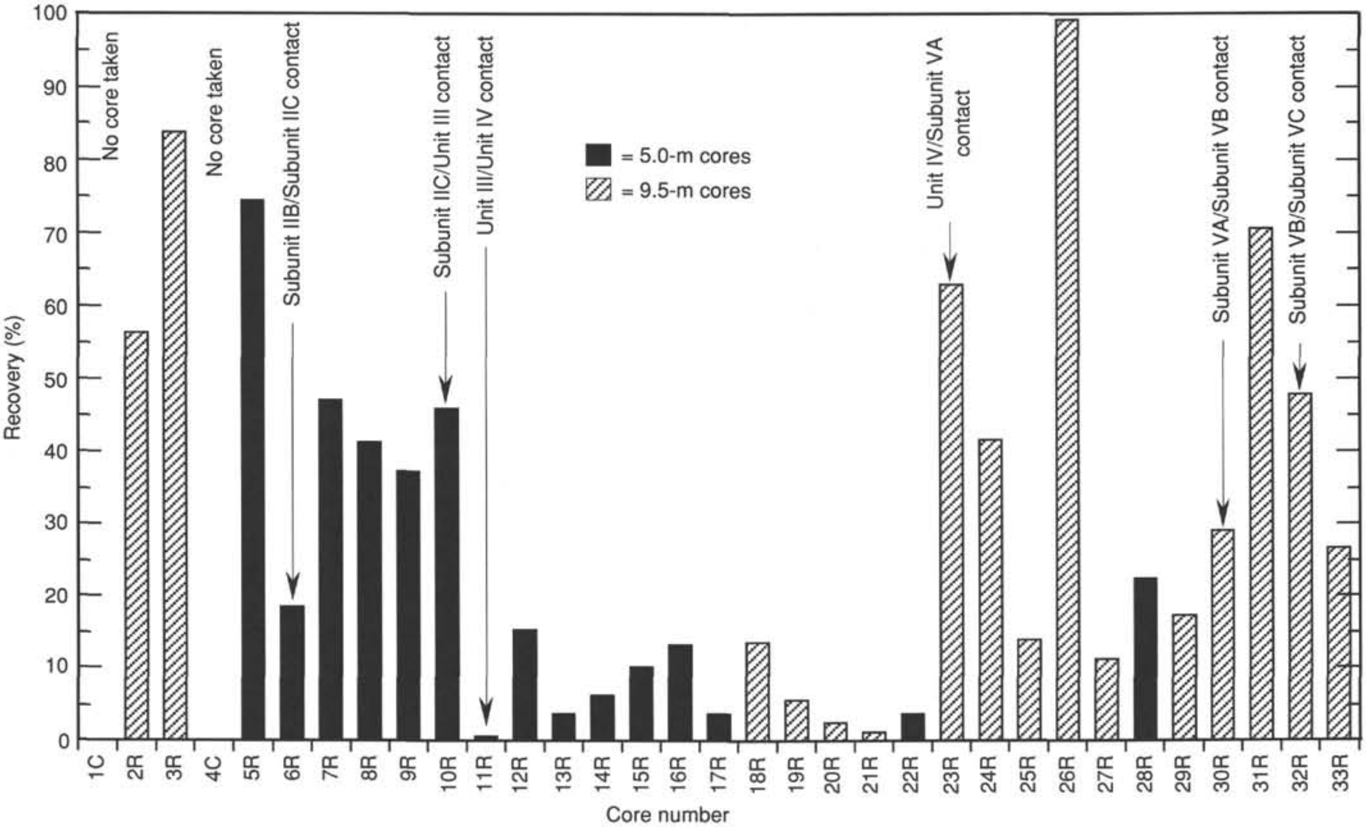

Figure 5. Core number versus recovery (%) for Hole 761C (RCB).

Subunit IIB (198.7–240.0 mbsf)

Interval 122-761B-24X-1, 0 cm, to -28X-CC, 0 cm and Interval 122-761C-5R-1, 0 cm, to -7R-1, 0 cm.

Subunit IIB consists of nannofossil chalk with foraminifers, and subordinate nannofossil chalk. Foraminifers are present in amounts ranging between 10% and 25%. Zeolite composes up to 5% of the sediment in Core 122-761B-24X. *Inoceramus* prisms (shell fragments) are common throughout the subunit, but are particularly abundant in Core 122-761B-25X. The color of the sediments is very pale brown (10YR 8/3), light gray (10YR 7/2) and white (10Y 8/2, 10YR 8/1, and 10YR 8/2, 5Y 8/1) with grayish brown (10YR 5/2) and light brownish gray (10YR 6/2) mottles. Bioturbation is extensive throughout. Vertical burrows with a grayish brown (10YR 5/2) and light brownish gray (10YR 6/2) filling, presumably enriched in organic matter, are typical of the subunit. Local faint laminations and color bands are preserved in the chalk, despite intense burrowing. Laminated intervals rhythmically alternate with completely bioturbated horizons of massive chalk in some sections. Brownish yellow (10YR 6/6) chert nodules are present but rare.

The lower boundary of Subunit IIB was placed at the lowermost occurrence of *Inoceramus* shell fragments, which coincides with the uppermost occurrence of calcispheres. Zeolite becomes abundant in the underlying Subunit IIC, together with calcisphere tests.

The age of Subunit IIB is Late Maestrichtian to early–middle Albian.

Subunit IIC (240.0–255.4 mbsf)

Interval 122-761B-29X-1, 0 cm, to -30X-1, 0 cm, and Interval 122-761C-7R-1, 0 cm, to -10R-1, 40 cm.

Subunit IIC predominantly consists of calcisphere nannofossil chalk and calcisphere chalk with nannofossils. Subordinate rock types include calcisphere nannofossil chalk with zeolites and zeolitic nannofossil chalk with calcispheres. Foraminifers are present in amounts less than 10%, increasing up to 10%–12% at the top of the unit. Chalks are extensively bioturbated and mottled. Colors range from white (2.5Y 8/2 and 10YR 8/2) to pinkish white (7.5YR 8/2) and light gray (2.5Y 7/2 and 10YR 7/2). Brownish shades include very pale brown (10YR 7/3), pale brown (10YR 8/3 and 10YR 6/3), light yellowish brown (2.5Y 6/4, 10YR 6/4, and 10YR 6/3), and pale yellow (2.5Y 7/4). Darker tones are yellowish brown (10YR 5/4) and light olive brown (2.5Y 5/4). Reddish brown (2.5YR 5/4) and brown (10YR 4/3) are dominant at the top of the subunit.

Rhythmic color banding over a 20–30 cm interval is present in some intervals, presumably reflecting subtle changes in organic matter or clay content. Darker lithologies are less bioturbated and preserve some faint lamination and banding. Lighter-colored rock types are massive and burrow-mottled.

Six layers of structureless, homogenous, waxy, very fine-grained smectite clay interpreted to be bentonite are present in the subunit, at Intervals 122-761C-7R-1, 36–64 cm, -7R-2, 30–56 cm, -8R-2, 19–32 cm, -9R-2, 5–22 cm, -9R-CC, 0–10 cm, and -10R-1, 20–40 cm. Large amounts of biotite grains are present in a smectite layer at Interval 122-761C-8R-2, 19–32 cm. These layers show a sharp contact at the base, and gradually mix with calcisphere nannofossil chalk at the top. Colors are white (5Y8/0 and 5Y 8/2), very pale brown (10YR 8/3 and 10YR 7/4), with pale yellow (7.5Y 7/4) shades, pink (5YR 7/4), light brownish gray (10YR 6/2), very dark gray (2.5Y 3/0), and gray (2.5Y 5/0).

Subunit IIC was poorly recovered in Hole 761B, but a better record was obtained from Hole 761C, where the lower

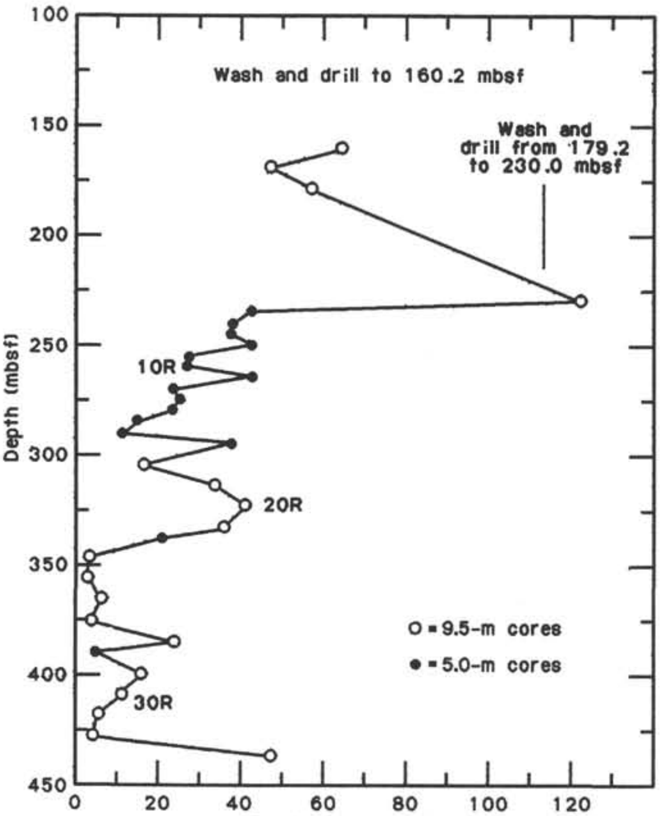

Figure 6. Penetration rate (m per hr) versus depth (mbsf) for Hole 761C (RCB).

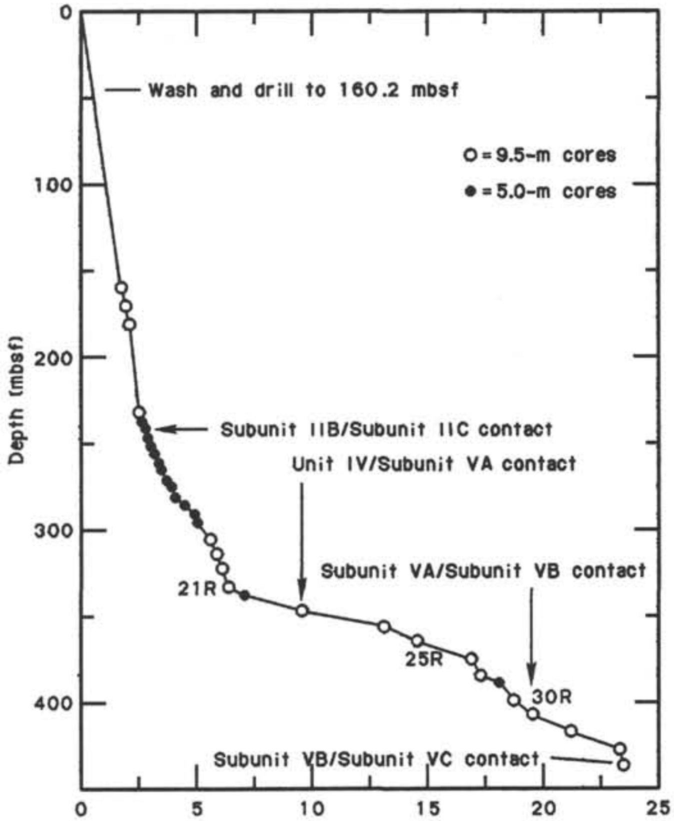

Figure 7. Total rotating time (hr) versus depth (mbsf) for Hole 761C, which was cored with the rotary bit.

boundary of the subunit was sampled. The lower boundary of Unit II is represented by the sharp contact between the lowermost bentonite layer and the reddish sandstone with belemnites of Unit III.

The age of Subunit IIC is Early Valanginian to late Berriasian.

Unit III (255.4–259.5 mbsf)

Interval 122-761B-30X-1, 0 cm, to -31X-1, 0 cm, and Interval 122-761C-10R-1, 40 cm, to -11R, 0 cm.

Unit III was recovered both in Hole 761B and Hole 761C. However, the section in Hole 761C is more complete. Unit III is almost 4.1 m thick and consists (from top to bottom) of three distinctive horizons: (1) an upper horizon, 0.40 m thick, of light yellowish brown (2.5Y 6/4) to light olive brown (2.5Y 5/6) nannofossil sandy and silty claystone; (2) an intermediate horizon, 0.80 m thick, of dark yellowish brown (10YR 4/6), yellowish brown (10YR 5/6) and very pale brown (10YR 7/3) quartzose, lithic, clayey sandstone. This intermediate sandstone is fine- to medium-grained, poorly-sorted, and rich in belemnite rostrums (Fig. 10); and (3) a lower horizon, >0.45 m thick, of unconsolidated brown (7.5YR 5/4) and yellowish brown (10YR 5/8) lithic quartzose clayey sand.

The sediments are unevenly parallel-laminated, with alternating 1-mm-thick laminae of white and reddish (iron-stained) quartz. Disruption of laminae occurred as a result of burrowing, differential sediment compaction around large belemnite rostrums, and drilling. Portions of Unit III are intensely biscuited.

The major components of the sediments in the three horizons of Unit III are: quartz, rock fragments, shell debris, micas (muscovite and biotite), heavy minerals (rutile and zircon), nannofossils, and clay; feldspar is a minor component, and dolomite, glauconite, zeolites, foraminifers, bioclasts, and calcispheres are accessory components. These components are mixed in different proportions in the three intervals, and the terrigenous fraction is always dominant.

Sandstone grains are typically coated by a conspicuous film of iron oxides. We found the intensely biscuited remnants of a dark brown and black (10YR 2/1) layer (Sample 122-761B-30X-2, 20 cm) to be enriched in iron and manganese oxides.

The contact with the underlying limestone of Unit IV was not recovered. We arbitrarily put the lower boundary of Unit III at the uppermost occurrence of limestone, at the top of Cores 122-761B-31X and 122-761C-11R in Holes 761B and 761C, respectively.

The age of Unit III is probably Early Valanginian to Late Berriasian, possibly Tithonian to early Valanginian.

Unit IV (259.5–338.3 mbsf)

Cores 122-761B-31X-1, 0 cm, to -33X-CC, 40 cm, and Interval 122-761C-11R-1, 0 cm, through -23R-1, 110 cm.

Unit IV is 78.8 m thick, and consists of poorly recovered white limestone. Lithologic facies vary from grainstone to wackestone-packstone or mudstone and indicate a littoral, subtidal, or intertidal environment. Fossils are abundant and include benthic foraminifers (mainly *Triasina* sp.), mollusks, calcareous algae, sponges, corals, and numerous thick-shelled valves of *Megalodon*.

Table 2. Lithologic units, Site 761. When two different depth values are available from coring data, the ones considered to be most reliable are italicized.

Unit	Lithology	Interval	Depth (mbsf)	Thick-ness (m)	Environment	Age
IA	White nannofossil ooze with foraminfers.	761B-1H-1, 0 cm to 761B-8H-1, 150 cm	0–62.7	62.7	Eupelagic.	Late Oligocene to Quarternary
IB	White nannofossil ooze.	761B-8H-1, 150 cm to 761-11X-1, 75 cm	62.7–90.5	27.8	Eupelagic.	Middle Eocene
IC	White nannofossil ooze with foraminfers and massive chert.	761B-11X-1, 75 cm to 761B-16X-1, 0 cm	90.5–122.7	32.2	Eupelagic.	Middle Eocene
ID	White nannofossil chalk with foraminifers.	761B-16X-1, 0 cm to 761B-21X-4, 122 cm and 761C-2R-1, 0 cm to 761C-3R-3, 70 cm	122.7–*175.9* 160.2–173.4	53.2	Eupelagic.	Early Paleocene (Danian) to Late Paleocene
IIA	White nannofossil chalk.	761B-21X-4, 122 cm to 761B-24X-1, 0 cm and 761C-3R-3, 70 cm to 761C-3R-6, 135 cm	*175.9–198.7* 173.4–(177.6)	22.8	Eupelagic.	Late Maestrichtian
IIB	Very pale brown nannofossil chalk with foraminifers and *Inoceramus* shells.	761B-24X-1, 0 cm to 761B-28X-CC, 0 cm and 761C-5R-1, 0 cm to 761C-7R-1, 0 cm	*198.7* (236.7) (230.0–) *240.0*	41.3	Eupelagic.	Early Middle Albian to Late Maestrichtian
IIC	Light to dark yellowish brown calcisphere nannofossil calcisphere chalk, with bentonite/smectite layers (altered volcanic ash).	761B-29X-1, 0 cm to 761B-30X-1, 0 cm and 761C-7R-1, 0 cm to 761C-10R-1, 40 cm	236.7–(254.2) *240.0 255.4*	15.4	Eupelagic.	Late Berriasian to Early Valanginian
III	Yellowish brown to dark brown ferruginous sandstone with belemnites.	761B-30X-1, 0 cm to 761B-31X-1, 0 cm and 761C-10R-1, 40 cm to 761C-11R-1, 0 cm	254.2–263.7 *255.4–259.5*	4.1	Hemipelagic, condensed horizon (relic deposit over pelagic high).	Neocomian (probably Late Berriasian to Early Valanginian)
IV	White, very pale brown limestone, with *Triasina hantkeni* and *Megalodon*.	761B-31X-1, 0 cm to 761B-33X-CC, 40 cm and 761C-11R-1, 0 cm to 761C-23R-1, 110 cm	263.7–(286.7) *259.5–338.3*	78.8	Neritic, shallow subtidal lagoon.	Rhaetian
VA	Very dark gray to black limestone and calcareous claystone, rythmically alternating.	761C-23R-1, 110 cm to 761C-30R-1, 65 cm	338.3–399.3	61.0	Neritic, open shelf.	Rhaetian
VB	Dark laminated claystone and crinoidal limestone.	761C-30R-1, 65 cm to 761C-32R-CC, 20 cm	399.3–422.4	23.1	Open shelf.	Rhaetian
VI	Black, carbonaceous silty claystone and claystone, with coal.	761C-32R-CC, 20 cm through 761C-33R-CC	422.4–436.7	14.3	Delta plain.	Norian

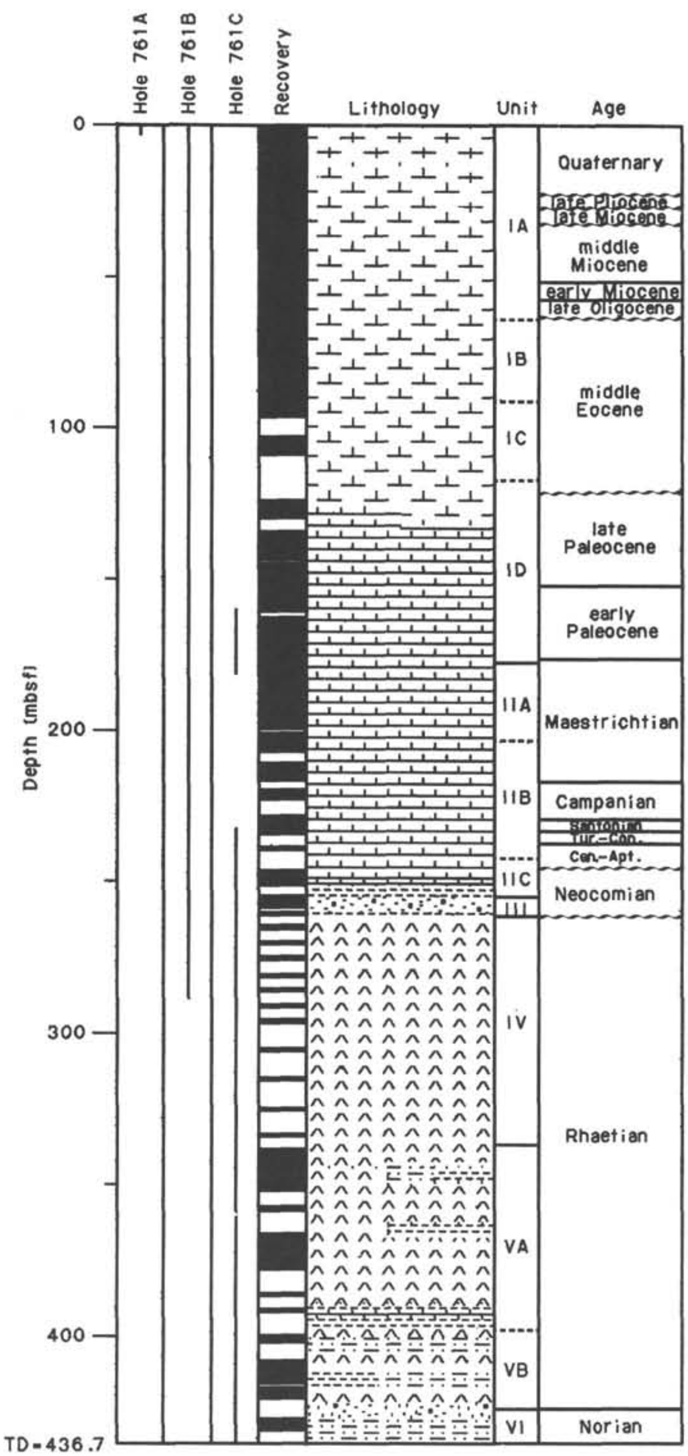

Figure 8. Lithologic column for Holes 761B and 761C. A key to lithologic symbols appears in the "Explanatory Notes" chapter (this volume).

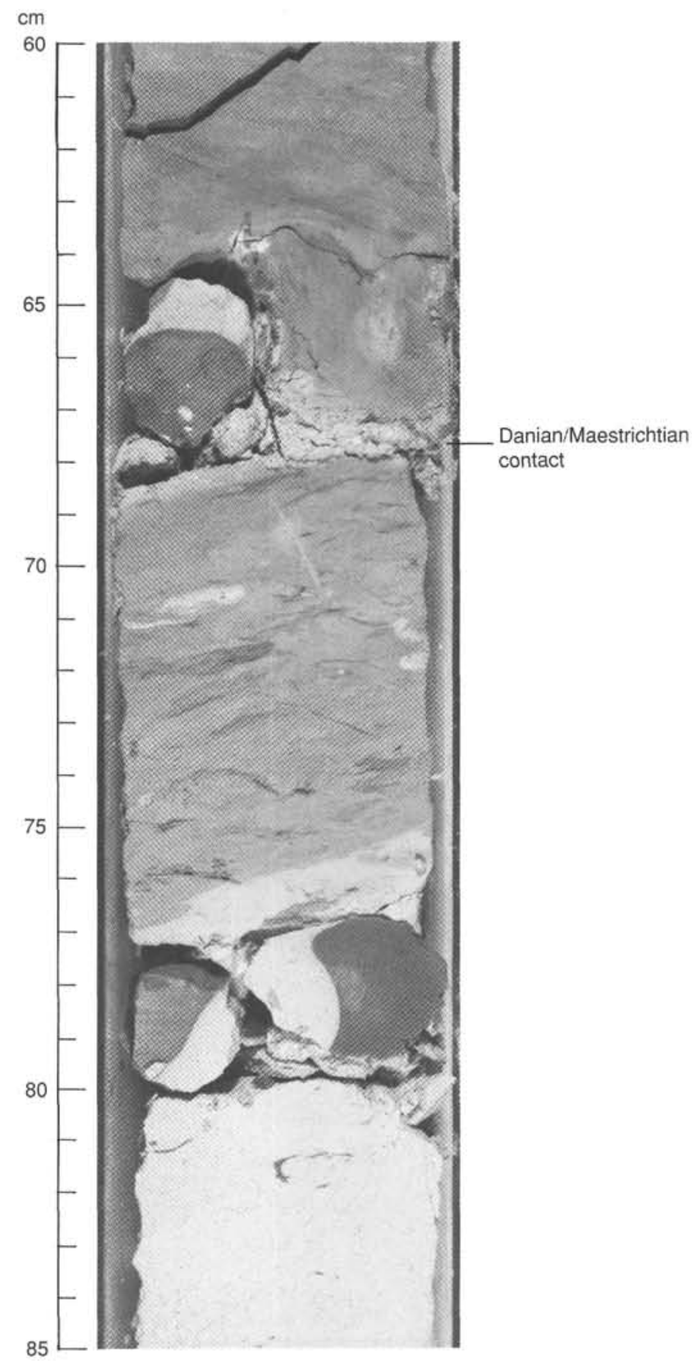

Figure 9. The Cretaceous/Tertiary boundary interval (Core 122-761C-3R-3, 60–85 cm) which is also the boundary between Units I and II. Dark-colored sediment above 68 cm is Danian, dark greenish gray nannofossil chalk. Beneath, is white to light brownish gray, bioturbated, Maestrichtian chalk, with porcellanite chert.

Dissolution is very common in these rocks. Although micrites are generally better preserved from dissolution, they are commonly affected by neomorphic replacement of calcite and dolomitization. Spar-cemented sediments (e.g., oolitic grainstones) are strongly dissolved, except for cortexes of ooids that have been previously micritized. Sponges and branching hermatypic corals are commonly observed, associated with wackestone-mudstone facies, whereas benthic foraminifers are very common in the grainstone facies.

We recognized five lithofacies in Unit IV (numbered IV-1 through IV-5); their vertical distribution is shown in Figure 11.

Lithofacies IV-1 consists of carbonate mudstone with frequent algal stromatolitic laminations (representing algal mats) and birdseye structures (Figs. 12, 13, and 14). This facies is typically dolomitized. Subaerial desiccation features

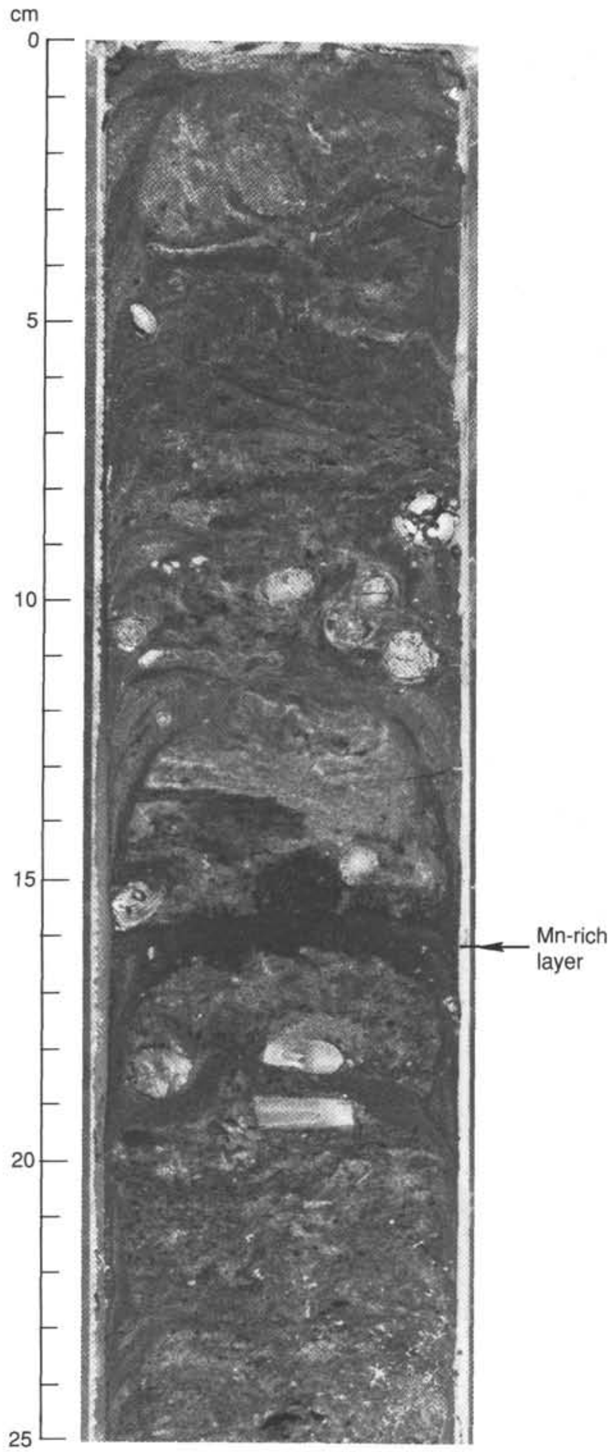

Figure 10. Ferruginous sand, with belemnite rostrums (Section 122-761B-30X-2, 0–25 cm). Sand is irregularly laminated due to bioturbation and drilling disturbance. Note dark brown-black manganese-oxide-rich layer at 16–17 cm. Belemnites lie horizontally, but do not seem to have any preferred orientation.

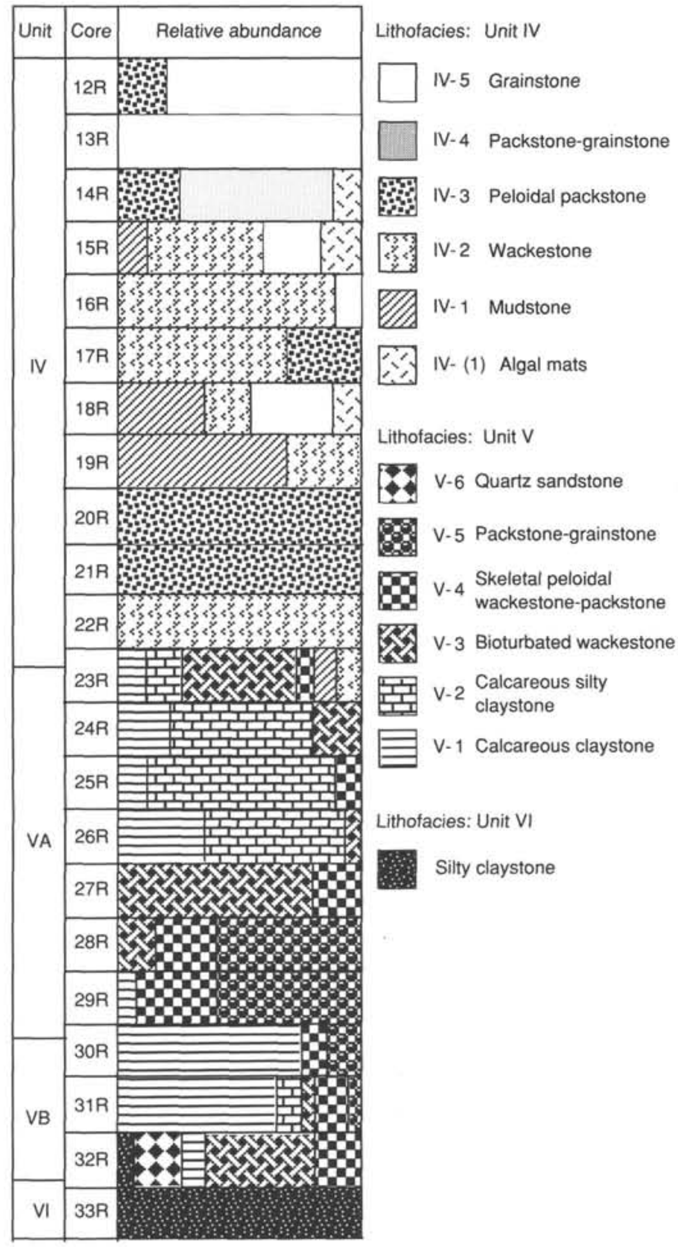

Figure 11. Vertical distribution of lithofacies in Units IV, V, and VI. Width of horizontal bar indicates relative abundance.

and cavities filled by sparry calcite (possibly *Stromatactis*-type voids, as discussed by Bathurst, 1959 and 1980; or dissolved megalodont shells) are present. Some thin mollusk shells may occur (less than 10%) and foraminifers are rare or absent. A typical example of this lithofacies is Sample 122-761C-15R-1, 38–41 cm (Fig. 12). Lithofacies IV-1 also occurs in Sections 122-761B-33X-1 (Fig. 14), and -33X-CC (Fig. 13), Sections 122-761C-14R-1 through -16R-1, and in Sections 122-761C-18R-1 and -23R-1.

Lithofacies IV-2 consists of skeletal wackestone and packstone, with abundant benthic foraminifers. Micrite matrix may be >60%. Bioclasts include mollusk shells, green algae, and some echinoderms. Peloids occur but are not as abundant as in Lithofacies IV-3. Branching corals and *Megalodon* shells are present (Fig. 12). Bioclasts are generally micritized. This facies may be strongly dolomitized. A typical example of this lithofacies is Sample 122-761C-20R-1, 10–12 cm. Other occurrences of Lithofacies IV-2 are in Sections 122-761C-16R-1, -19R-1, -20R-1, -21R-1, -21R-CC (Fig. 15), -22R-1, and -22R-CC.

Lithofacies IV-3 consists of skeletal-peloidal packstone with abundant foraminifers (Fig. 14, at 36–41 cm). The matrix is mainly composed of peloids (40%–50%) that are micritized

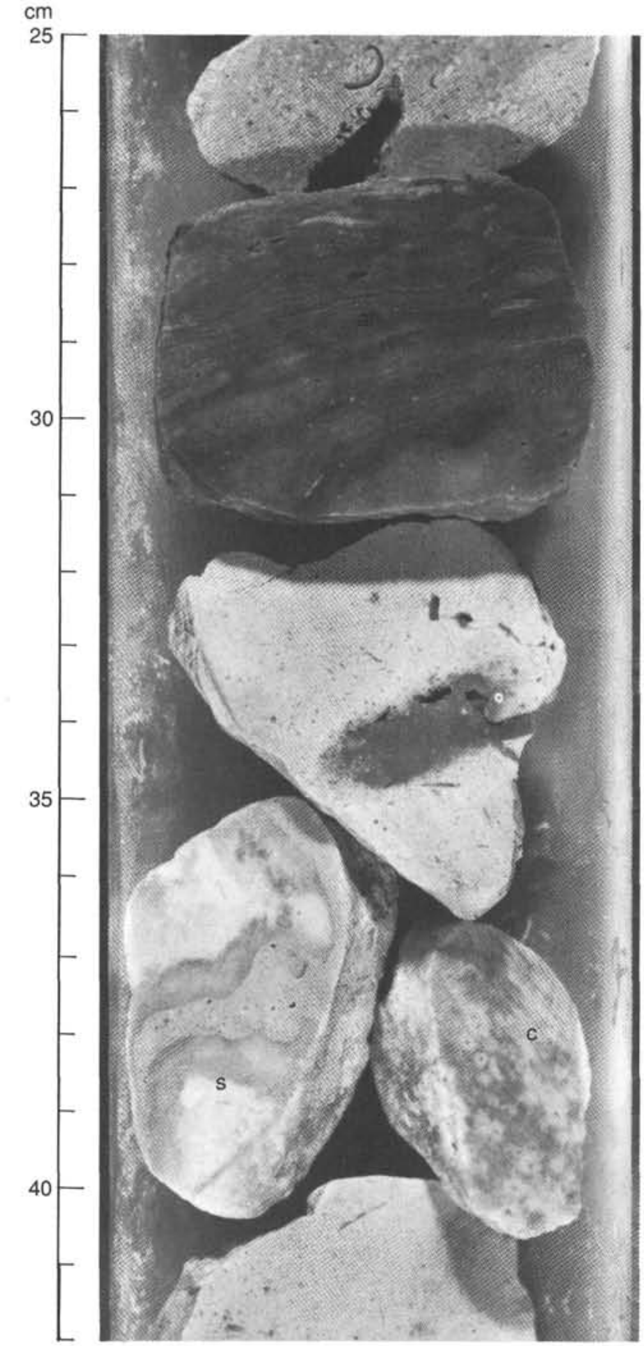

Figure 12. Lithologies from the upper part of Unit IV (Interval 122-761C-15R-1, 25–42 cm). Dominant lithologic type is light-colored, tan, skeletal peloidal wackestone and packstone with molluscan debris (lithofacies IV-1 and IV-2); (s) indicates large stromatactoid voids or *Megalodon* valves. Next to the (s) block is a fragment of a hermatypic coral head (c). The dark-colored block (al) has wavy algal stromatolitic lamination and fenestral voids (lithofacies IV-1).

grains and/or pellets of fecal origin. Bioclasts are abundant and include molluscs, green algae, and echinoderm plates and spines. Foraminifers are about 10%–30%. Patchy dolomitization may occur locally. Crinoids occur in Section 122-761C-22R-1. A typical example of this lithofacies is Sample 122-761C-14R-1, 15–18 cm. Occurrences of Lithofacies IV-3 are in Sections 122-761C-12R-1, -14R-1, -15R-1 through -18R-1, and -22R-1.

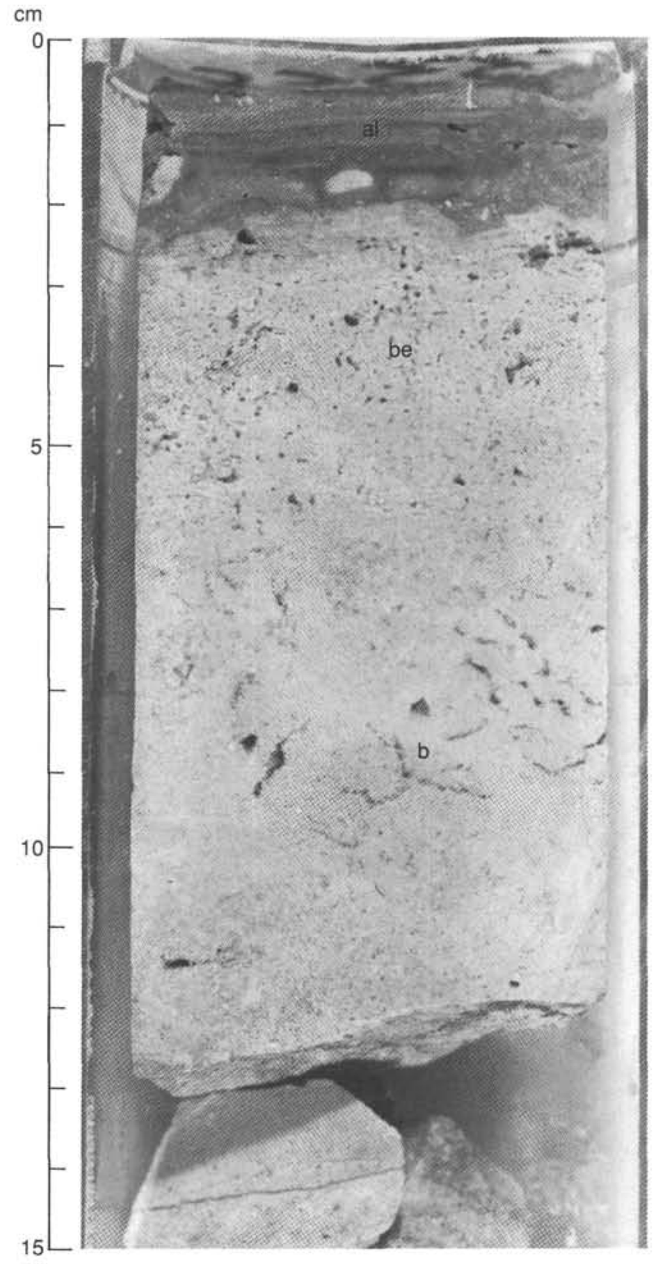

Figure 13. White peloidal-oncoidal packstone from the upper cores in Unit IV (Interval 122-761B-33X-CC, 0–15 cm. Note calcite-cemented burrows (b) in the middle part of the figure and birdseye-type of structures (be). Algal laminae (al) are present above. Birdseye structures in grainy sediments typically result from air entrapment after tidal flooding of emerged areas. Algal stromatolitic laminations are present above.

Lithofacies IV-4 consists of skeletal, peloidal packstone-grainstone. This lithofacies is transitional between Lithofacies IV-3 and -5. Peloids are dominant and the allochem composition is nearly the same as in Lithofacies IV-3, but some patchy microsparite cement is present. Corals are abundant in this facies (Fig. 16). A typical example of this lithofacies is in Sample 122-761C-12R-1, 2–4 cm. Other occurrences of Lithofacies IV-4 are in Sections 122-761C-12R-1, -13R-1, -15R-1, -16R-1.

Lithofacies IV-5 consists of moderately to well-sorted ooid-foraminifer grainstone. Current laminations are com-

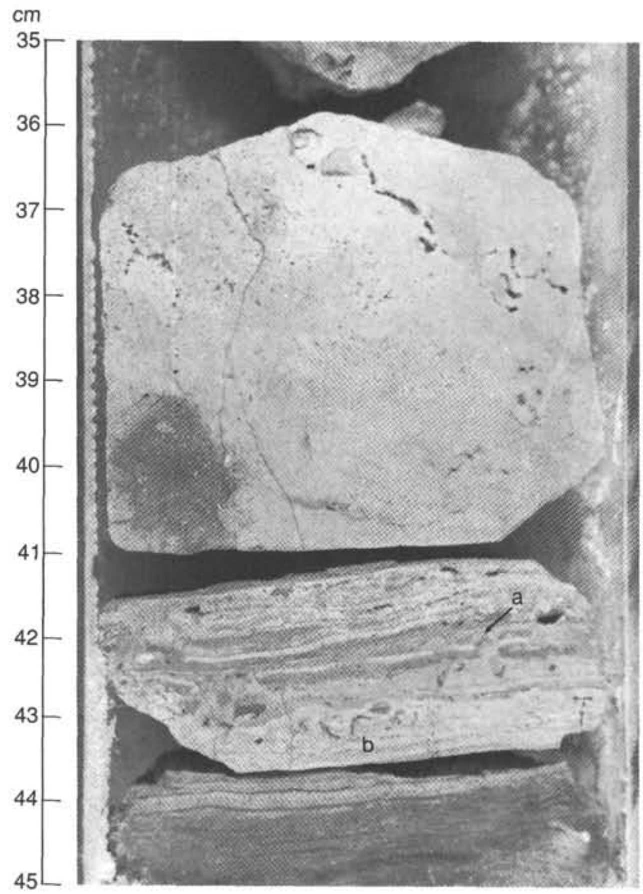

Figure 14. Algal-laminated, peloidal packstone from the upper part of Unit IV (Section 122-761B-33X-CC). Note the algal laminae disruption (a) and flat intraclasts in between the laminae (b).

mon, and birdseye or keystone vugs are locally present (Fig. 17). Components are ooids (generally with a micritized cortex), coated bioclastic grains, and rounded micritized grains. Abundant (20%–30%) benthic foraminifers (mainly *Triasina* sp.) are observed, mixed with the ooids. These foraminifers may be dominant in some grainstones. Lithofacies IV-5 is strongly affected by dissolution. Nuclei of ooids and intergranular sparite are selectively dissolved. Neomorphic calcite and dolomite are locally developed. A typical example of this lithofacies is Sample 122-761C-12R-1, 16–19 cm. Occurrences of Lithofacies IV-5 are in Cores 122-761C-12R-1, -13R-1, -15R-1, and -16R-1.

The colors of the limestones are generally tan to light gray. Mudstones tend to be white (5Y 8/1), and some algal-laminated facies types are yellowish red (5YR 5/8) or olive yellow (2.5Y 6/6) where dolomitized. Wackestones and packstones are white (10YR 8/1 and 10YR 8/2), pinkish white (5YR 8/2 and 7.5YR 8/2), and very pale brown (10YR 8/3), but are pale brown (10YR 6/3) and brown (7.5YR 5/4) or brownish yellow (10YR 6/6) where dolomitized. Grainstones are very pale brown (10YR 7/4 and 10YR 8/4).

The very poor recovery (less than 8%) severely hampered any sequential analysis. The relative abundance of each lithofacies recovered in Unit IV is reported in Figure 11.

The age of Unit IV is Rhaetian.

Unit V (338.3–422.4 mbsf)

Interval 122-761C-23R-1, 110 cm, to -32R-CC, 20 cm.

Figure 15. Internal mold of the pelecypod *Megalodon*, from the lower part of Unit IV (lithofacies IV-2 and IV-4; Section 122-761C-21R-CC).

Unit V is an 84.1-m-thick sequence of interbedded carbonate mudstone to grainstone and calcareous claystone to silty claystone. It is subdivided into two subunits on the basis of the relative proportion of carbonate to terrigenous sediments, and their vertical organization. The boundary between Subunits VA and VB is placed at Sample 122-761C-30R-1, 65 cm (399.3 mbsf). The rock color in both subunits is generally gray to dark gray, ranging from N3 to N5 or N6, with the carbonates being of lighter color than the argillaceous intervals.

Unit V is composed of six lithofacies (numbered V-1 to V-6), differentiated by composition and sedimentary structures. These are: (1) V-1, silty claystone to calcareous claystone; (2) V-2, carbonate mudstone; (3) V-3, carbonate wackestone with bioclasts; (4) V-4, carbonate packstone-wackestone; (5) V-5, carbonate grainstone-packstone; and (6) V-6, calcareous sandy siltstone to silty sandstone. Lithofacies V-1–V-5 occur in both Subunits VA and VB (associated in different proportions) whereas Lithofacies V-6 occurs only in Subunit VB. The stratigraphic distribution of these lithofacies is shown in Figure 11.

Lithofacies V-1 consists of silty claystone to calcareous claystone and occurs in 5-cm- to 2-m-thick intervals, interbedded with limestone (Figs. 18 and 19). It ranges in color

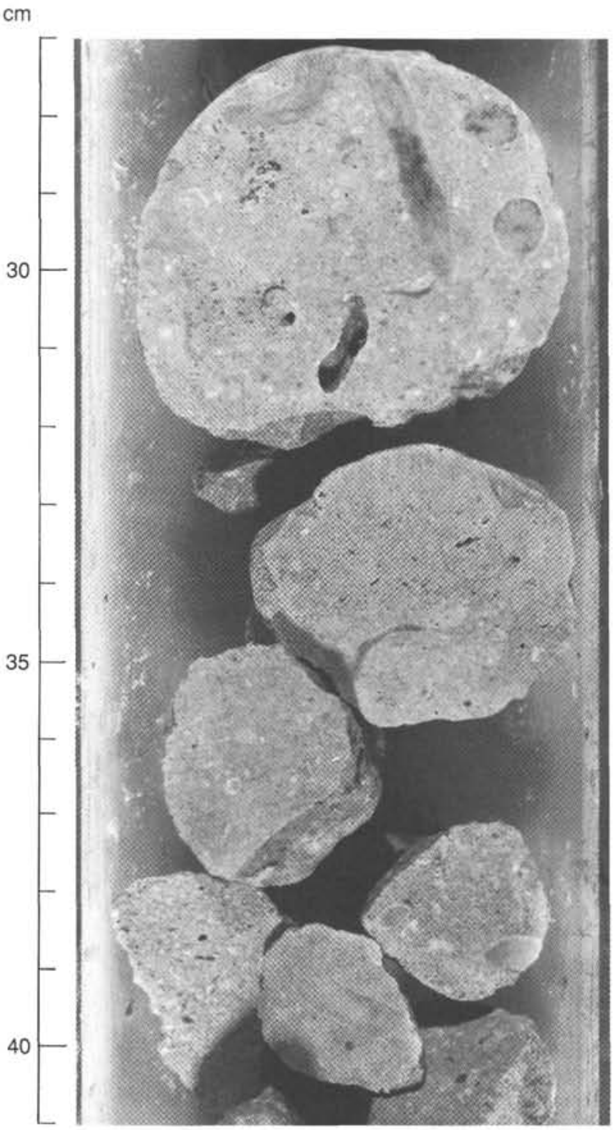

Figure 16. Branching hermatypic corals (at 36–41 cm) in Section 122-761C-16R-1, in skeletal peloidal calcarenite (grainstone); middle part of Unit IV (lithofacies IV-4).

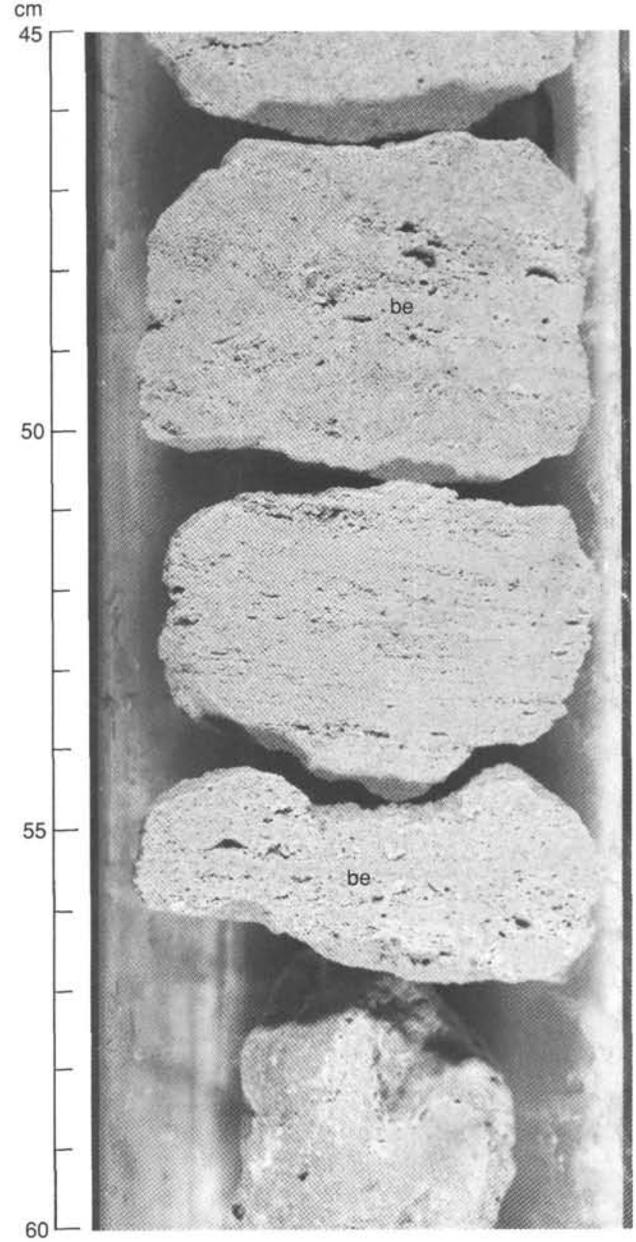

Figure 17. Coarse-grained, oolitic-foraminiferal calcarenite (grainstone), current-laminated and locally bioturbated (at 48–50 cm) with birdseye type of structures (be). Birdseye structures in grainy sediment result from air entrapment after tidal flooding of emerged areas (Section 122-761C-12R-1).

from black (N2) to dark gray (N4), with calcareous claystone being of lighter color. Parallel laminations characterize rock types of this lithofacies, although locally these are intensely bioturbated and structureless. Stringers of clayey siltstone and shell-rich laminae occur intermittently, being more common in Subunit VB than in Subunit VA. Skeletal fragments in these bioclastic laminae are oriented parallel to the bedding and this may indicate transport by currents.

Lithofacies V-2 consists of bioturbated carbonate mudstone, characteristically light gray (7.5YR 7/0) or gray to dark gray (N6–N4). Minor amounts of shell fragments (chiefly mollusks) and rare pellets are present. The mudstone is generally recrystallized and moldic porosity is locally present. A few burrows are partially infilled with pyrite. Carbonate mudstone comprises a substantial proportion of Subunit VA, occurring in 0.10–2.5-m-thick beds. It is a minor constituent of Subunit VB, where it occurs as thin, 1–5-cm-thick layers. Lithofacies V-1 and V-2 are interbedded in Unit V. In Subunit VA rhythmic alternations of the two rock types occur over intervals of 50–100 cm (Figs. 18 and 19).

Lithofacies V-3 is a carbonate wackestone with bioclasts, generally gray (N5) and mottled by bioturbation. Varieties of this lithofacies are found in Subunits VA and VB. In Subunit VA, wackestone occurs in 15–65-cm-thick beds that are generally bioturbated and grade upwards into parallel-laminated, slightly argillaceous wackestone. Mollusks are the most common bioclast, with lesser amounts of gastropods, echinoderms, corals, crinoid ossicles, and peloids. In Subunit VB, carbonate wackestone is a minor constituent, occurring in 20–50-cm-thick beds that overlie carbonate packstone and grade upwards into carbonate mudstone. Three varieties of wackestone occur in this subunit: peloid-crinoidal, coral-pellet-mollusk, and burrowed pellet-shelly.

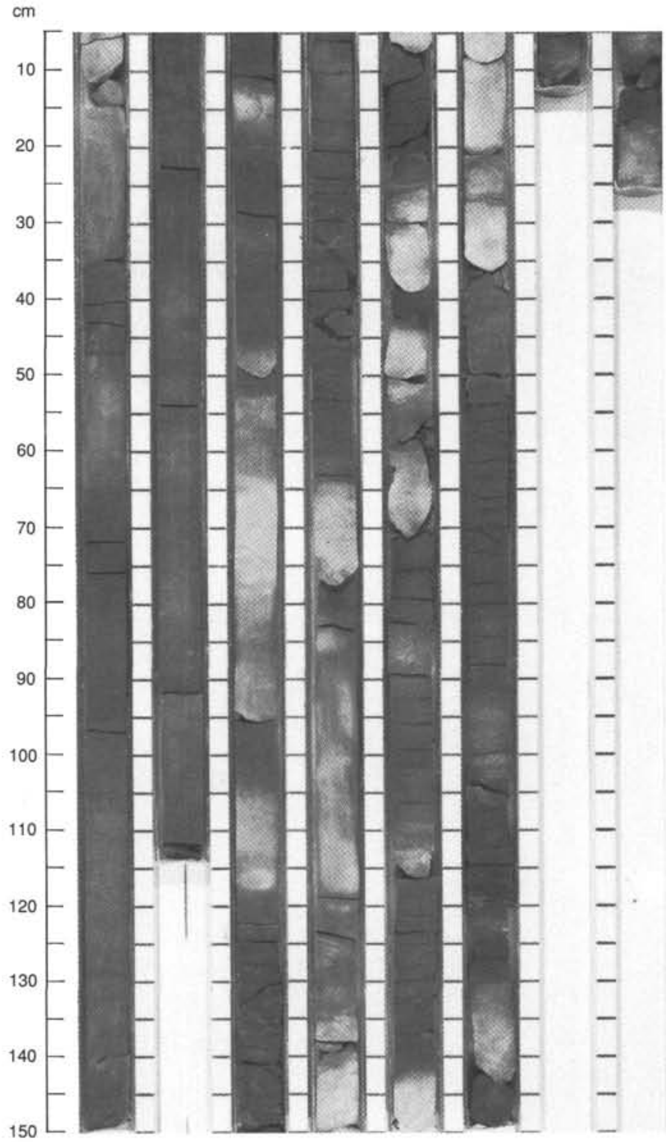

Figure 18. Lithofacies V-1 (Core 122-761C-26R). Limestone-calcareous claystone cycles that characterize the upper part of Subunit VA. Both limestone and calcareous claystone are dark gray. Limestone is light-colored in the photo.

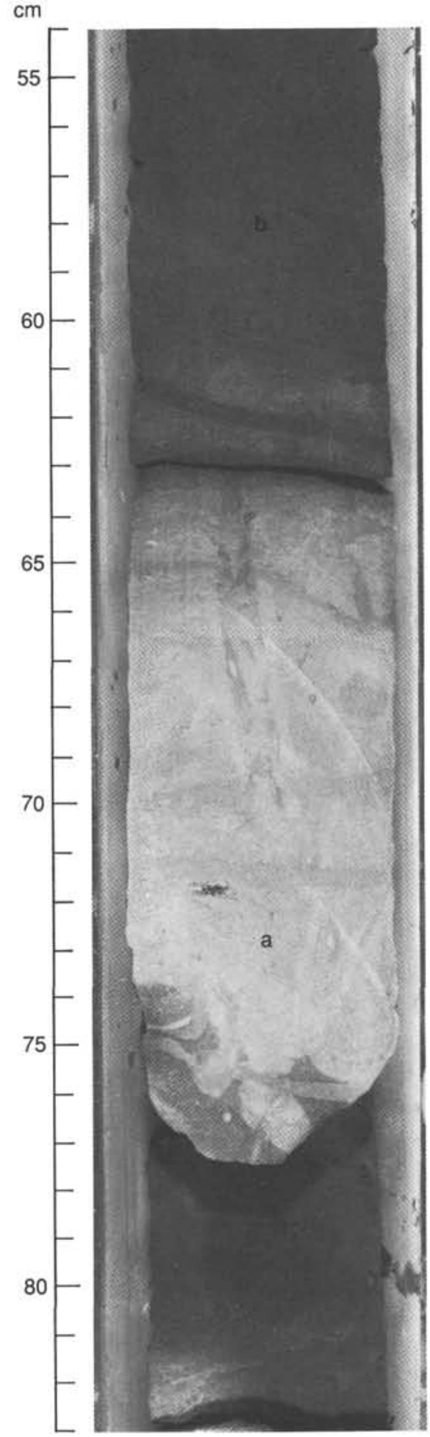

Figure 19. Lithofacies V-1 (Core 122-761C-26R-4, 54–83 cm; detail of Fig. 18). Note the gradual transition from pure limestone (a) to calcareous claystone (b). Both lithologic types are intensely bioturbated.

Lithofacies V-4 is carbonate packstone-wackestone. Fossiliferous, bioclastic, and peloidal packstone-wackestone occurs as dark gray (N4) to gray (N5), 10–50 cm-thick units (Fig. 20). These beds have a sharp base and generally grade upwards into carbonate wackestone. Dasycladacean algae, mollusks, crinoids, and peloids are the primary components, with the relative proportions among them quite variable. Lithofacies V-4 is common in Subunit VB, and is of secondary importance in Subunit VA.

Lithofacies V-5 is a carbonate grainstone and packstone with minor rudstone. Two end-member varieties were observed, with intergradations: (1) bioclastic grainstone-packstone containing mollusks and echinoderms, with lesser corals, coralline red algae, and benthic foraminifers, and (2) generally well-sorted ooid-peloid grainstone. Ooid-peloid grainstone occurs in 5–20-cm-thick beds, and is gradational into crinoid-peloid or crinoid-mollusk grainstone-packstone. A typical algal, hermatypic-coral, and sponge boundstone included in red clay was noted at Interval 122-761C-30R-1, 0–60 cm (Fig. 21). The thalli of red algae were in growth position. We consider this to be boundstone because of the micro-reefal association of encrusting organisms.

The grainstone-packstone is generally recrystallized and may be locally dolomitized. The colors vary from dark gray (N4 to 10YR 4/1) to olive gray (5Y 5/2), light olive brown (2.5Y

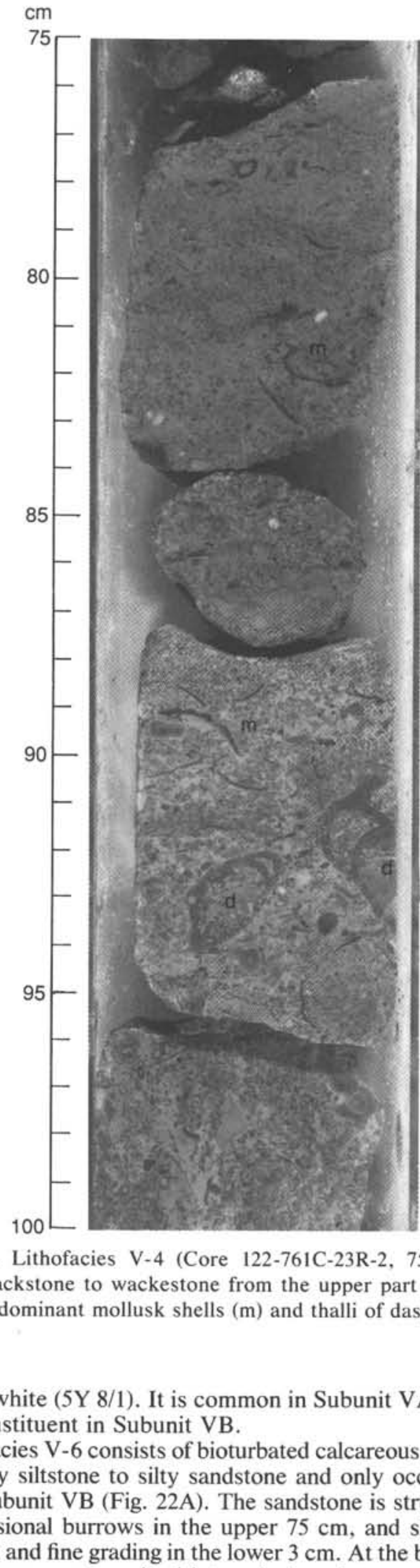

Figure 20. Lithofacies V-4 (Core 122-761C-23R-2, 75–100 cm). Skeletal packstone to wackestone from the upper part of Subunit VA. Note dominant mollusk shells (m) and thalli of dasycladacean algae (d).

5/4), and white (5Y 8/1). It is common in Subunit VA, and is a minor constituent in Subunit VB.

Lithofacies V-6 consists of bioturbated calcareous and quartzose sandy siltstone to silty sandstone and only occurs at the base of Subunit VB (Fig. 22A). The sandstone is structureless, with occasional burrows in the upper 75 cm, and shows faint lamination and fine grading in the lower 3 cm. At the base of this bed is a very coarse-grained interval of packstone and wackestone with coarse crinoidal debris and quartz sand that includes intraclasts of crinoidal packstone (Fig. 22B). This intraclast floatstone forms the basal interval of a 1-m-thick graded layer that directly overlies the top of Unit VI.

Subunit VA (338.3–399.3 mbsf)

Interval 122-761C-23R-1, 110 cm, through -30R-1, 65 cm.

Subunit VA is 61.0 m thick and consists of carbonate mudstone, wackestone, and packstone to grainstone, interbedded with calcareous to silty claystone. The upper 3.55 m (Interval 122-761C-23R-1, 110 cm, to -23R-4, 15 cm) consist of alternations of bioturbated wackestone and parallel-laminated, argillaceous wackestone, with minor peloid-skeletal packstone and wackestone. The underlying 26.95 m (Interval 122-761C-23R-4, 15 cm, to 761C-26R-2, 150 cm) are primarily composed of 0.30–1.5-m-thick beds of bioturbated carbonate mudstone, interbedded with thin (<35-cm-thick) calcareous claystone layers. Underlying this predominantly carbonate-mudstone interval are 7.55 m of rhythmically interbedded carbonate mudstone-wackestone and calcareous to silty claystone (Interval 122-761C-26R-2, 150 cm, to -27R-1, 105 cm; Fig. 18). The mudstone-wackestone layers are bioturbated and range in thickness from 5 to 80 cm. The calcareous to silty claystone layers are generally parallel-laminated and 5–90 cm thick. The lowermost 23.15 m of Subunit VA (Interval 122-761C-27R-1, 105 cm, to -30R-1, 70 cm) consist of bioclastic packstone to grainstone, with subordinate bioclastic wackestone and ooid-peloid grainstone.

The age of Subunit VA is Rhaetian.

Subunit VB (399.3–422.4)

Interval 122-761C-30R-1, 65 cm, through -32R-CC, 20 cm.

Subunit VB is 23.1 m thick. It contains more calcareous to silty claystone and less carbonate mudstone, wackestone, and grainstone than Subunit VA. The upper 15.1 m of Subunit VB consists primarily of 0.70–2-m-thick intervals of calcareous to silty claystone, with rare 60-cm-thick beds of packstone or grainstone, grading upward to wackestone or mudstone. Underlying this interval are 6.3 m of carbonate grainstone to mudstone and minor calcareous to silty claystone. The basal interval contains several 5-cm- to 1-m-thick graded beds of packstone-wackestone, with erosional scours or load casts at the base. The graded beds are rich in shell fragments and bioclastic crinoidal material, with shells oriented parallel to bedding. Graded packstone and wackestone are interbedded with bioturbated shell-rich wackestone and mudstone.

The upper part of the lowermost graded bed in Interval 122-761C-32R-4, 35 cm, to -32R-CC, 20 cm, is mostly quartzose sandstone and siltstone (Lithofacies V-6). The quartz sand is well sorted and does not show significant grain-size variations. The sandstone grades downward into a very coarse, intraclast-rich horizon, 20 cm thick. A 4–5 cm intraclast is crinoidal, skeletal packstone-grainstone with ooids, included in a quartzose, bioclastic sandstone matrix. This rather peculiar quartz-rich bed lies just above the Unit VI/Unit V boundary. The upper contact of Unit VI is actually a drilling contact, although the unrecovered lithologic contact is also presumed to be sharp. The age of Subunit VB is Rhaetian and that of the underlying Unit VI is Norian. We assume that the contact is unconformable and that a hiatus exists between the two units.

Unit VI (422.4–436.7 mbsf)

Interval 122-761C-32R-CC, 20 cm, through -33R-CC.

We only cored the topmost 14.3 m of Unit VI, and recovered 2.6 m of sediment. This unit consists of black (2.5Y 2/0) and dark greenish gray (10Y 4/2), parallel-laminated

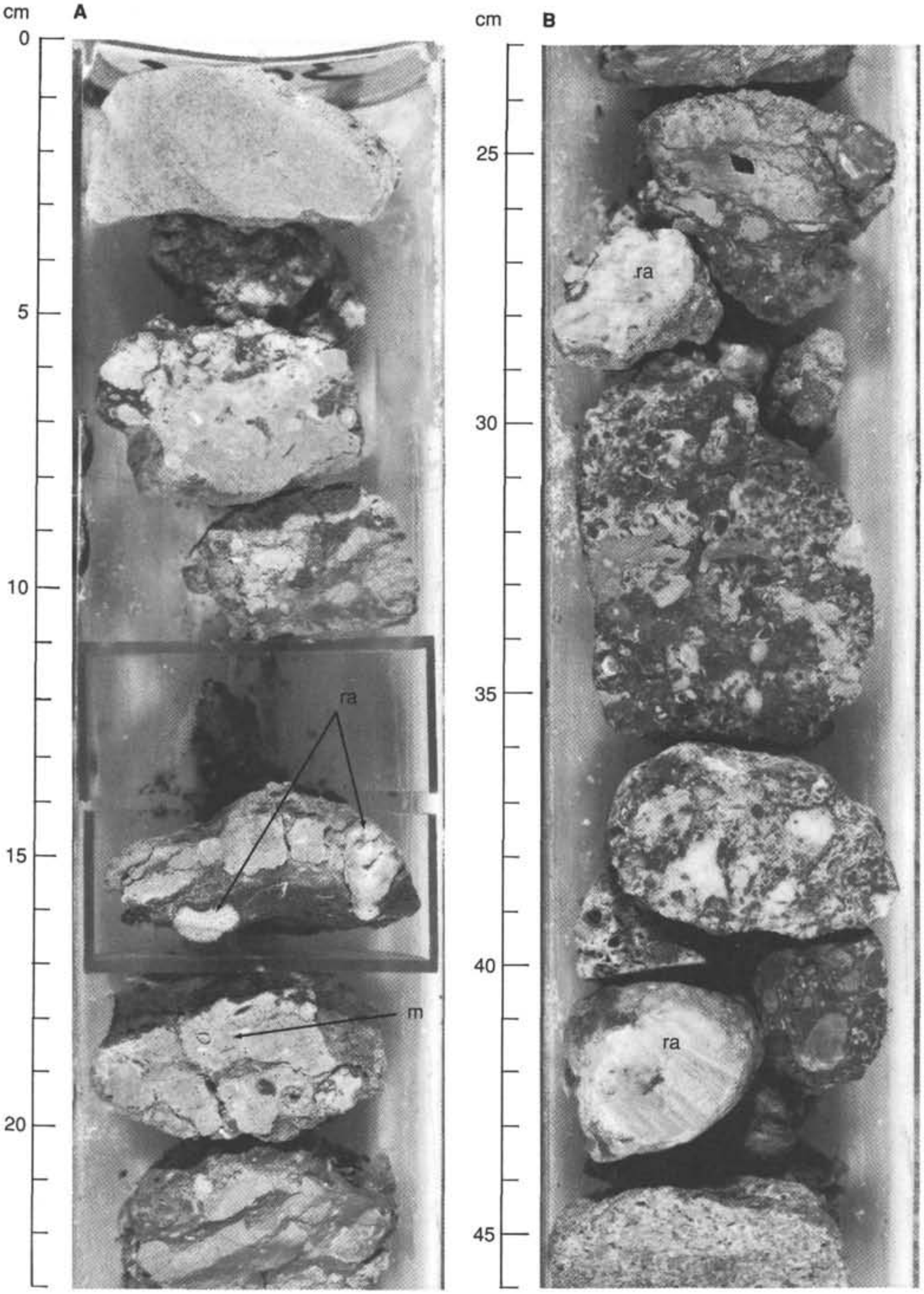

Figure 21. Lithofacies V-5 (Core 122-761C-30R-1, 0–46 cm). **A.** Micro-reefal association of red coralline algae and corals. Mollusks in life position (m) are associated. Note thalli of red algae (ra) in life position at 15–16 cm (upside down in the photograph). **B.** Continuation of A. Nodules of red algae ("rhodolites") are seen at 26–28 cm and 40.5–43.5 cm (ra).

clayey siltstone, with scattered pyrite nodules and coal seams. Minor burrowing is present.

The age of Unit VI is Norian.

Paleoenvironments and Sedimentation History at Site 761

The oldest sediments recovered at Site 761 are Norian in age and consist of carbonaceous silty claystone with pyrite and coal seams. Despite limited recovery of this unit (slightly >2 m), there are components that suggest that these rocks were deposited in a shallow-water, clastic-dominated, coastal environment. No open-marine fossils were observed in this unit, indicating limited circulation with the open ocean. Rocks from Unit VI are reminiscent of the coeval deltaic sediments of Site 760 (i.e., Units III and IV; see "Lithostratigraphy," Site 760 chapter, this volume).

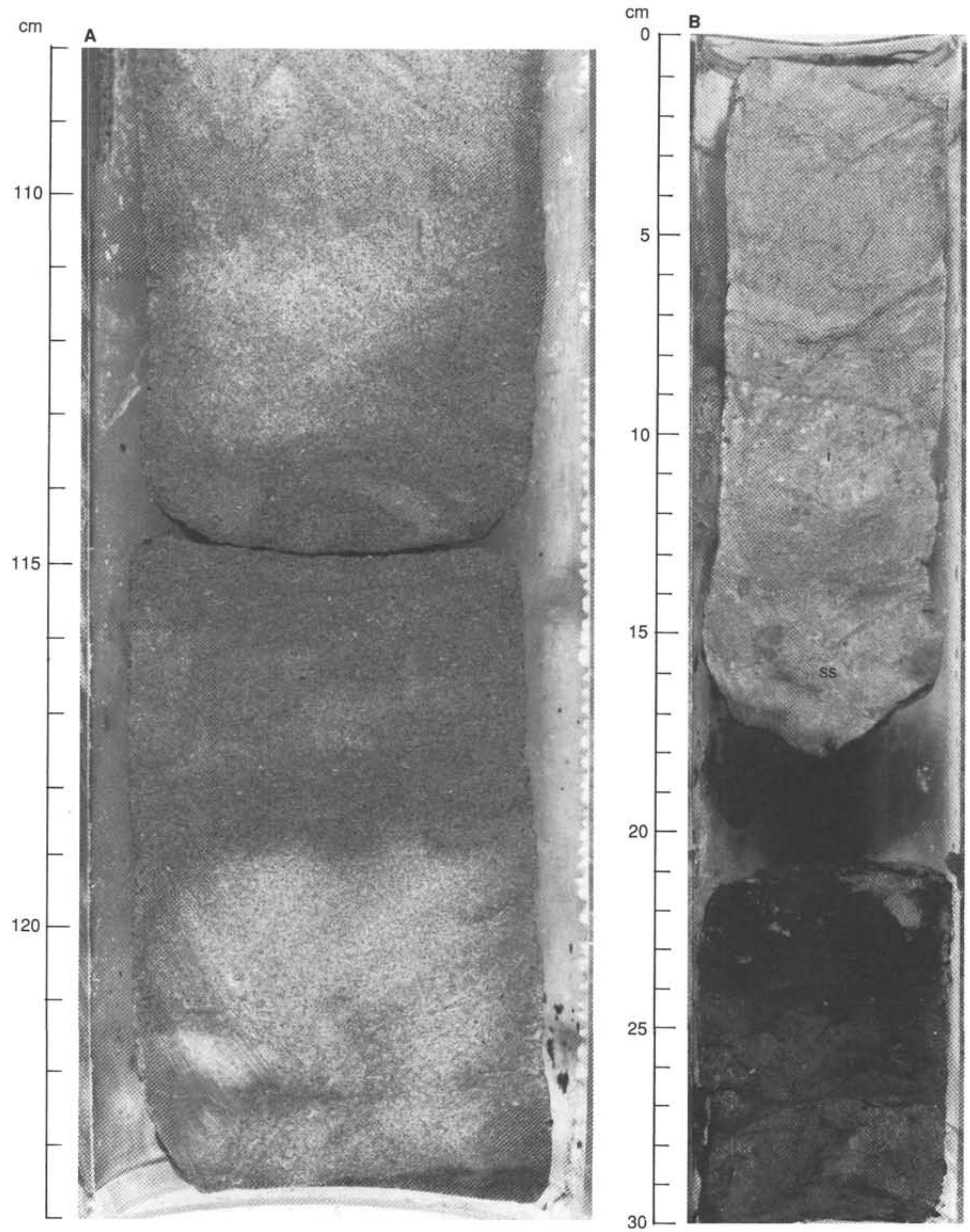

Figure 22. Boundary betweeen Units V and VI. **A.** Core 122-761C-32R-3, 108–124 cm. Fine-grained, well-sorted quartzose sandstone with faint size-grading and poorly developed parallel laminae. **B.** Core 122-761C-32R-CC, 0–30 cm. Below 20 cm, there is a black bioturbated carbonaceous silty claystone and clayey sandstone (c). Above 18 cm, there is a very coarse to granule-sized crinoidal-skeletal-quartzose sandstone (ss), incorporating a large subrounded intraclast of crinoidal skeletal calcarenite (i). This interval represents the basal horizon of a 1-m-thick graded bed showing structures that resemble those of turbidite layers.

Shallow-water coastal sediments of Unit VI are abruptly overlain by interbedded black claystone with an abundant nannoflora, and crinoidal limestone (plus a series of intermediate lithofacies that are described in the discussion of Subunit VB), indicating an open-marine environment. The depth at which Triassic crinoid colonies lived is open to discussion, as is the autochthonous or allochthonous nature of these deposits.

The crinoidal sediments of Subunit VB are Rhaetian, thus indicating that there is a remarkable deepening of the depositional environment at or near the Norian/Rhaetian boundary. The nature of this unit boundary at Site 761 is obscure because recovery was discontinuous. Nevertheless, we presume it to be sharp and unconformable, despite the lack of a biostratigraphically resolvable hiatus. Although we have no information on the actual boundary, details of the late Triassic shallow-to-deep water transition are preserved in the overlying record. The crinoidal limestones of Subunit VB (in part) occur in 1-m-thick graded units, with scour structures at their base. Abundant quartz sand mixed with the carbonate component suggests that the Norian substratum was syn-depositionally eroded; the presence of intraclasts likewise indicates syn-depositional erosion. The presence of crinoids indicates that on the Wombat Plateau, more open-marine conditions prevailed in the Rhaetian, as compared with the Norian.

Although the idea of a Rhaetian transgression is generally accepted by the shipboard sedimentologists, opinions differ regarding interpretation of the quartz sand input. One interpretation is that the episode of mass wasting and quartz input at the Norian/Rhaetian boundary documents erosion of the Wombat Plateau and shelf coinciding with the drowning of its distal edge. These processes might be related to the normal faulting and tilting that typically accompany the onset of rifting. Alternatively, the quartz input at the base of the Rhaetian sequence can be interpreted as neither proving nor precluding syndepositional tectonic events on the Wombat Plateau. Quartz may have been reworked from underlying siliciclastic formations and redistributed into marine environments (characterized by crinoids) owing to a *relative* sea-level rise and gradual flooding of the top-Norian erosional surface (considered to be a sequence boundary).

The basal detrital sequence, interbedded with mudstone, is overlain by a boundstone with red clay (Section 122-761C-30R-1) that represents a "biogenic hardground." Components of the boundstone include red algae, hermatypic coral, and sponges. The red coloration of the clay indicates highly oxic conditions on the seafloor, possibly in a regime of extremely slow deposition. As terrigenous deposition resumed, it formed rhythmic interbeds of limestone and claystone (Subunit VA). We interpret these rhythmic limestone and claystone interbeds to represent deposition in an outer shelf environment, in moderate water depth (below wave base). Rhythmic limestone-marlstone (calcareous claystone and clayey limestone in ODP nomenclature) alternations are known to be developed in the deep sea, but are also typical of many carbonate shelves (e.g., the Rhaetian of the Southern Alps). The mechanisms that produce such cycles in shallow-shelf, high-sedimentation-rate areas are not as well known as they are for open-ocean settings; possible causes include seasonality in productivity, driven by climatic changes and fluctuation of latitudinal zones (Ogg et al., 1987). For shelfal cycles, dilution factors (e.g., varying clay input) rather than productivity changes or dissolution could be important, and these might also be related to climatic changes driven by astronomic forcing.

The onset of littoral facies (beginning with Core 122-761C-22R) marks the restoration of near-sea-level deposition at Site 761. Grainstone facies of Unit IV indicate high-energy, oolitic environments. The presence of algal-laminated sediments, desiccation cracks, and birdseyes in the uppermost samples all indicate a tidally influenced environment, with temporary emersions and intertidal-supratidal algal marsh development. Benthic foraminifers (*Triasina* sp.) predominate in the grainstone facies. The pelecypod *Megalodon* is more typical of a subtidal (lagoonal) habitat. Corals seem to be associated with wackestone and packstone and thus typify a shallow-subtidal, enclosed environment (e.g., a lagoon) rather than a bank-edge setting (e.g., a patch reef). Owing to the limited recovery, we have no information on the spatial organization of these lithologic types. The association of dasycladacean green algae and hermatypic corals is typical of a "chlorozoan" type association, suggesting a low-latitude, tropical environment.

The lowermost Rhaetian strata represent relatively deep-water, outer-shelf crinoidal facies; littoral, coral-algal associations and tidal features characterize the uppermost strata. This apparently records an upward-shoaling sequence that might reflect the growth of a carbonate bank in a regime of high-standing sea level. The Rhaetian sequence is truncated by a major unconformity. The uppermost carbonates (Cores 122-761C-11R and -12R) contain calcite-cemented cavities whose origin might be related to the formation of this unconformity. Possible scenarios include uplift and paleokarst development over the emerged plateau, or dissolution after submergence and submarine cementation. Studies of the stable isotope composition of cavity-filling calcite might indicate the origin of these cavities and thereby elucidate the post-Rhaetian, pre-Tithonian history of the Wombat Plateau. Drilling results from Site 764 are instrumental for this interpretation.

A hiatus exists between the upper Rhaetian neritic limestone (Unit IV) and the overlying belemnite-rich sand (Unit III; Late Berriasian to Early Valanginian). This hiatus could have been produced by: (1) emergence as early as earliest Jurassic followed by nondeposition/erosion, (2) uplift and subaerial erosion of a Jurassic sequence during late Jurassic times, or (3) subsidence and submarine condensation/nondeposition during the duration of the Jurassic. Further shore-based studies will help to resolve this issue. Calcispheres in the overlying chalk (Unit III) indicate a pelagic environment (outer shelf–upper slope). We presume that the sand was deposited in a shallow-water nearshore environment, although the presence of iron-oxide-coated quartz grains and manganese-oxide micronodules suggests an open-marine environment of extremely slow deposition. Belemnites are thought to have inhabited such environments; alternatively, their presence may suggest a beach setting. One interpretaton is that the red, belemnite-rich sand is a relict sand, reworked by currents that swept across a drowned pelagic plateau.

Smectite (bentonite) layers occur in the basal Cretaceous strata. The smectite of Subunit IIC probably formed as an alteration product of ash layers; if so, this documents Berriasian through Valanginian volcanism. In comparison, ash layers (cinerites) of acidic composition in ocean-margin sequences of the Southern Alps record late Middle Jurassic Tethyan spreading.

The early Cretaceous strata of Site 761 record the initiation of hemipelagic carbonate deposition at upper bathyal depth ranges. Deposition occurred above the calcite compensation depth (CCD) at this depositional site up to and including the present. Periods of worldwide enhanced fertility and radiolarian blooms are reflected in the Eocene at Site 761 (Subunit IC). Episodes of siliceous deposition are recorded in most oceans at this time and are apparently of global significance.

BIOSTRATIGRAPHY

Introduction

Site 761 is located on the western edge of the Exmouth Plateau (2167.9 m water depth). Hole 761B was cored to a depth of 286.7 mbsf with a total recovery of 199.08 m of sediment. With the exception of two cores taken near the Cretaceous/Tertiary boundary, Hole 761C was washed to 230.0 mbsf and cored to a depth of 436.7 mbsf, with a total recovery of only 72.24 m of sediment. Biostratigraphic investigations were conducted on the core-catcher samples and on one or more additional samples from every core.

Calcareous nannofossil ages are summarized in Figure 23 for the Cenozoic, and Figure 24 for the Mesozoic. A summary of the biostratigraphic ages of the various lithologic units at Holes 761B and 761C are presented in Figure 25 and Table 3.

Units I and II were dated using nannofossils and foraminifers. Unit I (Paleocene to Quaternary) contains a major hiatus representing the upper Eocene to middle Oligocene. The transition from nannofossil chalk with foraminifers (Unit I) to nannofossil chalk (Unit II) roughly coincides with the Cretaceous/Tertiary boundary (Core 122-761B-21X). Unfortunately, the lowest part of the Danian Stage is missing, evidenced by the absence of nannofossil Zone NP1 (Fig. 23). The Cretaceous/Tertiary boundary interval in Hole 761C contains Zone NP1, but we cannot ascertain whether the boundary interval is complete. Unit II is late Berriasian to late Maestrichtian in age. The exact age of Unit III is unknown, but can be tentatively assigned a late Berriasian to early Valanginian age on the basis of the similarity of nannofossil assemblages to those in Subunit IIC. Jurassic sediments are absent in both holes. Units IV to VI are all Late Triassic (Rhaetian and Norian; Fig. 25). The sediments at Site 761 provide an upward continuation of the Triassic section drilled at Sites 759 and 760.

Calcareous Nannofossils

Occurrence and Preservation

Nannofossil abundance and preservational characteristics correspond well with the major lithologic units at Site 761. The upper eight cores of calcareous ooze (Subunit IA) in Hole 761B contain abundant, well-preserved assemblages. The interval from Sections 122-761B-8H-1 to -21X-4 and Section 122-761C-2R-CC, which consists of ooze and chalk (Subunits IB–ID), has abundant but generally moderately preserved calcareous nannofossils. The Cretaceous/Tertiary boundary interval (Sections 122-761B-21X-4 and 122-761C-3R-3) is characterized by few, moderately well-preserved nannofossils. Chalk (Subunits IIA and IIB) recovered from Sections 122-761B-21X-4 to -28X-CC and from Sections 122-761C-3R-3 to -6R-CC contains abundant, moderately preserved nannofossils.

The calcisphere-nannofossil chalk (Subunit IIC) recovered from Sections 122-761B-28X-1 to -30X-1 and Sections 122-761C-7R-1 to -10R-1 contains variably abundant nannofossils of moderate to poor preservation. The belemnite sands (Unit III) are characterized by short intervals with abundant and moderately well-preserved nannofossils. The shelfal limestone (Unit IV) is barren of nannofossils in both holes. The black limestone and calcareous claystone recovered in Hole 761C (Units V and VI) include numerous samples with few (but well-preserved) calcareous nannofossils. In our preliminary shipboard investigation of Hole 761, we studied at least one sample in each section and all core catchers.

Cenozoic Biostratigraphy

Hole 761B recovered a thick Cenozoic section composed predominantly of calcareous ooze, the age of which can be constrained within narrow limits using nannofossil stratigraphy (Fig. 23). We have applied the zonation of Martini (1971), using the primary zonal indicators in most cases. However, in a number of instances where the primary indicators were not observed, we relied on secondary markers; the biostratigraphic ranges of these taxa are summarized in Perch-Nielsen (1985a).

The uppermost part of the sequence from Section 122-761B-1H-1 to -3H-CC contains a mixed Quaternary assemblage of *Emiliania huxleyi*, *Gephyrocapsa oceanica*, and *Pseudoemiliania lacunosa*, indicating a possible range in age from Zone NN19 to Zone NN21. Sections 122-761B-4H-1 and -4H-2 possess *Discoaster surculus* and *Pseudoemiliania lacunosa*, suggesting a late Pliocene age within Zone NN16. The interval from Section 122-761B-4H-3 to -4H-6 is late Miocene in age (within the *Discoaster quinqueramus* Total Range Zone, or TRZ, NN11), as determined by the presence of the nominate species. A narrow interval within Section 122-761B-4H-6 (below 80 cm) marked by a color change, lies within the *Discoaster hamatus* TRZ (NN9), also determined by the presence of the nominate taxon. There may thus be a slight hiatus in Core 122-761B-4H-6, 80 cm, containing upper Miocene Zone NN10.

Sections 122-761B-4H-7 to -5H-2 are placed within Zone NN8, as suggested by the combined presence of *Catinaster coalitus*, and the absence of *D. hamatus*. The *Discoaster kugleri* TRZ is confined to Sections 122-761B-5H-3 and -5H-4 according to the presence of the nominate species. Sections 122-761B-5H-5 and -5H-6 lie within Zone NN6, as they fall between the last occurrence of *Sphenolithus heteromorphus* and the first occurrence of *Discoaster kugleri*. The interval from Section 122-761B-5H-7 to -6H-5 lies within the combined NN4 and NN5 Zones, between the last occurrence of *Sphenolithus belemnos* at the base, and the last occurrence of *S. heteromorphus* at the top. *Helicosphaera ampliaperta* was not observed, and thus this interval could not be subdivided. Sections 122-761B-6H-6 and -6H-CC are bounded by the last occurrence of *Triquetrorhabdulus carinatus* at the base and the last occurrence of *Sphenolithus belemnos* at the top, and are therefore constrained within the *Sphenolithus belemnos* Zone (NN3).

The overlying Sections 122-761B-7H-1 and -7H-2 lie in Zone NN2 as determined by the presence of *Discoaster druggii*. The lowermost Neogene zone (NN1) is confined to Sections 122-761B-7H-3 and -7H-4 on the basis of abundant *T. carinatus* and the absence of *D. druggii* and *Sphenolithus ciperoensis*.

The Paleogene occurs in Sections 122-761B-7H-5 to -8H-1. This interval lies in the uppermost Oligocene zone (NP25) according to the occurrence of *Sphenolithus ciperoensis* and the absence of *S. distentus* and *S. predistentus*. A pronounced hiatus occurs at the base of Section 122-761B-8H-1 (between 140 and 150 cm). The interval from Section 122-761B-8H-2 to -8H-CC is constrained to middle Eocene Zone NP16 on the basis of abundant *Sphenolithus furcatolithoides*, and of *Sphenolithus radians*, *Discoaster saipanensis*, and *Chiasmolithus grandis*. The upper Eocene and lower Oligocene are therefore missing. Core 122-761B-9H lies within upper Paleocene Zones NP15 or NP16 according to the presence of *Discoaster mohleri*, *S. furcatolithoides*, *Campylosphaera dela*, and *Reticulofenestra umbilica*.

Cores 122-761B-10H and -11X correspond to Zone NP15 on the basis of *Discoaster mohleri* and *Discoaster sublodoen-*

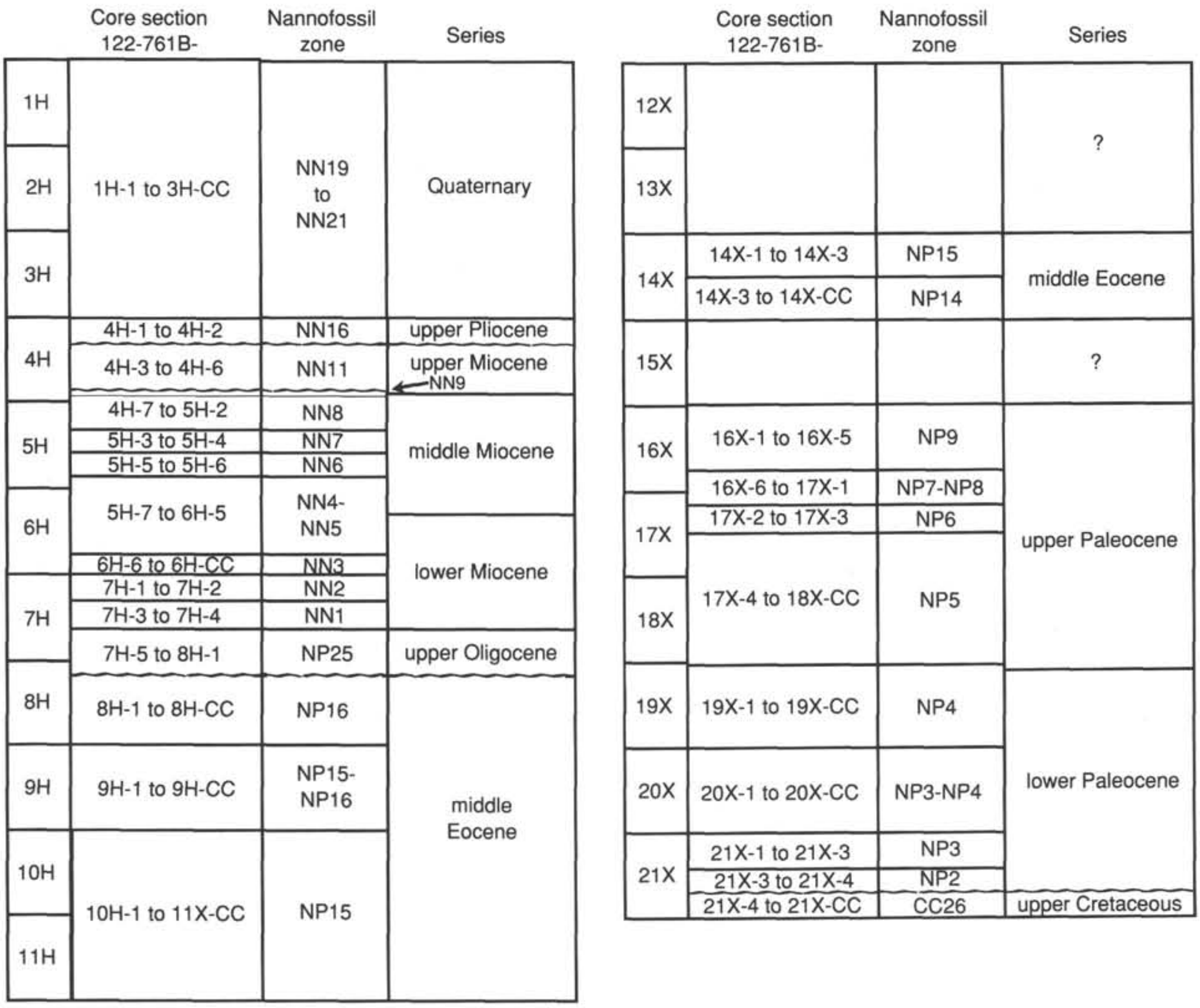

Figure 23. Cenozoic calcareous nannofossil stratigraphy of Hole 761B including zones of Martini (1971). Wavy lines indicate positions of hiatuses.

sis co-occurring. No material was recovered in Cores 122-761B-12X, -13X, or -15X, and the intermediate interval in Core 122-761B-14X is placed in Zones NP14 and NP15. The latter zone occurs from Sections 122-761B-14X-1 to -14X-3, and the former zone corresponds to the remainder of the core according to the combined presence of *Discoaster lodoensis* and *D. sublodoensis*. Sections 122-761B-16X-1 to -16X-5 lie within Zone NP9, as suggested by the combined presence of *Discoaster multiradiatus* and *Fasciculithus tympaniformis*, and by the occurrence of numerous other fasciculithids, including *Fasciculithus hayi* and *Fasciculithus alanii*, whose ranges are limited to that zone. The interval from Section 122-761B-16X-6 to -17X-1 has been correlated to Zones NP7 and NP8 given the presence of *Discoaster mohleri*, and the absence of *Discoaster multiradiatus*.

Sections 122-761B-17X-2 and -17X-3 belong in Zone NP6, as indicated by the occurrence of *Heliolithus kleinpellii* and the absence of *Discoaster mohleri*, and Sections 122-761B-17X-4 to -18X-CC are correlated to Zone NP5 on the basis of *Fasciculithus tympaniformis* occurring without *H. kleinpellii*. Core 122-761B-19X is placed in lower Paleocene Zone NP4, as suggested by the occurrence of *Fasciculithus magnicordis*, *Fasciculithus pileatus*, and *Cruciplacolithus tenuis*. Core 122-761B-20X corresponds to Zones NP3 or NP4, according to the presence of *Chiasmolithus danicus* and *Cruciplacolithus tenuis* and very rare *F. pileatus*. The interval from Section 122-761B-21X-1 to -21X-3 and Section 122-761C-2R-CC lie in Zone NP3, as determined by the presence of *C. danicus* and the absence of fasciculithids. The lowermost Paleocene zone observed in Hole 761B, Zone NP2, occurs in Sections 122-761B-21X-3 and -21X-4, which lie below the first occurrence of *C. danicus* in Section 122-761B-21X-2.

Cretaceous/Tertiary Boundary

The Cretaceous/Tertiary boundary interval was recovered in Holes 761B and 761C. The boundary interval in the former hole occurs in Core 122-761B-21X-4, 126 cm, where it is characterized by a distinct color change and is represented by a short hiatus (lowermost Paleocene Zone NP1 is clearly missing). Sample 122-761B-21X-4, 129 cm (from immediately below the boundary), contains a diverse upper Maestrichtian assemblage that we place in the *Micula murus* TRZ of Roth (1978) on the basis of the nominate species being present. In contrast, Sample 122-761B-21X-4, 125 cm (from immediately above the boundary), contains both *Cruciplacolithus primus* and *C. tenuis*, which indicate Zone NP2.

The boundary interval in Hole 761C occurs in Core 122-761C-3R-3, 66 cm, and although marked by slight coring disturbance and a distinct lithologic change, is more complete than the interval in Hole 761B. In Hole 761C, the lowermost Paleocene Zone NP1 is present and extends from Sample 122-761C-3R-3, 67 cm, which records the last *in situ* occurrence of late Cretaceous species, to Sample 122-761C-3R-3, 51 cm, containing the first occurrence of *Cruciplacolithus tenuis*. This zone is characterized by few, moderately preserved calcareous nannofossils, most of which have been reworked from the Cretaceous. Above and below this interval, however, nannofossils are abundant and quite well preserved. It is difficult to ascertain at present whether the boundary interval in Hole 761C is complete, as there are various opposing lines of evidence.

The thickness of Zone NP1 in Hole 761C (17 cm), is less than at other DSDP sites where it has been recovered. At DSDP Sites 356 and 577 it is 2.48 m and 1.04 m thick, respectively (Perch-Nielsen, 1977; Monechi, 1984), but at DSDP Site 384, it is only 24 cm thick (Thierstein and Okada, 1979). However, the overall thickness of NP1 may be related to sedimentation rate rather than to continuity of sedimentation. The first occurrences of *Cruciplacolithus primus* and *C. tenuis* occur at the same level in Hole 761C and DSDP Site 384, but are separated in DSDP Sites 356 and 577. This may indicate the absence of part of NP1 in the former two holes; it may also be explained by variable preservation between sites (Thierstein and Okada, 1979).

Likewise, Hole 761C does not contain the substantial bloom of the calcareous dinoflagellate, *Thoracosphaera*, which characterizes the Cretaceous/Tertiary boundary at other sites; clearly, its absence could have an environmental interpretation. The uppermost Maestrichtian marker *Micula prinsii* was not observed in Hole 761C, although its presence could easily be obscured by overgrowth, and there is some dispute as to whether its first occurrence lies above or below that of *Micula murus* (Thierstein, 1981). The occurrence of the Tertiary species *Biantholithus sparsus* and *Markalius astroporus* is lower in the relative sequence of events at Hole 761C than in other Deep Sea Drilling Project (DSDP) and Ocean Drilling Program (ODP) sites. This suggests that the Cretaceous/Tertiary boundary interval at Site 761 may be more complete than at the other DSDP/ODP sites.

Although it is clear that there has been some drilling disturbance of the boundary interval in Hole 761C, the calcareous nannofossil stratigraphy cannot at present determine how much, if any, is missing from the section. This will be clarified by shore-based investigations of foraminifers, magnetostratigraphy, and measurements of iridium and shocked-quartz contents.

Cretaceous Biostratigraphy

Hole 761B recovered a mostly complete Maestrichtian and upper Campanian sequence; however, the remainder of the upper Cretaceous appears to be disrupted by four hiatuses. Although the diversity of floras is high throughout the sequence, several of the zonal markers of Sissingh (1977) and Roth (1978) either were not observed or were found in low abundances. For this reason, we have relied largely on individual biohorizons for dating the sequences. Some of these events allow us to determine combined zonal units of Sissingh (1977) and Roth (1978) (Fig. 24). This zonation scheme can be correlated with the other zonations using common markers and the detailed stratigraphic scheme of Perch-Nielsen (1985b; see "Explanatory Notes" chapter, this volume).

The Maestrichtian and Campanian sequences appear to be mostly complete. There is one possible hiatus, within Section 122-761B-24X-5, as indicated by the coincidence of the last occurrences of *Reinhardtites levis*, *Broinsonia parca*, and *Eiffellithus eximius* (Fig. 24). Another unconformity lies within Section 122-761B-27X-1, as indicated by the coincidence of the first occurrence of *Lucianorhabdus cayeuxii* and the last occurrence of *Eprolithus floralis*; this hiatus is of middle Santonian age. A third Cretaceous unconformity was recovered in Section 122-761B-27X-4, and includes much of the Coniacian stage. This unconformity is indicated by the coincidence of the first occurrences of *Micula staurophora* and *Reinhardtites levis* in Section 122-761B-27X-4, immediately above an upper Turonian assemblage of much poorer preservation in Section 122-761B-27X-CC. Section 122-761B-28X-CC is represented by a probable lowermost Albian assemblage, as suggested by the combined presence of *Cribrosphaerella ehrenbergii* and absence of *Prediscosphaera cretacea*. Therefore, much of the Turonian, all of the Cenomanian, and much of the Albian are also missing.

Subunit IIB in Hole 761C was spot cored and therefore contains large sampling gaps. Core 122-761C-5R recovered chalk of Santonian age, as determined by the presence of *Micula staurophora* and absence of *Broinsonia parca*. Section 122-761C-6R-CC contains common *Vagalapilla matalosa*, few *Chiastozygus litterarius* and *Cretarhabdus coronadventis*, and rare *Braarudosphaera africana* and *Prediscosphaera cretacea*, suggesting a middle Albian age within Zone CC8 of Sissingh (1977).

The nannofossil calcisphere chalk (Subunit IIC) recovered in Cores 122-761B-29X to -30X and Cores 122-761C-7R to -9R, and intervals within the belemnite sands (Unit III) recovered in Cores 122-761B-30X and 122-761C-10R, are represented by a moderately well-preserved, but very-low-diversity nannoflora composed largely of the calcareous dinoflagellate, *Thoracosphaera* cf. *saxea*, but also with common *Watznaueria barnesae*, few *Parhabdolithus embergeri*, and rare *Microstaurus chiastius*, *Grantarhabdus meddii*, *Polypodorhabdus* sp., *Biscutum* sp., and *Crucibiscutum salebrosum*.

The most definitive age information for Subunit IIC is given by the occurrence (albeit of a single specimen) of *Rhagodiscus nebulosus* in Sample 122-761C-7R-1, 39–40 cm. This taxon has a rather restricted stratigraphic range, occurring in various sequences from the upper Berriasian to the lower Valanginian (Bralower et al., 1989). This age is supported by the occurrence of *C. salebrosum*, which ranges in the North Sea region from upper Ryazanian to lower Barremian, with a sharp acme in the Valanginian (Jakubowski, 1987). The age of this unit is therefore probably late Berriaisan to early Valanginian. At present, there is no reason to suggest that Unit III has a significantly different age, as it contains a similar nannoflora in several intervals.

The low-diversity nannoflora of Subunit IIC and Unit III is composed of several taxa known to tolerate stressful environments, including *Thoracosphaera*, *Watznaueria*, and *Biscutum*. In this case, sedimentological data indicate that this unit may represent an elevated-salinity environment. Clearly these unusual assemblages warrant further, more detailed investigation.

Triassic Biostratigraphy

As in the previous two sites (Sites 759 and 760), Triassic nannofossils were recovered at Site 761. In Hole 761C, these occurred in most samples processed from Cores 122-761C-23R to -30R. The assemblages appear to be well preserved (composed of original calcite) and consist predominantly of the holococcolith genus *Prinsosphaera*. Two taxa described by Jafar (1983) were observed (*Prinsosphaera triassica* and *Prinsosphaera triassica punctata*) and several undescribed forms of this genus were also noted. These taxa have been

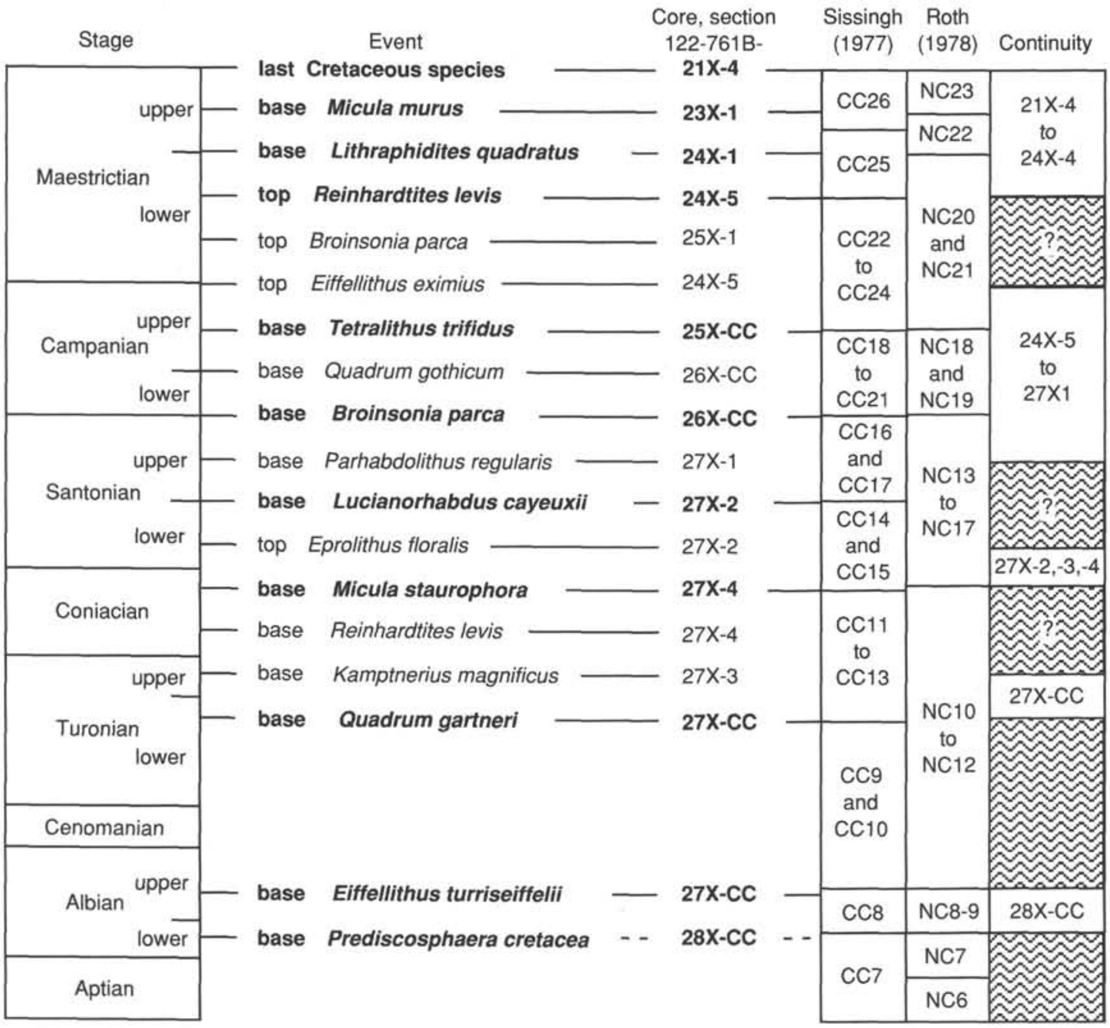

Figure 24. Upper Cretaceous calcareous nannofossil stratigraphy of Hole 761B, including zonations of Sissingh (1977; CC zones) and Roth (1978; NC zones). Bold type indicates zonal markers. Wavy pattern indicates stratigraphic positions of possible unconformities.

observed in underlying units in Holes 759B and 760B, but never in such high abundance. In addition, we noted a few occurrences of *Hayococcus floralis*, *Crucirhabdus* sp., and other forms observed in the previous holes.

Foraminifers

Planktonic foraminiferal faunas recovered from the Cenozoic and upper Cretaceous (down to the Turonian) parts of Holes 761B and 761C are generally rich and diverse. Below the Cenomanian, the faunas are very restricted, except in one sample of Albian age that yielded an abundant but low-diversity planktonic assemblage. The Rhaetian foraminiferal faunas are exclusively benthic and are dominated by miliolids, involutinids, and ammodiscids in the limestones, and by nodosariids in the calcareous claystones. The latter also contain rich ostracode faunas.

Neogene Biostratigraphy

Quaternary faunas were recovered from Sections 122-761B-1H-CC through -3H-CC. These all contain *Globorotalia truncatulinoides*, and are dominated by *Globigerinoides sacculifer*, *Globorotalia tumida*, *Globorotalia menardii*, *Pulleniatina obliquiloculata*, and *Sphaeroidinella dehiscens*, which form a typical low-latitude fauna. The combined presence of *G. truncatulinoides* and *Globorotalia tosaensis* in Section 122-761B-3H-CC assigns this sample to Pleistocene Zone N22, while the higher section is tentatively assigned to Zone N23.

Detailed biostratigraphic analysis was carried out on Core 122-761B-4H. Sample 122-761B-4H-2, 45–47 cm, contains *G. tosaensis* and *Globigerinoides fistulosus* and belongs to upper Pliocene Zone N21. The interval from Samples 122-761B-4H-3, 45–47 cm, through -4H-6, 45–47 cm, is late Miocene in age and is placed within Zones N15 and N16 as indicated by the presence of *Globigerina nepenthes*, *Globoquadrina dehiscens*, and *Globogerinoides bollii*. Section 122-761B-4H-CC and Core 122-761B-5H-2, 44–46 cm, are late middle Miocene in age, with both *G. nepenthes* and *Globorotalia siakensis* present, indicating Zone N14. Lower Pliocene and uppermost Miocene sediments appear to be missing in this hole.

The lower part of Core 122-761B-5H and the upper part of Core 122-761B-6H show a rapid succession of Middle Miocene Zones N12 or N11 to N9, as indicated by the successive representatives of the *Globorotalia fohsi* group, and the presence of *Orbulina* spp. The base of the Middle Miocene was recognized by the evolutionary appearance of *Orbulina* *suturalis* (from *Praeorbulina glomerosa*) in Core 122-761B-6H-2, 45–47 cm.

The middle part of Core 122-761B-6H belongs to Zone N8. This is indicated by the presence of successive members of the *Globigerinoides sicanus-Praeorbulina* lineage in Samples 122-761B-6H-3, 45-47 cm, and -6H-4, 45–47 cm.

Section 122-761B-6H-CC belongs to Zone N5 as indicated by the presence of *Globigerinoides primordius*, *Globoquadrina binaiensis*, *Globoquadrina praedehiscens*, and *G. dehiscens*, but *Globorotalia kugleri* is absent. The first downhole appearance of *G. kugleri* is in Sample 122-761B-7H-2, 45–47 cm, indicating the top of Zone N4. The Miocene/Oligocene boundary was placed within Zone N4, at the lowest occurrence of *Globoquadrina dehiscens*, in Sample 122-761B-7H-2, 45–47 cm.

Paleogene Biostratigraphy

Samples 122-761B-7H-3, 45–47 cm, and -7H-4, 45–47 cm, contain *Globorotalia kugleri*, *G. binaiensis*, and *G. praedehiscens*, indicating uppermost Oligocene Zone N4A. Below that, *Globigerina tripartita* and *Globigerina ciperoensis* indicate the presence of Zone P22 down to the appearance of *Globorotalia opima opima* (a species marking the top of Zone P21) in Sections 122-761B-7H-CC and -8H-1. This is the lowest occurrence of Oligocene taxa in this hole.

Sections 122-761B-8H-2 and -8H-CC contain *Acarinina bullbrooki*, *Turborotalia frontosa*, *Morozovella spinulosa*, and *Hantkenina alabamensis*, indicating a middle Eocene age (Zone P12 or P11). Lower Oligocene and Upper Eocene sediments appear to be missing in Hole 761B.

Cores 122-761B-9H through -14X are middle Eocene to uppermost Lower Eocene. Section 122-761B-9H-CC contains *H. alabamensis*, *A. bullbrooki*, *M. spinulosa*, and *Truncorotaloides* spp., indicating a middle Eocene age. Below this, Sections 122-761B-10H-CC and -11X-CC are characterized by the occurrence of *Morozovella aragonensis* and *Morozovella caucasica*, and therefore belong to Zone P9 or P10. *M. aragonensis*, *Acarinina broedermanni*, and *Acarinina soldadoensis* were found in Section 122-761B-14X-CC. The presence of these species assigns this section to upper Lower Eocene (Zones P8–P9). We found no sediments of the Eocene/Paleocene boundary interval (P7 to P5), possibly owing to the lack of core recovery in Core 122-761B-15H.

Sections 122-761B-16X-CC to -18X-CC belong to Upper Paleocene Zone P4, as determined by the occurrence of *Planorotalites pseudomenardii* accompanied by *Acarinina mckanni*. Cores 122-761B-19X to -21X are lower Paleocene (Zones P3–P1). The upper part of Core 122-761B-19X is characterized by *Planorotalites compressus* and *Morozovella angulata*, indicating Zone P3. Below this, Core 122-761B-20X contains *P. compressus* and *Morozovella pseudobulloides*. *Morozovella trinidadensis* occurs in Sample 122-761B-20X-4, 134–136 cm, which assigns this section to Zone P1C.

Cretaceous Biostratigraphy

The highest Cretaceous section studied (Section 122-761B-21X-CC) contains a planktonic foraminiferal fauna with *Abathomphalus mayaroensis* and is clearly of late Maestrichtian age (*A. mayaroensis* Zone). This species is present down to and including Sample 122-761B-24X-1, 82–84 cm. It is remarkable that several species that are usually quite common in this part of the Maestrichtian (e.g., *Rosita contusa* and *Globotruncana stuarti*) are present rarely, whereas others (e.g., *Trinitella scotti* and *Gansserina gansseri*) were absent. These assemblages are clearly dominated by *Rugoglobigerina* spp., *Gueblerina cuvillieri*, and representatives of the *Globotruncana arca* and *Globotruncana rosetta* groups.

A Maestrichtian age is also certain for Sample 122-761B-24X-4, 82–84 cm, which contains *Abathomphalus intermedius* and can be assigned to the *Rosita contusa* Zone, although the zonal marker was not found.

From the bottom of Core 122-761B-24X through Sample 122-761B-25X-3, 43–45 cm, a *Rugoglobigerina*-dominated fauna without Maestrichtian marker species occurs, and is assigned a questionable Maestrichtian age on the strength of the presence of a primitive form *Gueblerina* sp.

Below Section 122-761B-25X-CC, *Gueblerina* is absent. An assemblage with both *Globotruncana ventricosa* and *Globotruncanita elevata* is present throughout Core 122-761B-26X; the age of this fauna is somewhat problematic. These species do not commonly occur together, as the former is an upper Campanian marker and the latter is a lower to mid-Campanian marker. However, calcareous nannofossil evidence suggests an upper Campanian age for this interval.

No planktonic foraminiferal evidence of Santonian and Coniacian was seen in shipboard analysis of Hole 761B.

Section 122-761B-27X-CC yielded *Dicarinella imbricata* and *Falsotruncana maslakovae*, which together indicate a late Turonian age. Section 122-761B-28X-CC contains only very rare planktonic foraminifers including *D. imbricata* and *Marginotruncana pseudolinneiana*. The presence of these taxa probably represent contamination, but otherwise would indicate a Turonian age.

One section from Hole 761C (Section 122-761C-6R-CC) contains an abundant planktonic microfauna with *Hedbergella delrioensis*, *Hedbergella planispira*, and possibly *Ticinella bejaouaensis*, most probably indicating an early to middle Albian age. Below this, only benthic foraminifers (including abundant polymorphinids and a few nodosariids, together with superabundant small calcispheres) occur in Section 122-761C-7R-CC. None of these are age diagnostic in themselves. The Cretaceous foraminifers at Site 761 show a fluctuating Tethyan influence, alternating with more temperate, low-diversity interludes.

Triassic Biostratigraphy

Preliminary analysis of thin sections of samples from Cores 122-761B-32X and -33X revealed the presence of *Glomospirella* sp. in Samples 761B-32X-CC, 21–23 cm, -33X-1, 4–6 cm, and -33X-CC, 10–12 cm. This suggests that the lowermost cores in Holes 761B are Triassic, as was confirmed by the foraminiferal record in Hole 761C.

The first evidence of Triassic in Hole 761C was found in Sample 122-761C-12R-1, 2–4 cm, with *Triasina hantkeni* indicating a Rhaetian age. Below this, we examined numerous thin sections down to Core 122-761C-32R-2, 32–36 cm. Regular occurrences of *Triasina hantkeni* were recorded in Cores 122-761C-12R through -17R, and in Samples 122-761C-20R-1, 10–11 cm, and -20R-1, 20–22 cm. Washed residues from Sections 122-761C-23R-CC through -30R-CC contained fairly rich and diverse ostracode faunas with a few nodosariid, miliolid, and involutinid foraminifers. A thin section from Sample 122-761C-31R-2, 50–52 cm, contains a questionable specimen of *T. hantkeni*, along with *Trocholina* sp. and *Involutina* sp.; these are the lowermost foraminifer occurrences in Hole 761C.

It appears that the local range of *T. hantkeni* covers most (if not all) of the Rhaetian, as dated using palynology. We propose a *Triasina hantkeni* Total Range Zone of Rhaetian age on the basis of its occurrence at Site 761.

Radiolarians

The radiolarians recovered from Holes 761B and 761C are seldom abundant and thus were studied as wet-sieved residues instead of as strewn slides. Sample 122-761A-1H-CC contains middle to late Quaternary radiolarians including *Arcosphaera spinosa*, *Anthrocyrtidium ophirense*, *Axoprunum stauroaxonium*, *Didymocyrtis tetrathalamus*, *Euchitonia elegans*, *Giraffospyris angulata*, *Lamprocyrtis nigriniae*, *Lamprocyclas* spp., and *Stylacontarium acquilonium*. Samples 122-761B-1H-CC to -2H-4, 138–142 cm, contain relatively well-preserved radiolarians assignable to either the upper Quaternary *Buccinosphaera invaginita* Zone or *Collosphaera tuberosa* Zone (Sanfilippo et al., 1985).

Samples 122-761B-2H-4, 138–142 cm, -2H-5, 23–27 cm, -2H-CC, and -3H-5, 81–83 cm, contain *Anthrocyrtidium angulare*, *Didymocyrtis tetrathalamus*, and *Theocorythium trachelium*, all of which are assignable to either the lower Quaternary *Amphirhopalum ypsilon* or *Anthrocyrtidium angulare* Zones of Sanfilippo et al. (1985). Radiolarians are extremely rare and only fragmentary in Samples 122-761B-6H-CC and -7H-CC. Poorly preserved middle Eocene (*Theocotyle cryptocephala* to *Podocyrtis ampla* Zones of Sanfilippo et al., 1985) radiolarians, including *Podocyrtis sinuosa* and *Podocyrtis* spp., were recovered from Sample 122-761B-8H-CC. Core catchers from Cores 122-761B-9H, -10H, -11H, and -14X, are all barren of radiolarians.

Samples 122-761B-16X-3, 67–69 cm, through -19X-1, 134–136 cm, all contain well-preserved (but mostly undescribed) upper Paleocene radiolarian taxa, although *Bathropyramis* sp., *Buryella pentadica*, *Carposphaera subbotinae*, *Lamptonium pennatum*, *Lychnocanoma* sp., *Pterocodon*? *anteclinata*, *Phormocyrtis striata*, *Phormocyrtis exquisita*, *Spongodiscus pulcher*, *Stylotrochus alueatus*, and *Theocotylissa auctor* could be identified. The Paleocene Series still remains unzoned with respect to radiolarian biostratigraphy, but many of the upper and middle Paleocene taxa cited above were described by Foreman (1973). Samples 122-761B-19X-2, 72–74 cm, to -19X-CC contain very rare and fragmental lower Paleocene radiolarian taxa. No radiolarians were recovered from Cores 122-761B-20X to -24X. Fragments of *Dictyomitra* spp. and *Phaseliforma* spp. were recovered in Sample 122-761B-25X-CC, which indicates a late Cretaceous (Campanian?) age. Cores 122-761B-26X and -27X are barren.

A chert horizon in Section 122-761B-28X-CC contains early Cretaceous (upper Albian) radiolarians assignable to the *Petasiforma formanae* Zone of Pessagno (1977; equivalent to the upper part of *Acaeniotyle umbilicata* Zone of Sanfilippo and Riedel, 1985), including *Acaeniotyle diaphorogona*, *Alievium* spp., *Archaeodictyomitra simplex*, *Mita gracilis*, *Thanarla pulchra*, *Spongocapsula zamoraensis*, *Stichomitra*(?) *communis*, and *Zifondium lassenensis*. Sample 122-761B-29X-1, 73–75 cm, contains a poorly preserved lower to mid-Aptian fauna assignable to either the *Stichomitra euganea* Zone or the lowermost part of the *Acaeniotyle umbilicata* Zone of Sanfilippo and Riedel (1985). Age-diagnostic taxa include *Eucyrtis micropora*, *Pseudodictyomitra carpatica*, *Pseudodictyomitra lodogaensis*, *Sethocapsa trachyostraca*, *Stichomitra* spp., *Theocorys antiqua*, and *Xitus alievi*. Section 122-761B-29X-CC contains radiolarians largely preserved as casts, but also includes rare specimens of *Praeconocaryomma*, *Pseudodictyomitra*, *Stichomitra*, and *Thanarla*, all of which indicate an undifferentiated late Early Cretaceous age. Samples 122-761B-30X-CC to -33X-CC are barren of radiolarians.

Most of the sediments in Hole 761C contain poorly preserved radiolarian faunas with the exception of Section 122-761C-2R-CC. This section contains rare but well-preserved middle to lower Paleocene radiolarians including *Bathropyramis* sp., *Buryella tetradica*, *Lithomespilus mendosa*, and *Lychnocanoma* sp. Samples 122-761C-3R-CC and -9R-CC are barren of identifiable radiolarians. Chert horizons in Samples 122-761C-5R-2, 147–149 cm, and -6R-1, 31–33 cm, both contained mid-Cretaceous radiolarian faunas. The chert horizon in Sample 122-761C-5R-2, 147–149 cm, contains a mid to upper Cenomanian fauna assignable to the *Rotaforma hessi* Zone of Pessagno (1976, equivalent to the lower part of the *Obesacapsula somphedia* Zone of Sanfilippo and Riedel, 1985). Age-diagnostic taxa include *Archaeodictyomitra sliteri*, *Archaeodictyomitra*(?) *turris*, *Halesium sexangulum*, *Mita gracilis*, *Pseudodictyomitra pseudomacrocephala*, *Novixitus mclaughlini*, *Novixitus* spp., *Patulibracchium inaequalum*, *Stichomitra communis*, *Stichomitra*(?) *euganea*, *Stichomitra*(?) *zamoraensis*, and *Thanarla elegantissima*.

Another chert horizon in Sample 122-761C-6R-1, 31–33 cm, contains mid-Albian taxa with concurrent ranges near the boundary separating the *Kozurium zingulai* and *Petasiforma formanae* Zones of Pessagno (1977; equivalent to the upper part of the *Acaeniotyle umbilicata* Zone of Sanfilippo and Riedel, 1985). Diagnostic taxa include *Acaeniotyle diaphorogona*, *A. umbilicata*, *Acanthocircus dendrocanthus*, *Archaeodictyomitra squinaboli*, *Mita magnifica*, *Pseudodictyomitra carpatica*, *Xitus spicularius*, *Xitus spineus*, and *Zifondium lassenensis*.

Nearly all the radiolarians from Sample 122-761C-7R-CC are preserved as casts with little or no meshwork visible. However, several specimens can be identified as *Mita* cf. *M. magnifica* and *Xitus* cf. *X. spicularius*, both of which indicate an undifferentiated late Early Cretaceous (Aptian-Albian) age. Below this, in Sample 122-761C-11R-CC, a poorly preserved fauna with questionably assigned taxa (*Holocryptocanium?* sp. and *Obesacapsula?* sp.) also suggests an undifferentiated early Cretaceous age. Cores 122-761C-23R to -30R are all barren of identifiable radiolarians.

Palynology

All samples analyzed from Hole 761B and the interval from Core 122-761C-2R through -22R are barren of palynomorphs. Samples 122-761C-23R-CC, -24R-CC, 27R-1, 69–71 cm, and -31R-2, 135–138 cm, contain a few specimens of bisaccate pollen, organic coatings of foraminifers (termed "foraminifer liners" or "inner organic layers"), and the dinoflagellate cysts *Rhaetogonyaulax* sp., *Rhaetogonyaulax uncinata*, *Suessia swabiana*, and *Suessia listeri*. The foraminifer liners are abnormally abundant in comparison to foraminifer liners in other Triassic samples investigated at Site 759 and 760. Their presence suggests that the interval from Core 122-761C-23R through -31R belongs to one specific palynological paleoenvironment.

Dinoflagellate biostratigraphy indicates that this interval is early to middle Rhaetian in age (*Rhaetogonyaulax rhaetica* dinoflagellate Zone; *Ashmoripollis reducta* spore/pollen Zone; Helby et al., 1987). Samples 122-761C-28R-CC and -29R-CC are barren of palynomorphs.

Samples 122-761C-32R-CC and -33R-CC exhibit an assemblage of terrestrial palynomorphs dominated by cuticles. No foraminifer liners were visible. The presence of *Falcisporites australis*, *Minutosaccus crenulatus*, and *Samaropollenites speciosus* suggests the spore/pollen *Minutosaccus crenulatus* Zone (after Helby et al. 1987), which is Norian in age.

Discussion

Table 3 and Figure 25 show the various intervals cored, the assigned lithologic units, the corresponding biostratigraphic zonations, and approximate age ranges for each lithologic unit.

Hole 761B sediments yielded a fairly complete Cenozoic calcareous nannofossil and planktonic foraminiferal succes-

Table 3. Biostratigraphic summary, Site 761.

Interval	Unit	Foraminifer zone	Nannofossil zone	Radiolarian zone	Palynological zone	Age
761B-1H-1 to 761B-8H-1	IA Nannofossil ooze with foraminifers	N22–P21	NN21–BP25	*B. invaginata*/ *C. tuberosa* Zone to unzoned		Quaternary to Late Oligocene
761B-8H-1 to 761B-11X-1	IB Nannofossil ooze	P11/12 to P9/10	NP16–NP15			Middle Eocene
761B-11X-1 to 761B-16X-1	IC Nannofossil ooze with foraminifers and chert	P9/10 to P8/9	NP15–NP14			Middle Eocene
761B-16X-1 to -21X-4; 761-2R-1 to -3R-3	ID Nannofossil chalk with foraminifers	P4/5 to P1b	NP7/8–NP2			Paleocene
761B-21X-4 to -24X-1; 761-3R-3 to -3R-6	IIA Nannofossil chalk	*A. mayaroensis* to *A. mayaroensis*/*R. contusa*	CC26–CC25			Late Maestrichtian
761B-24X-1 to -28X-CC; 761C-5R to -7R-1	IIB Nannofossil chalk with foraminifers	*A. mayaroensis*/*R. contusa* to unzoned	CC25 to CC9/10			Late Maestrichtian early middle Albian
761B-29X-1 to -30X-1; 761-7R-1 to -10R-1	IIC Nannofossil chalk with clay	Unzoned	NK2/3 to unzoned			Early Valanginian to Late Berriasian
761B-30X-1 to -31X-1; 761C-10R-1 to -11R-1	III Sandstone with belemnites	Unzoned				Early Valanginian? to Late Berriasian
761B-31X-1 to -33X-CC; 761-11R-1 to -23R-1	IVA Limestone with *Triasina*	*Triasina hantkeni* Zone				Rhaetian
761C-23R-1 to -30R-1	VA Limestone and silty calcareous claystone	*Triasina hantkeni* Zone			*Rhaetogonyaulax rhaetica* dinoflagellate Zone	Rhaetian
761C-30R-1 to -32R-CC	VB Claystone and limestone	*Triasina hantkeni* Zone			*Rhaetogonyaulax rhaetica* Zone?	Rhaetian
761C-32R-CC to -33R-CC	VI Silty claystone and coal	Unzoned			*Minutosaccus crenulatus* pollen Zone	Norian

sion in which two hiatuses were defined (Fig. 23). The ages obtained from nannofossils and foraminifers at Holes 761B and 761C are in agreement, as each suggests that lower Pliocene and uppermost Miocene sediments are missing in the upper cores of Hole 761B. The lower Cenozoic hiatus lies between the upper Oligocene and middle Eocene. Upper Cretaceous nannofossil assemblages indicate four missing time intervals (Fig. 24). Determination of hiatuses for the Lower Cretaceous and Triassic intervals was impossible due to poor preservation and sporadic age control.

Holes 761B and 761C both contain Cretaceous/Tertiary boundary intervals, each characterized by a distinct color change; however, the lowermost Paleocene nannofossil zone (Zone NP1) is missing in Core 122-761B-21X. Although nannofossil biostratigraphic evidence suggests that the Cretaceous/Tertiary boundary interval in Hole 761C is complete, there is coring disturbance at the boundary; additional foraminiferal, magnetostratigraphic, and isotopic studies and iridium measurements are required to determine the extent of missing section.

As at the previous two sites, Triassic nannofossils were recovered in Hole 761C. However, the discovery of marine Rhaetian foraminifers in the Australian region is new and offers ample scope for further investigations. The best age control for the Triassic sediments at both holes was provided by palynology. The Rhaetian and Norian sections in Hole 761C should provide critical age control both for described and undescribed upper Triassic nannofossils found at the sites.

Finally, excellently preserved middle and upper Paleocene radiolarian assemblages were discovered in Sections 122-761B-16X-3 through -19X-1 and 122-761C-2R-CC, although much of the fauna is undescribed. The Paleocene is, at present, unzoned with respect to radiolarians (Sanfilippo et al., 1985). The excellent preservation of these faunas, combined with the age control offered by nannofossils and fora-

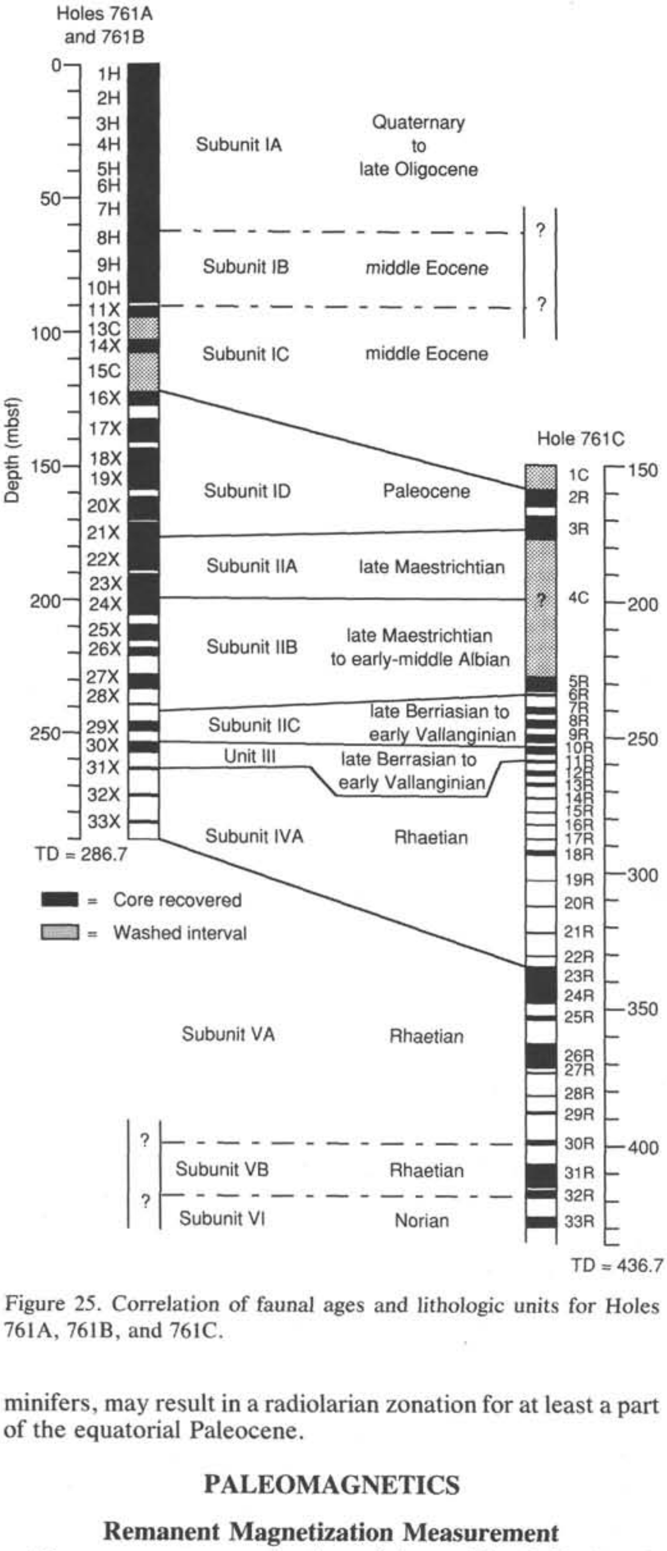

Figure 25. Correlation of faunal ages and lithologic units for Holes 761A, 761B, and 761C.

minifers, may result in a radiolarian zonation for at least a part of the equatorial Paleocene.

PALEOMAGNETICS

Remanent Magnetization Measurement

The remanent magnetization of the archive half of each core from Holes 761B and 761C was measured using the pass-through, three-component cryogenic magnetometer. Each core section was then demagnetized using the maximum field available (9 mT) and its remanence remeasured. Discrete samples were measured using the Molspin magnetometer, and step-wise alternating-field demagnetization (AFD) was performed on one sample from each core using the shipboard Schonstedt AC Geophysical Specimen Demagnetometer (Model GSD-1). Zijderveld diagrams were plotted from demagnetization data for all samples that were subjected to AFD.

Depending upon the stability of the magnetic components, the demagnetization curves plotted for individual samples commonly fall into one of three shape categories. The most commonly observed shape is similar to that in Figure 26A, and indicates the gradual removal of a single, stable magnetic vector. In contrast, some samples exhibit curves similar to that in Figure 26B. This type of demagnetization is characterized by the removal of an extremely large component at very low peak fields (i.e., 3 mT) and there is random change in direction beyond the low fields. This indicates an unstable magnetization, and the data corresponding to this type of demagnetization are excluded. Finally, a significant proportion of our samples have curves similar to that in Figures 26C and 26D. This type of curve is characterized by the easy removal of a soft secondary component by 5 or 10 mT alternating current (AC) field. This unstable component is of normal polarity and is probably a viscous remanent magnetization.

Figure 27 shows the variation of magnetization before and after AF demagnetization with a 9-mT field. Although there is no significant change in intensity, there is a drastic variation in direction, especially inclination. The data from discrete samples that have a stable magnetization exhibit an excellent agreement with whole-core measurements (Fig. 27B). Predicted magnetic inclinations are about $-32°$ (the dashed line in Fig. 27B) for the site, but observed values differed appreciably from this. The inclinations are substantially biased toward high values, with some exceeding $-80°$. While this bias is partially removed during demagnetization, some of it still remains after 9 mT AC field.

The interpretation of magnetic polarity for Hole 761B is on the basis of whole-core measurement and should be considered very speculative because of coring disturbance and poor magnetic properties of the sediments. However, whole-core and discrete-sample measurements provide a reasonably complete magnetostratigraphic section for the Quaternary sedimentary section (Fig. 27). Using the age constraints provided by paleontological data, a few reversal boundaries have been correlated to the geomagnetic reversal time scale (Fig. 27B). For example, the magnetic polarity sequence from Cores 122-761B-1H to -3H can be correlated to the Brunhes and upper Matuyama chrons (Haq et al., 1987).

Considering the low sedimentation rate during middle Miocene to upper Oligocene time at Site 761 (Cores 122-761B-4H-7 to -8H-1), correlation of the polarity record obtained at Hole 761B with the geomagnetic reversal time scale is difficult. In spite of coring disturbance, a higher sedimentation rate and the acceptable recovery of Cores 122-761B-16X through -27X allow us to recognize the principal polarity features of the upper Paleocene to upper Campanian.

Considering the poor recovery and severe disturbance of cores from Hole 761C, little interesting magnetic data were obtained during shipboard analysis. Shore-based analyses will be carried out on discrete samples.

Magnetic Susceptibility Measurements

Measurement of volume susceptibility was made at 5-cm intervals on whole, unsplit, 1.5-m sections from Cores 122-761B-1H to -9H. The shipboard Bartington Instruments Model MS-1 magnetic susceptibility meter with a 80-mm loop sensor was employed. This instrument is capable of measuring susceptibility with a sensitivity of 1×10^{-7} cgs. The susceptibility reflects variations in the concentration of magnetic material in the sediment. Susceptibility values were generally high

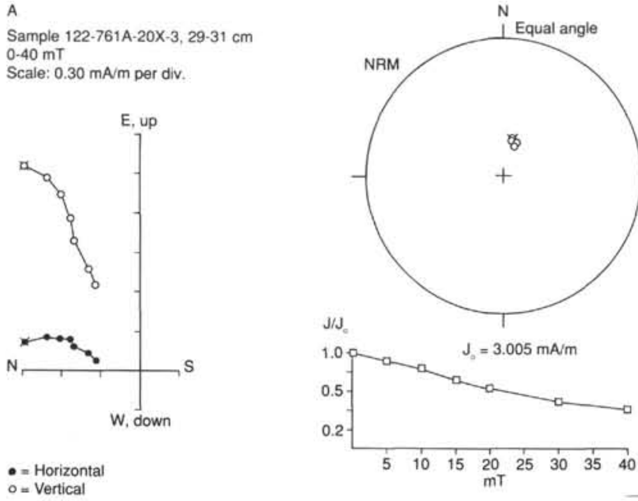

Figure 26. Vector endpoint diagrams, equal angle stereographic projections, and intensity decay curves. **A.** Sample 122-761A-20X-3, 29–31 cm, showing a single, stable component of magnetization. **B.** Sample 122-761B-17H-7, 23–25 cm, showing an unstable magnetization. **C.** Sample 122-761B-3H-1, 115–117 cm, showing a soft secondary component. **D.** Sample 122-761B-4H-2, 54–56 cm, showing a stable component.

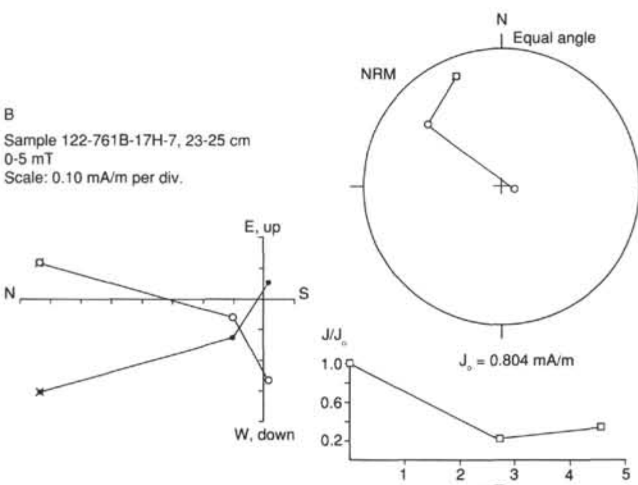

Figure 26 (continued).

(approximately 5–10 × 10^{-6} cgs units). However, the susceptibility versus depth record (Fig. 28) is punctuated with some high-amplitude spikes, especially in the upper 20 m of the hole.

SEDIMENTATION RATES

The sedimentation rates for the Cenozoic and upper Cretaceous sediments at Hole 761B are graphically illustrated in Figures 29 and 30. A discussion of the techniques used to calculate sedimentation rates at this site is given in the "Explanatory Notes" chapter (this volume).

Sediment recovery was variable for the upper Cretaceous sediments at Hole 761B (Fig. 30), and therefore the sedimentation rates are more speculative. Upper Cretaceous sedimentation rates dramatically increased from 0.1 cm/k.y. for basal Santonian and Turonian sediments to nearly 2.0 cm/k.y. for the interval represented by Zone CC26.

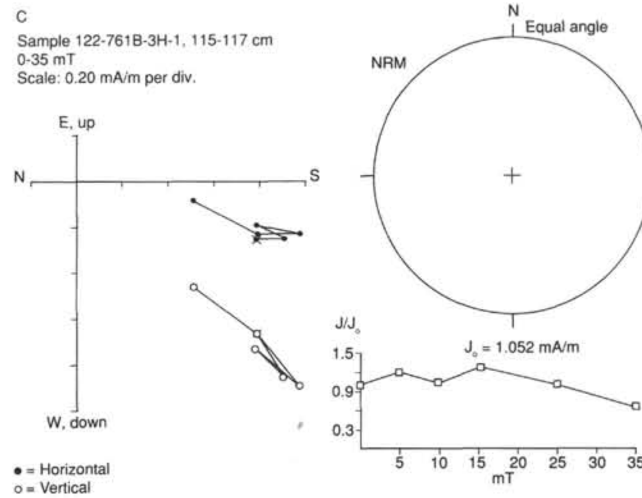

Figure 26 (continued).

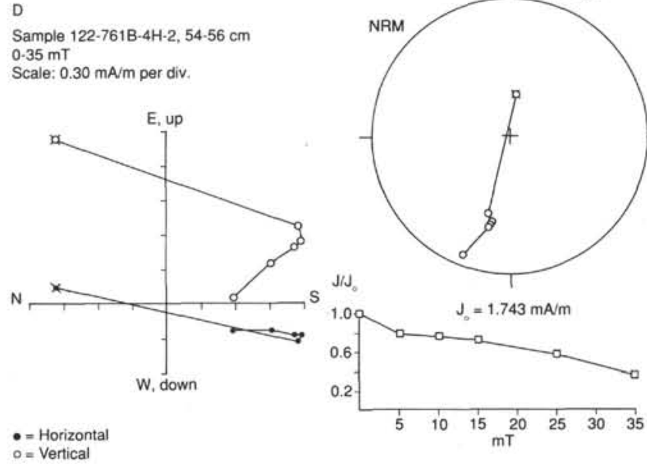

Figure 26 (continued).

Sedimentation rates dropped dramatically, resulting in the highly condensed interval between Zones NP3 and NP2 (Fig. 29) near the Cretaceous/Tertiary boundary. The boundary itself may represent a slight hiatus and thus will be studied in greater detail onshore.

The sedimentation rates decreased steadily from a high of 1.2 cm/k.y. in the lower Paleocene (i.e., the interval between NP4 and NP3; Fig. 29) to a minimum of about 0.25 cm/k.y. for the Eocene interval. The higher Paleocene sedimentation rate may be responsible for the excellent preservation of middle and late Paleocene radiolarian faunas in Sections 122-761B-16X-3 to -19X-1. A long hiatus (12.9 m.y.) occurs between the upper Oligocene and middle Eocene, as determined by nannofossil and foraminifer zonal evidence.

Sedimentation rates for the Neogene sediments range from 0.7–0.28 cm/k.y., but average about 0.15 cm/k.y. Three hiatuses representing 0.5, 1.9, and 2.0 m.y. occur between the Pliocene and Miocene (Fig. 29). These hiatuses are substantiated by both calcareous nannofossil and foraminifer zonal evidence (see "Biostratigraphy," this chapter). The sedimentation rates for the Quaternary are about 1.2 cm/k.y., and probably reflect the high porosity and water content of the relatively uncompacted sediments.

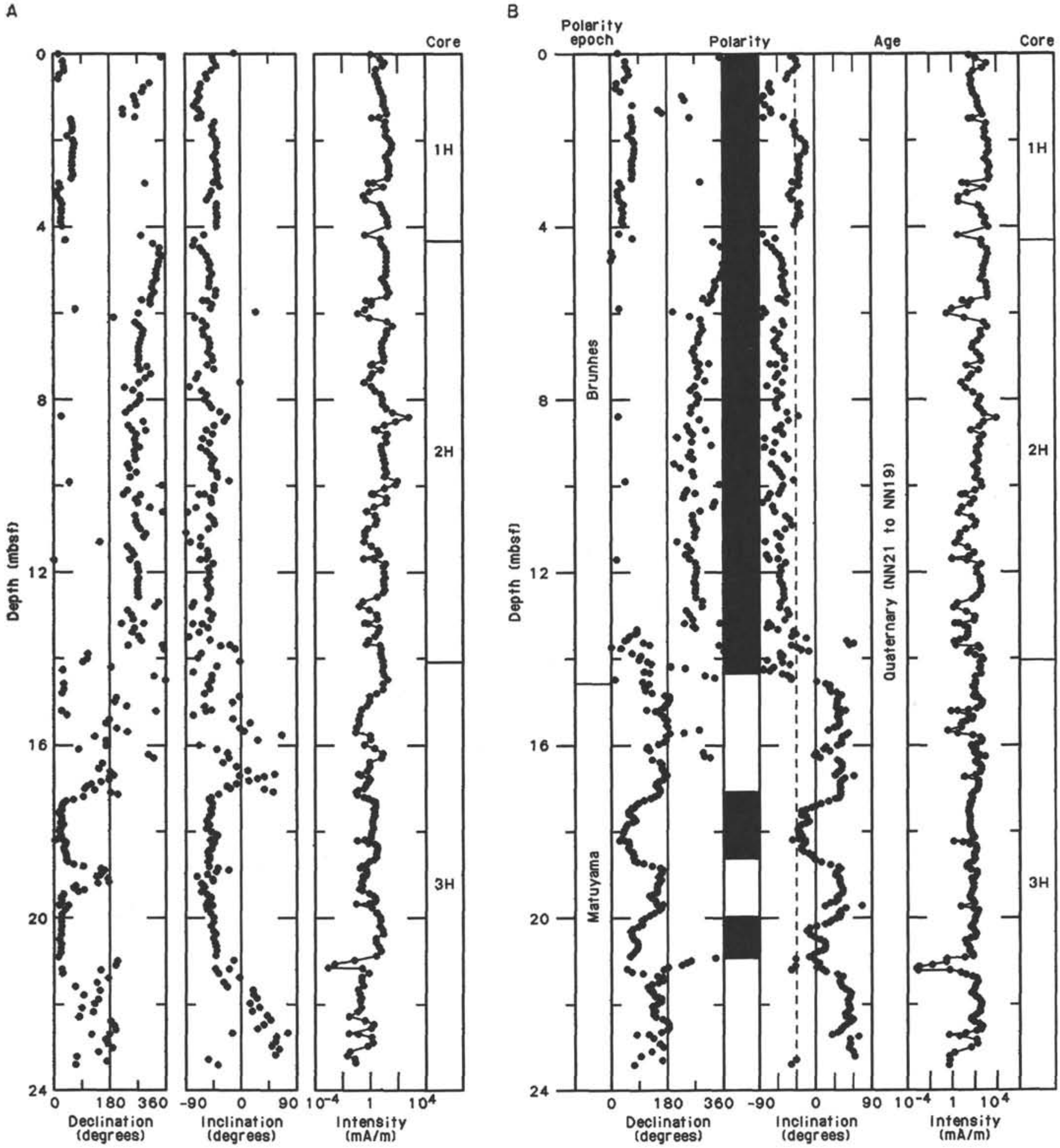

Figure 27. Declination, inclination, and intensity plot of magnetization. **A.** Before AF demagnetization at 9 mT. **B.** After 9-mT demagnetization. Black (white) corresponds to normal (reversed) polarity. Small circles represent declination and inclination of discrete samples. Dashed line indicates the expected inclination for the site.

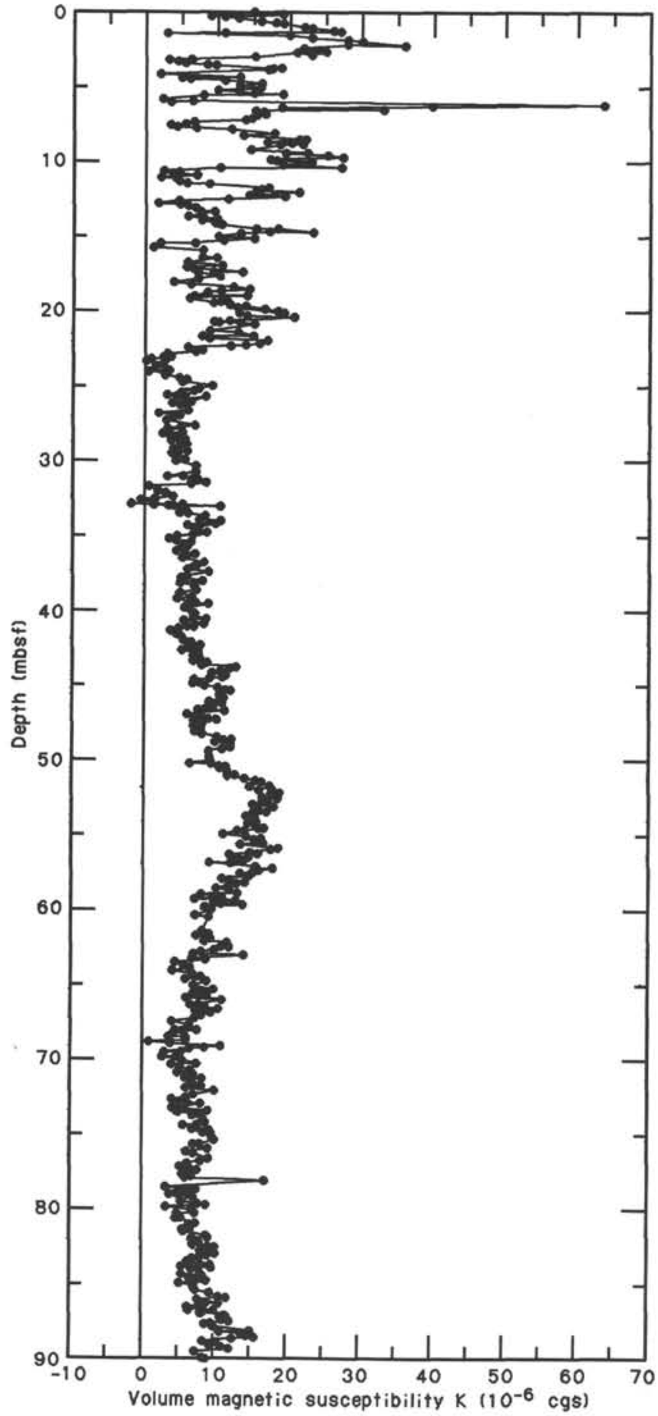

Figure 28. Whole-core-volume magnetic-susceptibility measurements plotted versus depth for Cores 122-761B-1H to -10X.

In summary, the sedimentation rates for the lower Upper Cretaceous were low, increasing in the upper upper Cretaceous and Paleogene to 2.0 cm/k.y. Neogene sediments correlate well with normal values for pelagic calcareous oozes.

ORGANIC GEOCHEMISTRY

Shipboard organic geochemical analyses at Site 761 consist of 84 determinations of inorganic carbon, 59 Rock-Eval and total organic carbon (TOC) analyses, and 58 measurements of low-molecular-weight hydrocarbons. The procedures used for these determinations are outlined in the "Explanatory Notes" (this volume) and are described in detail by Emeis and Kvenvolden (1986).

Inorganic and Organic Carbon

The results of the analyses of inorganic carbon in samples from Holes 761B and 761C are listed in Table 4. Included in this listing are percentages of calcium carbonate, calculated from the inorganic carbon percentages assuming that calcite is the only carbonate mineral present. Nearly all of the samples are rich in carbonate, reflecting the dominance of calcareous oozes in the Tertiary parts of these holes and of limestones in the Triassic portion of Hole 761C.

Percentages of organic carbon are given for selected samples. These values, determined on a whole-sediment basis, are generally less than 0.1% sediment dry weight. The calcareous oozes, rare chert samples, and many of the limestones contain little organic matter. Only the dark-colored limestones and the black claystones encountered near the bottom of Hole 761C have significant concentrations of organic carbon. Sample 122-761C-33R-2, 40–42 cm, for example, is a Norian black claystone that contains over 3% organic carbon.

Rock-Eval and TOC

Rock-Eval and TOC results of analyses of samples from Holes 761B and 761C are listed in Table 5. The very low (ca. <0.1%) concentrations of organic carbon and hence pyrolyzable material make most of the ratio calculations (e.g., hydrogen index, oxygen index, production index) undefined (i.e., almost zero divided by almost zero) and the absolute measured values of primary parameters (T_{max}, S_1, S_2, S_3, and TOC) subject to large errors because the instrument was operating at its level of sensitivity.

In the lower (Triassic) interval of Hole 761C, dark-colored limestones and claystones contain 0.4%–5% TOC. On the basis of the low hydrogen index values of these samples, their organic matter is interpreted to be type III (higher land plant) material, which probably came to this ocean-margin setting from nearby Australia at the time of sediment accumulation.

The level of thermal maturity is interpreted to be immature to marginally mature (equivalent to vitrinite reflectance levels of 0.4%–0.6%) on the basis of the analyses of a few samples from Section 122-761C-33R-2, which gave S_2 yields of >2 mg hydrocarbons/g rock.

Low-Molecular-Weight Hydrocarbons

Amounts of low-molecular-weight, gaseous hydrocarbons were monotonously low in samples from Holes 761B and 761C (Table 6). Methane concentrations usually were between 1 and 4 parts per million (ppm) of analyzed gas volumes, and ethane levels were generally below detection. In Cores 122-761C-30R to -33R gas amounts did increase, but only to 6 or 7 ppm. These cores contain Triassic dark-colored limestones and black claystones having 1%–5% TOC. Because gas concentrations roughly follow organic carbon concentrations in marine sediments (e.g., Schaefer and Leythaeuser, 1984), the low-molecular-weight hydrocarbons found in these Triassic rocks may be locally thermally generated from type III, land-plant organic matter therein. Even in the Triassic section of this site, the low amounts of gaseous hydrocarbons precluded calculation of C_1/C_2 ratios, unlike the Carnian section of nearby Site 760, where these ratios verified the thermogenic origin of the gases (see Site 760 chapter, this volume).

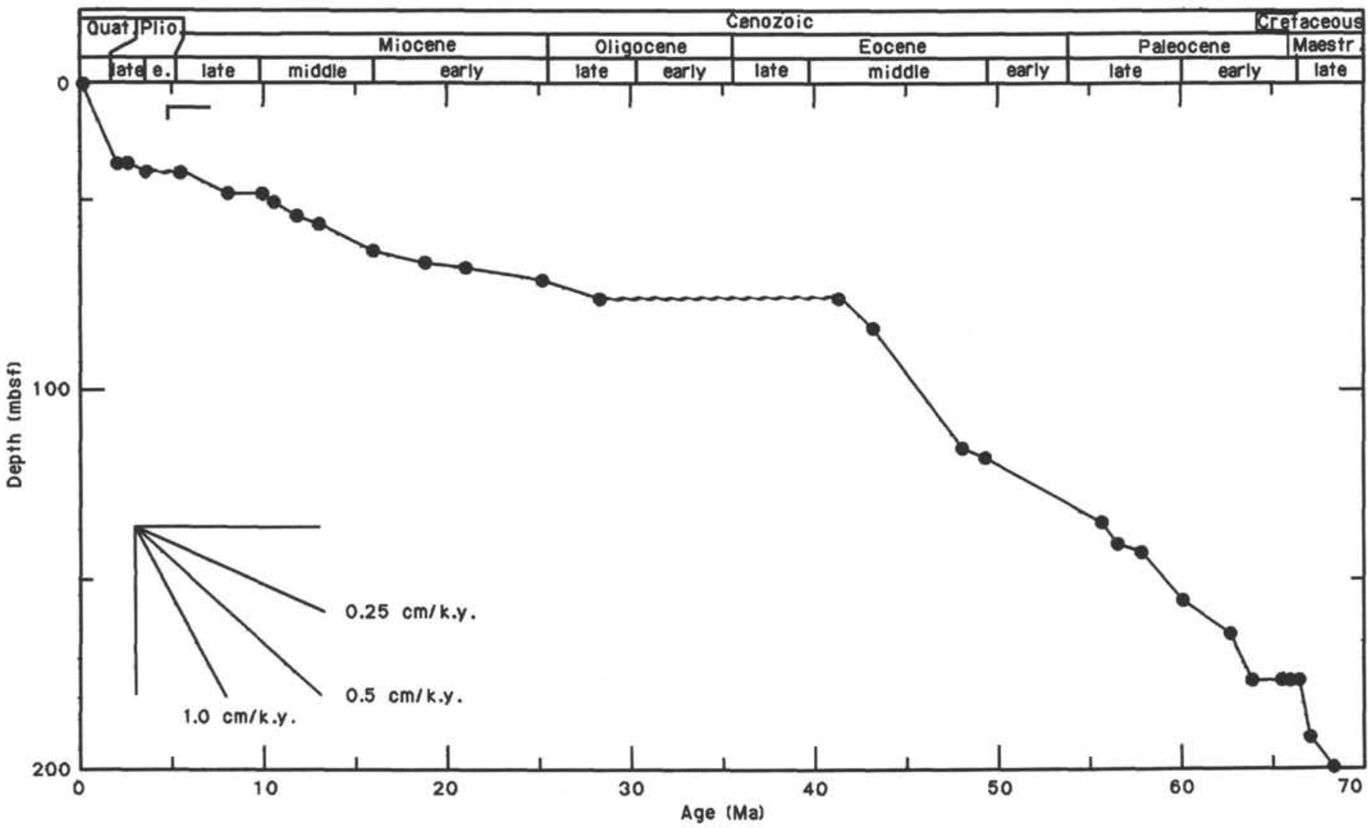

Figure 29. Graphic illustration of the sedimentation rates for the Cenozoic of Hole 761B. Hiatuses shown in wavy lines. Standard error bars for depth and age are shown at top left. See "Explanatory Notes," this volume, for a discussion of sedimentation-rate calculation methods.

INORGANIC GEOCHEMISTRY

Introduction

In addition to the normal sampling program, the detailed interstitial water sampling carried out in the first 100 m of Site 760 was continued at Site 761. Five- or 10-cm whole-round samples were taken, as warranted by the sediment recovery, squeezed, and analyzed as previously described (see "Explanatory Notes," this volume). Seventeen water samples were obtained, and only the lowermost (Samples 122-761C-26R-2, 140–150 cm and -31R-3, 140–150 cm) did not yield a sufficient volume of pore water to allow a complete set of analyses; hence alkalinity and pH were not determined on these samples. Surface seawater was also collected at Site 761 and used as a reference sample, although seawater from a few meters above the sediment/seawater interface would have been a more suitable reference.

Concentration gradients observed at Site 759 and Site 760 suggested that similar processes control the pore water chemistry in the upper 275 m of the sediments of each site. It was hoped that interstitial water sampling at Site 761 would provide complementary information to that obtained at the previous sites and further enhance our understanding of the seawater/sediment interactions taking place on the Wombat Plateau.

The restoration of regulated power allowed us to carry out X-ray diffraction (XRD) studies on selected samples, although the X-ray-fluorescence (XRF) instrument remained inoperative and thus no solid-phase chemical analyses were performed. Results of XRD analyses for all samples from the Wombat Plateau are combined and appear in the Site 759 report.

Interstitial Waters

Magnesium (Mg^{2+}) and Calcium (Ca^{2+})

In contrast to the decrease in Mg^{2+} observed immediately below the mudline at Sites 759 and 760, the Mg^{2+} concentration in the upper 100 m of Hole 761B exhibits no significant decrease, and ranges between 51.6 and 52.4 mM (Table 7 and Fig. 31). A slight gradient (−2.01 mM/100 m) is observed between 87.6 and 257.1 mbsf. The negligible concentration gradient in the uppermost 87.6 m and the weak negative gradient observed between 87.6 and 257.1 mbsf in Hole 761B (the average gradient = −1.46 mM/100 m over the entire interval) suggest that carbonate diagenesis has only taken place to a limited extent, or that diffusion processes through these unconsolidated oozes and chalks have smoothed out concentration gradients (Lasaga and Holland, 1976; Gieskes et al., 1982).

It is only in the lower portions of Hole 761C (where, unfortunately, only two samples were obtained) that large changes in Mg^{2+} occur. Between 257.1 and 412.6 mbsf the dissolved Mg^{2+} content decreases from 48.7 to 15.1 mM, which corresponds to a gradient of −21.6 mM/100 m. The actual location of the concentration drop observed within this depth interval is unknown, as no samples were obtained between 257.1 mbsf (Hole 761B) and 368.6 mbsf (Hole 761C) owing to the presence of lithified material. It is likely that a sharp decrease in Mg^{2+} occurs somewhere between the two samples, and that a reduced concentration gradient exists further downhole, as suggested by the two lowermost samples (−7.20 mM/100 m).

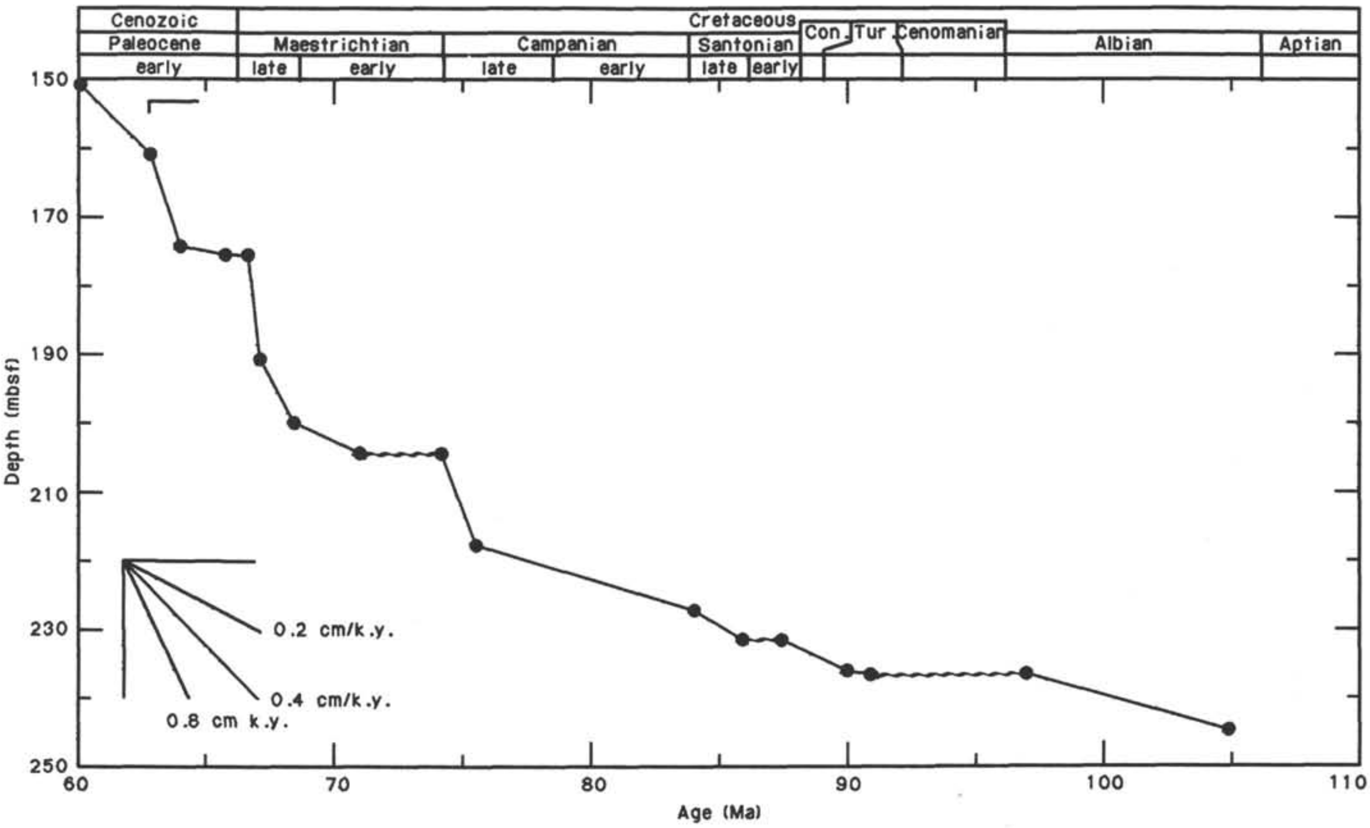

Figure 30. Sedimentation rates for the Cretaceous of Hole 761B. Hiatuses shown in wavy lines. Standard error bars for depth and age are shown at top left. See "Explanatory Notes," this volume, for a discussion of sedimentation-rate calculation methods.

The observed decrease in Mg^{2+} concentration below 257.1 mbsf corresponds to a change from the brown ferruginous sandstones (eupelagic condensed horizon) of Unit III, to the limestones of Unit IV (not sampled for interstitial water), to the dark, laminated, shallow-marine claystones of Subunits VA and VB (near 368.6 mbsf) (see "Lithostratigraphy," this chapter). Unfortunately, inadequate recovery from the deepest core (Core 122-761C-33R) in Unit VI precluded the whole-round sampling necessary to obtain interstitial water from this core, which contains nonmarine silty claystone with coal beds.

Dissolved Ca^{2+} exhibits a very small increase in concentration in the upper 230 m of Hole 761B (Fig. 31). The concentration gradient of 0.735 mM/100 m between 3.0 and 230.1 mbsf is approximately half the negative gradient observed for Mg^{2+} over the same depth interval. This suggests that a one-to-one exchange of these ions in calcite is not the only process responsible for the observed fluid composition. A decrease in Ca^{2+} between 230.1 and 257.1 mbsf is associated with a gradual change from eupelagic nannofossil chalk (Subunit IIB), to hemipelagic chalk (Subunit IIC), to brown ferruginous sandstone (Subunit III). Below 257.1 mbsf, the Ca^{2+} concentration increases again with a gradient of 2.85 mM/100 m. The gradient between the lowermost two samples is nearly twice that in overlying samples, but does not correspond to that necessary for a direct ion exchange of Ca^{2+} for Mg^{2+}.

Interstitial waters at Site 761 exhibit much smaller changes in the Mg^{2+}/Ca^{2+} ratio than at the previous two sites (Fig. 31). This is a direct result of the more subtle variations exhibited by each element at Site 761. A small decrease in the Mg^{2+}/Ca^{2+} ratio from a value approximately 10% less than seawater exists between 3.0 mbsf and 230.1 mbsf (4.76–3.96). A small increase in the ratio (to 4.33) is observed at 257.1 mbsf, overlying an interval in which values decrease (to 0.96) near the bottom of Hole 761C. The latter is of the same order as observed in Triassic sediments from Sites 759 and 760 and probably reflects similar geochemical processes.

Overall variations in Ca^{2+} and Mg^{2+} at Site 761 are much more subdued than those observed at the previous two sites, except in the lowermost portion of Hole 761C. It is likely that this reflects more subtle changes in lithology in the first 250 m of Site 761. Additionally, the highly porous nature of oozes and chalks could allow rapid diffusion, hence readily erase concentration gradients. Below 257.1 mbsf the Ca^{2+} and Mg^{2+} gradients are larger.

Sulfate (SO_4^{2-})

Examination of Table 6 reveals that SO_4^{2-} concentrations at Site 761 generally decrease slightly with depth, in a very narrow range of values between the normal seawater concentration of 28.9 mM (at 3.0 mbsf) and 26.1 mM (at 412.6 mbsf) in Hole 761C. The depth profile for SO_4^{2-} (Fig. 31) shows an alternating series of decreases and increases throughout the entire sedimentary sequence. Although the lowest SO_4^{2-} concentration was found in the deepest sample, it represents less than a 10% depletion of this constituent relative to normal seawater. This relatively small variation sharply contrasts with that observed in the sediments of Sites 759 and 760, where more than 80% of the SO_4^{2-} was removed from interstitial fluids in the lower parts of the holes. The absence of large variations at Site 761 suggests, as proposed above, that an extensive circulation of seawater and/or a lack of signifi-

Table 4. Concentrations of inorganic carbon, calcium carbonate, and total organic carbon (TOC) in samples from Holes 761B and 761C. Inorganic carbon concentrations were measured coulometrically. Calcium carbonate percentages were calculated assuming the carbonate contents to be pure calcite. TOC values were determined by Rock-Eval analysis. All percentages are on a whole sediment, dry-weight basis. Samples are listed according to sub-bottom depth.

Hole, core, section, interval (cm)	Depth (mbsf)	Inorganic carbon (%)	$CaCO_3$ (%)	TOC (%)	Lithology
761B-1H-2, 90–93	2.4	10.0	83.3	0.04	Nannofossil ooze
761B-1H-3, 58–60	3.6	9.9	82.8	na	Nannofossil ooze
761B-2H-1, 65–68	4.9	9.9	82.1	na	Nannofossil ooze
761B-2H-3, 75–78	8.0	9.6	80.1	0.09	Nannofossil ooze
761B-2H-5, 70–73	10.9	9.8	81.5	na	Nannofossil ooze
761B-3H-1, 70–73	14.4	9.5	78.8	na	Nannofossil ooze
761B-3H-2, 33–36	15.5	9.6	79.9	0.10	Nannofossil ooze
761B-3H-6, 66–69	21.9	9.3	77.5	na	Nannofossil ooze
761B-4H-2, 30–35	25.0	9.6	80.3	na	Nannofossil ooze
761B-4H-4, 80–84	28.5	10.5	87.3	0.04	Nannofossil ooze
761H-4H-7, 30–35	32.5	11.2	93.3	na	Nannofossil ooze
761B-5H-2, 103–105	33.7	10.0	83.7	na	Nannofossil ooze
761B-5H-4, 103–105	38.2	10.1	84.5	<0.01	Nannofossil ooze
761B-5H-6, 103–105	41.2	10.6	88.0	na	Nannofossil ooze
761B-6H-2, 85–87	44.8	10.1	84.5	na	Nannofossil ooze
761B-6H-4, 85–87	47.8	11.0	91.3	0.02	Nannofossil ooze
761B-6H-6, 85–87	50.8	9.6	79.8	na	Nannofossil ooze
761B-7H-4, 73–75	56.9	9.5	78.8	na	Nannofossil ooze
761B-7H-6, 73–75	59.7	10.3	86.1	<0.01	Nannofossil ooze
761B-8H-1, 90–92	62.1	10.6	88.0	na	Nannofossil ooze
761B-8H-2, 78–80	63.6	10.9	91.2	0.01	Nannofossil ooze
761B-8H-6, 20–23	68.9	11.2	93.2	na	Nannofossil ooze
761B-9H-2, 72–74	72.9	11.0	91.8	na	Nannofossil ooze
761B-9H-6, 94–96	79.1	11.0	91.8	0.01	Nannofossil ooze
761B-10H-2, 68–70	82.4	10.9	91.0	na	Nannofossil ooze
761B-10H-6, 68–70	88.4	10.7	88.8	0.01	Nannofossil ooze
761B-11X-1, 80–83	90.5	<0.1	<0.1	na	Chert
761B-11X-3, 86–88	94.6	10.7	89.2	<0.01	Nannofossil ooze
761B-14X-2, 85–90	103.1	10.8	90.0	0.01	Nannofossil ooze
761B-14X-4, 45–50	104.7	10.7	88.9	na	Nannofossil ooze
761B-16X-1, 114–115	23.8	10.5	87.5	<0.01	Nannofossil ooze
761B-16X-3, 117–118	126.9	10.2	85.0	na	Chalk
761B-17X-2, 14–16	133.3	10.1	84.3	na	Chalk
761B-17X-4, 21–23	136.9	10.3	86.0	0.01	Chalk
761B-17X-5, 73–75	138.9	10.1	84.0	na	Chalk
761B-18X-2, 11–13	143.3	10.1	84.5	na	Chalk
761B-18X-4, 37–39	146.6	10.1	84.5	<0.01	Chalk
761B-18X-6, 146–148	150.7	10.6	88.4	na	Chalk
761B-19X-2, 142–144	154.1	10.7	88.9	<0.01	Chalk
761B-19X-4, 146–150	157.2	10.3	85.9	na	Chalk
761C-2R-1, 44–47	160.7	9.8	81.2	na	Chalk
761B-20X-2, 69–70	162.9	8.3	69.1	0.06	Chalk
761B-21X-1, 25–28	170.5	9.3	77.0	0.01	Chalk
761B-22X-2, 130–132	182.5	10.5	87.4	na	Chalk
761B-22X-4, 111–113	185.3	10.6	87.9	0.05	Chalk
761B-22X-6, 40–42	190.6	10.8	89.7	na	Chalk
761B-23X-2, 110–112	191.8	10.7	89.3	<0.01	Chalk
761B-23X-4, 32–35	194.0	10.2	85.1	na	Chalk
761B-23X-4, 73–75	194.4	0.1	1.1	<0.01	Chert
761B-24X-2, 54–56	200.7	10.2	85.1	na	Chalk
761B-24X-4, 37–39	203.6	10.7	89.3	0.10	Chalk
761B-25X-2, 22–25	209.9	10.6	87.9	0.01	Chalk
761B-25X-4, 9–11	212.8	10.7	88.8	na	Chalk
761B-25X-4, 133–135	214.0	10.5	87.2	na	Chalk
761B-26X-1, 12–14	217.8	11.0	91.5	na	Chalk
761C-5R-1, 24–26	230.2	10.7	89.2	<0.01	Chalk
761C-5R-3, 24–26	233.2	10.2	84.8	na	Chalk
761C-6R-1, 59–61	235.6	10.1	84.1	0.02	Chalk
761B-28X-CC, 10–11	236.6	6.5	53.8	na	Orange chert
761C-7R-1, 60–63	240.6	<0.1	0.2	na	Gray claystone
761C-7R-2, 7–9	241.6	8.0	66.8	0.01	Calcareous sandstone
761B-29X-1, 38–41	245.1	9.6	79.6	na	White chalk
761C-9R-1, 24–27	250.3	0.8	6.2	<0.01	Chert
761C-9R-1, 145–147	251.5	1.5	12.2	0.08	Sandstone
761C-9R-2, 8–10	251.6	1.4	11.3	na	Claystone
761B-30X-2, 69–71	256.4	0.6	4.6	na	Brown sandstone
761C-10R-2, 4–6	256.5	0.4	3.1	0.13	Silty sandstone
761C-10R-2, 37–39	256.9	0.3	2.2	0.02	Silty sandstone
761C-12R-1, 70–71	265.2	11.8	98.6	<0.01	Limestone
761B-31X-CC, 34–35	273.1	11.8	98.5	na	Pink limestone

Table 4 (continued).

Hole, core, section, interval (cm)	Depth (mbsf)	Inorganic carbon (%)	$CaCO_3$ (%)	TOC (%)	Lithology
761C-15R-1, 23–27	279.7	11.8	98.6	na	Limestone
761B-32X-CC, 3–5	282.6	11.8	98.4	na	Pink limestone
761B-33X-CC, 26–28	286.6	11.3	93.8	0.03	Limestone
761C-23R-4, 48–52	342.2	9.8	81.2	0.14	Gray limestone
761C-24R-2, 27–28	348.5	4.0	33.1	0.78	Dark gray limestone
761C-25R-CC, 34–36	365.7	10.3	86.2	na	Dark gray limestone
761C-26R-2, 102–104	368.2	8.3	69.4	na	Dark gray mudstone
761C-26R-4, 144–147	371.7	10.9	90.5	na	Dark gray limestone
761C-30R-2, 98–100	401.2	2.3	19.2	0.94	Black claystone
761C-31R-2, 74–76	410.4	5.9	49.4	0.39	Calcareous silty claystone
761C-31R-4, 129–131	414.0	11.6	96.7	0.02	Calcareous silty claystone
761C-32R-2, 111–113	420.3	11.4	94.8	na	Gray limestone
761C-32R-3, 115–118	423.4	6.1	50.7	na	Gray sandstone
761C-33R-2, 40–42	429.1	0.2	1.4	3.02	Black claystone

Note: na = not analyzed.

cant oxidation of organic matter by SO_4^{2-} occurs in the sediments.

Silica (SiO_2)

The downhole SiO_2 concentrations at Site 761 range between 0.40 and 1.68 mM (Fig. 31), except for the extremely low surface seawater value (0.01 mM). However, surface seawater is a poor reference for silica because biological uptake almost always depletes this nutrient in the photic zone. In the first 12 m of the sediment a small increase in concentration (from 1.23 to 1.46 mM) is observed. A sharp decrease in SiO_2 (to 0.47 mM by 30.7 mbsf) is consistent with the disappearance of radiolarians from the sediments (see "Biostratigraphy," this chapter) resulting from early-diagenetic dissolution (Schrader, 1972); SiO_2 then remains nearly constant to 49.9 mbsf. Between 49.9 and 138.1 mbsf a significant gradient (1.38 mM/100 m) exists, with the maximum concentration for this site (1.68 mM) at 138.1 mbsf. The observed increase probably results from the dissolution of amorphous silica in this section of the sediments. It also corresponds to Subunits IB and IC and uppermost ID. In Subunit IC massive cherts occur (see "Lithostratigraphy," this chapter), indicating major SiO_2 mobilization from the dissolution of skeletal opal and the reprecipitation of authigenic silica.

Below 138.1 mbsf, SiO_2 decreases gradually (to 0.78 mM at 257.1 mbsf). A small increase is observed between 257.1 and 368.6 mbsf. As mentioned above it is difficult to interpret this increase because no data are available for this important limestone–calcareous claystone interval (Subunit VA; see "Lithostratigraphy," this chapter). The return to dark laminated claystone in Subunit VB is accompanied by a negative SiO_2 gradient that reflects silica incorporation into clay minerals (Kastner and Gieskes, 1976). The maintenance of SiO_2 gradients throughout Site 761 sediments reflects the local lithology and high reactivity of this constituent, as well as its relative insensitivity to diffusion processes (Gieskes, 1981). In addition, there is evidence from DSDP studies that high dissolved SiO_2 concentrations persist even after all skeletal opal-A has been dissolved and reprecipitated as opal-CT (Gieskes, 1981).

Salinity and Chlorinity

As noted for Mg^{2+} and Ca^{2+} (Fig. 31), the Cl^- content of Site 761 interstitial waters exhibits only small variations between 3.0 and 238.6 mbsf. A gradual rise is observed from the local surface seawater concentration of 550.8 mM to 563.6 at 40.2 mbsf. This trend appears to be paralleled by the salinity profile (Fig. 31), although the latter exhibits considerably more scatter associated with the use of the optical refractometer. A slight decrease in both Cl^- and salinity occurs from 40.2 to 165.1 mbsf, followed by a subtle increase to 230.1 mbsf. In this interval there is a much better agreement between the Cl^- and salinity profiles. The relatively significant drop exhibited by each of these parameters below 230.1 mbsf is reminiscent of that observed in the nonmarine Triassic sediments encountered at Sites 759 and 760. Overall, the decrease in salinity between 230.1 and 412.6 mbsf essentially reflects the variations in Cl^- and other major seawater constituents.

Alkalinity and pH

The alkalinity in sediments of Site 761 (Fig. 31) initially increases from the local surface seawater value of 2.61 mM to 3.87 mM at 21.2 mbsf. It then exhibits an alternating series of decreases and increases within a narrow range of 3.31 to 3.84 mM, down to 87.6 mbsf. At 138.1 mbsf a decreasing trend is observed, with the lowest alkalinity value (3.12 mM) occurring at 257.1 mbsf. An inverse relationship between SiO_2 and alkalinity appears to exist between 30.6 and 59.2 mbsf that suggests the occurrence of silica diagenesis, although the associated Ca^{2+} variations (Gieskes, 1981) are not as expected. Below 138.1 mbsf a steady decrease in alkalinity (Fig. 31) occurs down to 257.1 mbsf, mirrored by a steady increase in pH. The alkalinity change below 138.1 mbsf is paralleled by the SiO_2 content of the pore waters, suggesting a change in the chemistry of the sediments in this portion of Hole 761B. No alkalinity data are available for Hole 761C, where larger changes in the concentrations of many constituents occur.

Variations in the pH of Site 761 interstitial waters are slight (Fig. 31) and lie in the narrow range between 7.50 and 7.84. The pH of local surface seawater is 8.44, which is considerably higher than the highest value (7.84) observed downhole. The pH profile generally mirrors alkalinity, but exhibits less scatter in the shallow section of Hole 761B; two low values of 7.50 each occur between 68.6 and 78.2 mbsf. Exclusion of these two samples further narrows the downhole pH range (7.60–7.84).

X-Ray Diffraction Analysis (XRD)

Bulk XRD studies were performed on samples exhibiting significant morphological differences relative to the rest of the section or to complement available data. Three samples were initially selected from Hole 761C; the first two are pinkish-white clays found at the bottom of Core 122-761C-9R and the top of Core 122-761C-10R, just above laminated sands with abundant belemnites. These consist primarily of bentonitic/

Table 5. Rock-Eval data from Holes 761B and 761C. Total organic carbon (TOC) percentages are on a whole-sediment, dry-weight basis. Samples are listed according to sub-bottom depth.

Hole, core, section interval (cm)	Depth (mbsf)	Wt. (mg)	T_{max}	S_1	S_2	S_3	PI	S_2/S_3	PC	TOC	HI	OI	Lithology
761B-1H-2, 90–93	2.40	99.9	299	0.06	0.12	5.48	0.33	0.02	0.01	0.04	300	13700	
761B-2H-3, 75–79	7.95	101.3	350	0.07	0.19	2.26	0.27	0.08	0.02	0.09	211	2511	Soft ooze
761B-2H-5, 145–150	11.65	101.9	366	0.17	0.27	1.81	0.39	0.14	0.03	0.08	337	2262	
761B-3H-2, 33–36	15.53	100.6	367	0.06	0.28	2.08	0.18	0.13	0.02	0.10	280	2080	Soft ooze
761B-4H-4, 80–84	28.50	101.0	262	0.10	0.21	1.56	0.33	0.13	0.02	0.04	525	3900	Soft ooze
761B-5H-4, 103–105	38.23	100.8	299	0.14	0.22	1.73	0.39	0.12	0.00	0.00	3733	5766	
761B-6H-4, 85–87	47.75	100.7	249	0.01	0.00	1.10	0.00	0.00	0.00	0.02	0	5500	Soft ooze
761B-7H-6, 73–75	59.93	100.7	327	0.00	0.00	0.99	0.00	0.00	0.00	0.00	0	0	Soft ooze
761B-8H-2, 78–80	63.48	100.8	261	0.00	0.01	0.77	0.00	0.01	0.00	0.01	100	7700	Soft ooze
761B-8H-5, 145–150	68.65	102.1	305	0.00	0.07	0.45	0.00	0.15	0.00	0.02	350	2250	
761B-9H-5, 145–150	78.15	102.3	265	0.00	0.05	0.54	0.00	0.09	0.00	0.00	0	0	
761B-9H-6, 94–96	79.14	100.7	514	0.01	0.02	0.84	0.50	0.02	0.00	0.01	200	8400	
761B-10H-6, 68–70	88.38	101.7	413	0.02	0.14	0.87	0.12	0.16	0.01	0.01	140	8700	
761B-11X-3, 86–88	93.56	101.5	310	0.01	0.01	0.84	0.50	0.01	0.00	0.00	0	0	Ooze
761B-14X-2, 85–90	104.05	101.1	389	0.01	0.16	0.90	0.06	0.17	0.01	0.01	1600	9000	Ooze
761B-16X-1, 114–115	123.84	101.2	422	0.00	0.03	0.58	0.00	0.05	0.00	0.00	0	0	
761B-17X-4, 21–23	136.91	99.8	310	0.09	0.05	0.85	0.64	0.05	0.01	0.01	500	8500	
761B-18X-4, 37–39	146.57	100.6	338	0.01	0.01	0.83	0.50	0.01	0.00	0.00	0	0	Chalk
761B-19X-2, 142–144	154.12	101.4	272	0.01	0.03	0.75	0.25	0.04	0.00	0.00	0	0	Chalk
761B-20X-2, 69–79	162.89	100.9	275	0.00	0.00	1.30	0.00	0.00	0.00	0.06	0	2166	Chalk
761B-21X-1, 25–28	170.45	100.5	296	0.04	0.04	0.88	0.50	0.04	0.00	0.01	400	8800	Chalk
761B-22X-4, 111–113	185.31	100.8	250	0.00	0.01	0.66	0.00	0.01	0.00	0.05	20	1320	Chalk
761B-23X-2, 110–112	191.80	102.7	237	0.02	0.00	0.74	1.00	0.00	0.00	0.04	0	1850	Chalk
761B-23X-4, 73–75	194.43	100.2	340	0.00	0.04	0.18	0.00	0.22	0.00	0.00	0	0	White chalk
761B-23X-4, 140–150	195.10	103.1	378	0.01	0.00	0.64	0.00	0.00	0.00	0.02	0	3200	
761B-24X-4, 37–39	203.57	100.0	310	0.21	0.09	0.84	0.70	0.10	0.02	0.10	90	840	Chalk
761B-25X-2, 22–25	209.92	100.8	542	0.00	0.22	0.94	0.00	0.23	0.01	0.01	2200	9400	Chalk
761B-25X-3, 96–97	212.16	99.8	467	0.03	0.00	1.50	1.00	0.00	0.00	0.00	0	7500	
761B-25X-4, 140–150	214.10	102.1	477	0.01	0.63	0.20	0.02	3.15	0.05	0.51	123	39	
761B-27X-2, 140–150	230.10	102.8	310	0.01	0.02	0.63	0.50	0.03	0.00	0.00	0	0	
761C-5R-1, 24–26	230.24	101.5	445	0.00	0.00	0.84	0.00	0.00	0.00	0.00	0	0	White chalk
761C-6R-1, 59–61	235.59	100.6	446	0.00	0.00	0.94	0.00	0.00	0.00	0.02	0	4700	Mottled chalk
761C-7R-2, 7–9	241.57	101.8	363	0.01	0.00	1.35	0.00	0.00	0.00	0.01	0	13500	Calcareous sandstone
761C-9R-1, 24–27	250.24	100.5	226	0.00	0.00	0.39	0.00	0.00	0.00	0.00	0	0	Chert
761C-9R-1, 145–147	251.45	101.5	490	0.00	0.43	0.83	0.00	0.51	0.03	0.08	537	1037	
761C-10R-2, 4–6	256.54	101.4	366	0.21	0.83	0.63	0.20	1.31	0.08	0.13	638	484	Bioclastic sandstone
761C-10R-2, 37–39	256.87	101.6	481	0.00	0.26	0.26	0.00	1.00	0.02	0.02	1300	1300	Silty sandstone
761B-30X-2, 140–150	257.10	103.8	464	0.00	0.50	0.10	0.00	5.00	0.04	0.04	1250	250	
761C-12R-1, 70–71	265.20	101.8	451	0.00	0.00	0.29	0.00	0.00	0.00	0.00	0	0	Porous limestone
761B-33X-CC, 26–28	283.82	99.8	259	0.00	0.00	0.89	0.00	0.00	0.00	0.03	0	2966	Limestone
761C-23R-4, 48–52	342.18	101.6	267	0.00	0.00	0.80	0.00	0.00	0.00	0.14	0	571	Grey muddy carbonate
761C-24R-2, 27–29	348.47	101.4	407	0.04	0.28	1.94	0.12	0.14	0.02	0.78	35	248	Dark grey carbonate
761C-25R-1, 93–95	357.13	98.7	411	0.00	0.03	1.63	0.00	0.01	0.00	0.36	8	452	
761C-25R-CC, 34–36	357.90	99.9	304	0.01	0.01	0.56	0.50	0.01	0.00	0.09	11	622	Dark grey limestone
761C-26R-2, 113–115	368.33	101.2	313	0.00	0.01	0.60	0.00	0.01	0.00	0.47	2	127	
761C-26R-2, 140–150	368.60	100.3	391	0.08	0.18	1.18	0.31	0.15	0.02	0.45	40	262	
761C-27R-CC, 0–2	376.27	102.9	213	0.00	0.00	0.36	0.00	0.00	0.00	0.02	0	1800	
761C-29R-2, 0–2	390.70	104.1	217	0.00	0.00	0.21	0.00	0.00	0.00	0.00	0	0	
761C-30R-2, 98–100	401.18	100.9	432	0.04	0.16	1.79	0.20	0.08	0.01	0.94	17	190	Black laminated claystone
761C-30R-2, 113–115	401.33	100.6	415	0.01	0.17	2.00	0.06	0.08	0.01	0.85	20	235	
761C-31R-2, 74–76	410.44	100.9	328	0.00	0.01	1.04	0.00	0.00	0.00	0.39	2	266	Limestone/packstone
761C-31R-3, 140–150	412.60	100.2	304	0.00	0.00	1.08	0.00	0.00	0.00	0.39	0	276	
761C-31R-4, 0–2	412.70	101.7	341	0.00	0.06	1.28	0.00	0.04	0.00	0.50	12	256	
761C-32R-2, 111–113	420.31	99.9	226	0.00	0.00	0.79	0.00	0.00	0.00	0.02	0	3950	Grey limestone
761C-32R-2, 149–150	420.69	101.2	304	0.00	0.03	0.44	0.00	0.06	0.00	0.10	30	440	
761C-32R-3, 115–118	421.85	101.5	239	0.00	0.00	0.77	0.00	0.00	0.00	0.08	0	962	Grey calcareous sandstone
761C-33R-2, 0–2	428.70	102.5	429	0.01	2.40	2.86	0.00	0.83	0.20	4.75	50	60	
761C-33R-2, 0–2	428.70	100.6	425	0.04	2.78	2.80	0.01	0.99	0.23	4.91	56	57	
761C-33R-2, 40–42	429.10	99.8	437	0.03	2.40	3.08	0.01	0.77	0.20	3.02	79	101	Black organic claystone

smectitic clays. As no interstitial water was taken from Core 122-761C-33R, we performed XRD studies on the clay and coarse fractions of the sediment recovered in the core-catcher sample to characterize the environmental setting. Kaolinite (or chlorite) and illite dominate the clay fraction, with minor amounts of quartz and feldspar also present; however, without heat treatments we are unable to differentiate between chlorite and kaolinite. As anticipated, the coarse fraction of this sample is similar to the clay fraction, except that quartz and feldspar are more abundant than the clay minerals. The mineral phases encountered in this sample are characteristic of terrigenous material.

Restoration of regulated power later in the cruise (during the transit to Singapore) allowed further XRD studies; these are tabulated in the Site 759 chapter (this volume).

Conclusions

The chemistry of interstitial waters in the upper 250 m of Site 761 appears to be dominated by diffusion processes with all constituents except SiO_2 displaying weak concentration gradients. The concentration profile of silica, less affected by diffusion, reflects the local lithology and the diagenesis of opal-A. Below 257.1 mbsf, significant changes in the intersti-

Table 6. Concentrations of low-molecular-weight hydrocarbons of samples from Holes 761B and 761C. Analyses were done with the Carle gas chromatograph. Except where noted, data are from headspace samples. Concentrations are given in parts per million of headspace or vacutainer volume. Samples are listed according to sub-bottom depth.

Hole, core, section interval (cm)	Depth (mbsf)	C_1	C_2	C_1/C_2
761B-1H-3, 100–105	4.0	2	nd	—
761B-2H-6, 0–5	11.7	2	nd	—
761B-3H-6, 0–5	21.2	2	nd	—
761B-4H-6, 0–2	30.7	2	nd	—
761B-5H-6, 0–2	40.2	2	nd	—
761B-5H-6, 93–94[a]	41.1	3	nd	—
761B-6H-6, 0–2	49.7	2	nd	—
761B-7H-5, 143–145	59.1	2	nd	—
761B-7H-6, 20–21[a]	59.4	2	nd	—
761B-8H-6, 0–2	68.7	2	nd	—
761B-8H-6, 72–73[a]	69.4	2	nd	—
761B-9H-6, 0–2	78.2	2	nd	—
761B-10H-6, 0–2	87.7	2	nd	—
761B-11H-3, 0–2	92.7	2	nd	—
761B-14X-4, 0–5	100.2	2	nd	—
761B-16X-4, 145–150	128.7	2	nd	—
761B-17X-4, 123–125	137.9	2	nd	—
761B-18X-4, 145–150	147.7	2	nd	—
761B-19X-3, 148–150	155.7	3	nd	—
761C-2R-4, 0–2	164.7	4	nd	—
761B-20X-3, 123–125	164.9	2	nd	—
761C-3R-5, 0–2	175.7	3	nd	—
761B-21X-4, 148–150	176.2	2	nd	—
761B-22X-4, 145–150	185.7	2	nd	—
761B-23X-4, 113–115	194.8	2	nd	—
761B-24X-4, 0–2	203.2	1	nd	—
761B-25X-4, 0–2	212.7	2	nd	—
761B-26X-2, 0–2	219.2	2	nd	—
761B-27X-3, 0–2	230.3	2	nd	—
761B-27X-3, 18–19[a]	230.4	3	tr	—
761C-5R-2, 0–2	231.5	2	nd	—
761C-6R-1, 0–2	235.0	3	nd	—
761C-7R-2, 0–2	241.5	3	nd	—
761B-29X-2, 0–2	246.2	3	nd	—
761C-8R-2, 53–55	247.0	3	nd	—
761C-9R-2, 0–2	251.5	2	nd	—
761C-10R-1, 148–150	256.5	2	nd	—
761B-30X-3, 0–2	257.2	3	nd	—
761C-12R-1, 74–75	265.2	2	nd	—
761C-13R-1, 35–37	269.9	2	nd	—
761C-14R-1, 0–2	274.5	2	nd	—
761C-15R-1, 0–2	279.5	2	nd	—
761B-33X-1, 0–2	282.7	2	nd	—
761C-16R-1, 0–2	284.5	2	nd	—
761C-18R-1, 0–2	294.5	2	nd	—
761C-19R-1, 0–2	304.0	2	nd	—
761C-20R-2, 0–2	313.5	2	nd	—
761C-21R-CC, 0–2	332.5	2	nd	—
761C-24R-3, 0–2	349.7	4	nd	—
761C-25R-1, 93–95	357.1	4	nd	—
761C-26R-2, 113–115	368.8	3	nd	—
761C-27R-CC, 0–2	384.5	3	nd	—
761C-28R-1, 0–2	384.7	2	nd	—
761C-29R-2, 0–2	390.7	3	nd	—
761C-30R-2, 113–115	401.3	7	tr	—
761C-31R-4, 0–2	412.7	6	tr	—
761C-32R-2, 149–150	420.7	2	nd	—
761C-33R-2, 0–2	428.7	6	tr	—

Note: nd = not detectable; tr = trace.
[a] Vacutainer sample.

tial water chemistry occur that are reminiscent of those encountered in Triassic sediments of Sites 759 and 760.

PHYSICAL PROPERTIES

Introduction

Routine physical-property measurements on sediments from Site 761 include compressional wave velocity, velocity anisotropy, thermal conductivity, and the index properties (wet-bulk density, grain density, porosity, and water content; see "Explanatory Notes," this volume). Hole 761B was cored to 89.7 mbsf using the APC, and to 286.7 mbsf using the XCB. As core recovery and preservation were excellent throughout the APC interval, we were able to conduct all the routine physical-properties measurements. Below 89.7 mbsf, the core material became progressively firmer and recovery was more fragmentary. Only velocity and index-property measurements were taken below 149.93 mbsf. Coring was continued in Hole 761C (using the RCB) to a total depth of 436.7 mbsf. Few samples were measured below about 286 mbsf owing to poor core recovery. The values of the various physical properties are listed in Tables 8 and 9, and are plotted versus depth in Figures 32 to 34.

Sonic Velocity

The velocity versus depth data (Fig. 32) show two distinctive trends, separated by a minor interval between approximately 240 and 258 mbsf. The uppermost zone extends from the seafloor to about 240 mbsf, within which the average velocity increases (from about 1.53 km/s to 1.85 km/s), reflecting a typical compaction curve with depth. Three measurements taken from chert horizons at 90.5, 194.0, and 236.8 mbsf reveal prominent "faster" intervals (average velocities range from 2.37 km/s to 5.68 km/s).

An interval of lower velocities between 240 and 258 mbsf is attributed to the presence of clay-rich layers and unlithified bioclastic sandstone. Below 258 mbsf, the second major velocity trend displays a marked departure from the normal compaction trend shown in the uppermost zone. This is attributed to the first occurrence of lithified limestone at the top of the Triassic section. Velocities below 258 mbsf are variable (ranging from an average of 1.7 km/s in calcareous claystone to 5.0 km/s in bioclastic limestone). The variable trend of the velocity plot reflects the interbedded nature of these lithologies. Velocity anisotropy (Fig. 32) seems to be evenly distributed about zero, and shows no trend with depth.

Index Properties

The grain density of the sediment from Holes 761B and 761C (Fig. 32) is as expected for quartz- and calcite-dominated lithologies (2.6 to 2.8 g/cm^3). From the mudline to approximately 240 mbsf, the sediments from Holes 761B and 761C display properties typical of shallow marine sections undergoing compaction, wherein decreasing porosity and water content are matched by increasing bulk density (Fig. 32). A porosity decrease (from 72% at the mudline to about 50% at 240 mbsf) is matched by a decrease in the water content (from nearly 50% to 27%). The rate of decrease is most rapid in the uppermost 50 m of the section where the sediments consist of soft, unconsolidated oozes. The rate of decrease is slowest below the Cretaceous/Tertiary boundary interval, at about 174 mbsf. The latter trend reflects the transition from uncompacted oozes to more consolidated chalks. Similarly, the bulk density increases most rapidly in the top 50 m (values range from 1.49 g/cm^3 at the mudline to 1.73 g/cm^3 at 50 mbsf, and to 1.90 g/cm^3 at approximately 240 mbsf). Departures from these trends occur at chert intervals, as porosity and water

Table 7. Interstitial water composition, Site 761.

Core, section, interval (cm)	Depth (mbsf)	Vol. (cm^3)	pH	Alk. (mM)	Sal. (g/kg)	Mg^{2+} (mM)	Ca^{2+} (mM)	Mg^{2+}/Ca^{2+}	Cl^- (mM)	SO_4^{2-} (mM)	SiO_2 (mM)
Surface seawater	0.0		7.44	2.608	35.0	54.0	10.4	5.19	551	28.9	0.010
122-761B-											
1H-2, 145–150	3.0	55	7.79	3.631	35.8	52.4	11.0	4.76	553	28.9	1.226
2H-5, 145–150	11.7	50	7.62	3.661	35.6	52.4	11.0	4.77	555	29.0	1.455
3H-5, 145–150	21.2	50	7.62	3.870	35.6	52.0	11.2	4.63	559	29.2	1.097
4H-5, 145–150	30.7	45	7.63	3.575	36.3	52.0	11.1	4.67	560	28.2	0.468
5H-5, 145–150	40.2	40	7.59	3.397	35.4	52.2	11.2	4.64	564	28.4	0.519
6H-5, 145–150	49.2	42	7.60	3.689	36.1	51.6	11.4	4.53	562	28.6	0.463
7H-5, 145–150	59.2	30	7.66	3.584	35.5	51.7	11.3	4.57	559	27.3	0.610
8H-5, 145–150	68.7	25	7.50	3.844	35.5	51.7	11.3	4.56	558	27.4	0.810
9H-5, 145–150	78.2	30	7.50	3.314	35.5	51.9	11.5	4.51	558	27.2	1.164
10H-5, 145–150	87.7	40	7.70	3.589	35.7	52.1	11.9	4.37	558	28.1	1.218
17X-4, 140–150	138.1	50	7.72	3.700	35.5	50.5	12.4	4.06	555	27.3	1.683
20X-3, 140–150	165.1	50	7.69	3.572	35.6	49.3	12.5	3.94	554	26.4	1.409
23X-4, 140–150	195.1	45	7.64	3.420	35.8	49.3	12.5	3.93	556	27.2	1.405
27X-2, 140–150	230.1	53	7.68	3.347	35.5	50.3	12.7	3.96	562	27.9	1.172
30X-2, 140–150	257.1	30	7.84	3.119	35.5	48.7	11.2	4.34	555	27.6	0.776
122-761C-											
26R-2, 140–150	368.6	5			34.6	18.2	13.3	1.37	536	26.4	0.944
31C-3, 140–150	412.6	4			33.8	15.1	15.6	0.96	511	26.1	0.401

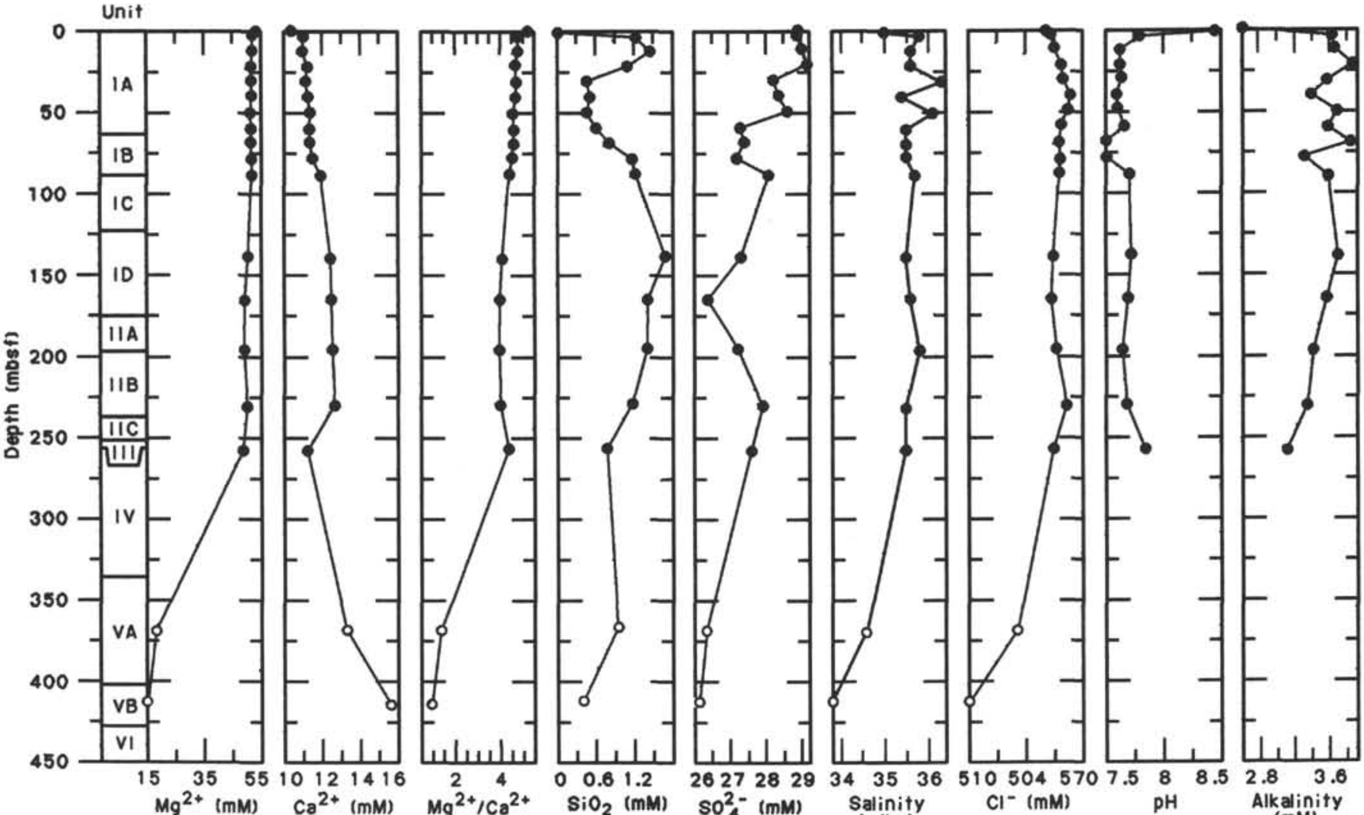

Figure 31. Summary of interstitial-water analyses, Site 761, as a function of depth. Solid circles = Hole 761B, open circles = Hole 761C.

content drop (to <2%) and the bulk density increases (to about 2.4 g/cm^3).

Highly variable index properties between 240 and 258 mbsf reflect a range of lithologies. Clay-rich layers within this interval are characterized by high porosity and water contents (averages = 65% and 40%, respectively), and low bulk densities (average = 1.65 g/cm^3). In contrast, the chert layers have lower porosity and water contents (<2.5%) and higher bulk density (1.84 g/cm^3). Unlithified bioclastic sandstones between 240 and 258 mbsf display intermediate porosity and water contents (average = 50% and 30%, respectively), with variable bulk densities (from 1.82 to 2.09 g/cm^3).

Below 258 mbsf there is a significant drop in the average porosity and water content (Fig. 32), reflecting the lithological change below the Triassic/Cretaceous boundary. There is a corresponding increase in bulk density, especially in the limestone horizons (values range from 2.12 to 2.64 g/cm^3). Mudstone interbeds within this section display slightly lower bulk densities (approximate average = 2.0 g/cm^3), whereas porosity and water content are generally higher (approximate averages = about 50% and 25%, respectively).

Thermal Conductivity

Thermal conductivity measurements (Table 9, Fig. 33) were only taken in sediments from Hole 761B down to 150 mbsf, as underlying material was too compacted for this type of analysis. The values display a general trend of increasing conductivity with depth (1.134 W/m·K just below the mudline to 1.566 W/m·K at 150 mbsf). This can be explained by the decrease in porosity and water content with depth (pore water is a relatively poor heat conductor).

Shear Strength

Shear-strength measurements (Fig. 33) were primarily made on APC cores, which have minimal sample disturbance, although some measurements were made on XCB cores from Hole 761B (down to 126.85 mbsf). Below this, the sediments were too firm to use the motorized shear-vane device.

Shear strengths over the measured section are highly variable, but between 2.46 and 56.93 mbsf there is a general increase in the values with depth, consistent with the increase in bulk density over this interval. A zone of decreased shear strength values between 56.93 and 78.88 mbsf correlates well with the undercompacted interval identified from velocity and index-property measurements. This reflects the close relationship between the porosity and shear strength of a sediment. Below 78.88 mbsf, the data points are widely scattered and are of little interpretive value, especially given the effects of drilling disturbance in XCB cores.

Formation Factor

Formation-factor measurements at Hole 761B were made down to a depth of 126.85 mbsf, and the results are shown in Figure 33. The increase in formation factor with depth is typical of a compacting sedimentary section and reflects the effect that decreasing porosity and water content have on the resistivity of the sediment. Marked increases in the formation factor at approximately 40 mbsf and 50 mbsf appear to correlate with an increase in the shear strength of the sediment, which is in turn the product of a slight decrease in the porosity and water content of the sediment.

GRAPE and *P*-wave Logger

GRAPE and *P*-wave-logging measurements were conducted on cores from Hole 761B down to a depth of 145 mbsf (Fig. 34). The GRAPE wet-bulk density estimates correlate well with the general trends established from index-property measurements.

Sonic velocity data from the *P*-wave logger appear to be less reliable than the bulk density results and display a large amount of scatter, especially compared with the Hamilton Frame sonic velocities. However, *P*-wave-velocity measurements reveal higher-velocity intervals that broadly correspond with chert horizons at about 65 and 90 mbsf.

Heat Flow

Two temperature-probe measurements were conducted in Hole 761B to check the equipment in preparation for Exmouth Plateau drilling, and to provide information for a comparison of the thermal properties of the Exmouth and Wombat plateaus. The measurements were performed at 32.7 and 89.7 mbsf while a calm sea state prevailed. At 32.7 mbsf, the probe stayed at the mudline for 5 min on both the ascent and descent, remaining on the bottom for 10 min. At 89.7 mbsf, the probe stayed at the mudline for 6–7 min on both the ascent and descent, and remained on the bottom for 12 min. The bottom temperature at 32.7 mbsf was 10.9°C, and at 89.7 mbsf was 5.6°C (Figs. 35A and 35B). The temperature value at 32.7 mbsf did not reach equilibrium, which indicated that the probe did not penetrate the sediment. The value at 89.7 mbsf appeared noisy, indicating that the probe was repeatedly inserted (Fig. 35B). However the probe cooled after each insertion to approximately the same temperature (5.6°C), and the value is regarded as acceptable. Assuming a mudline temperature of 2.8°C, a temperature gradient of 31.2°C/km can be determined for Site 761 (Fig. 36). Using thermal-conductivity measurements of 1.37 W/m·K averaged over the upper 89.7 m of Hole 761B, heat flow for the sediments can be calculated (Garland, 1979) as 42.8 mW/m^2. This value is comparable both with values from Jurassic-age ocean crust or cool, stable continental crust (Sclater et al. 1981).

Discussion

Physical-property measurements from Holes 761B and 761C display a good degree of correlation between the various index properties, and also with the lithologies identified from core material. Above approximately 240 mbsf, all the physical properties display characteristics generally typical of a marine sediment section undergoing compaction. Lithologically this uppermost section correlates well with Units I and II, which consist of white nannofossil ooze and white to pale brown nannofossil chalk, respectively. The Cretaceous/Tertiary boundary interval (approximately 174 mbsf) is not obviously discernible from the physical properties, although a slight change in the trend of the compaction curve above and below the boundary is inferred.

Between about 140 and 158 mbsf the occurrence of clay-rich layers within Subunit IIC, and ferruginous sandstone in Unit III, can be readily correlated with the physical-property measurements. For example, clay layers are characterized by very high porosities and water content, which probably reflects the water-retaining capabilities of expanding clays. The sandstone intervals are characterized by higher porosities and water contents than the overlying chalk and underlying limestone, as expected.

The marked change in the physical-property results below 258 mbsf correlates well with the Triassic/Cretaceous unconformity. Below this unconformity, lithified bioclastic limestone units are characterized by low porosities and water contents, with correspondingly high bulk densities. Calcareous claystones in this interval display higher porosities and lower densities. The unconformity can also be easily identified by the transition from the typically high velocity limestones in the Triassic to the slower overlying Cretaceous sediments.

SEISMIC STRATIGRAPHY

See "Seismic Stratigraphy," Site 764 chapter, for a combined report of Sites 759, 760, 761, and 764.

DOWNHOLE MEASUREMENTS

Operations

Hole conditioning of Hole 761C for well logging began at 1800 hr (all times given in local time) on 23 July 1988; 5.5 hr were spent. Cable and tool preparations commenced at 2330 hr, and the first tool string was in the pipe at 0120 hr, 24 July. This string contained the DIT-E, SDT, NGT, and the GPIT. At 0125 hr the computer crashed as a result of a telemetry overload. The GPIT was removed from the tool string and the run into the hole was begun at 0210 hr.

At 0255 hr the tools lost power and the tool string was run out of the hole. The problem was a shorted cable termination

Table 8. Physical-property data collected from Holes 761B and 761C.

Core, section, interval (cm)	Depth (mbsf)	V_{ph} (km/s)	V_{pv} (km/s)	Anisotropy (%)	Water content (%)	Porosity (%)	Wet-bulk density (g/cm^3)	Grain density (g/cm^3)	Shear strength (kPa)	Formation factor horizontal	Formation factor vertical
122-761B-											
1H-2, 96	2.46	1.660			49.80	72.4	1.49	2.58	4.5	2.33	
1H-3, 56	3.56	1.566			46.26	69.8	1.55	2.63	11.2		2.24
2H-1, 68	4.86	1.565			45.67	69.5	1.56	2.65	9.0	1.99	2.03
2H-3, 78	7.96	1.538			48.27	71.5	1.52	2.62	6.7	2.04	2.15
2H-5, 68	10.88	1.565			46.88	72.4	1.58	2.66	6.7	2.02	2.82
3H-1, 65	14.35	1.530			46.23	70.3	1.56	2.69	8.3		1.99
3H-2, 33	15.53	1.528			47.95	72.3	1.54	2.65	15.5		
3H-6, 70	21.88	1.558			45.03	69.9	1.59	2.59	11.0		
4H-2, 30	25.00	1.597			40.79	65.4	1.64	2.59	19.3		
4H-4, 80	28.50	1.612			37.56	63.3	1.73	2.65	10.6		
4H-7, 30	32.50	1.564			40.91	65.5	1.64	2.65	.70		
5H-2, 104	35.24	1.588			39.04	69.0	1.81	2.67	6.1	2.44	2.14
5H-4, 104	38.24	1.589			39.20	65.8	1.72	2.70	20.7	3.51	2.76
5H-6, 104	41.24	1.612			38.13	62.8	1.69	2.60	15.7	3.51	2.93
6H-2, 85	44.75	1.561			38.94	63.8	1.68	2.59	35.0	2.56	2.18
6H-4, 85	47.75	1.560			35.35	59.7	1.73	2.69	12.8	2.79	2.48
6H-6, 85	50.75	1.621			35.99	60.7	1.73	2.57	35.9	3.66	3.23
7H-2, 73	53.93	1.601			33.98	59.8	1.80	2.75	35.9	3.59	3.44
7H-4, 73	56.93	1.588			33.65	57.3	1.78	2.68	28.1	3.44	2.89
7H-6, 73	59.93	1.616			34.30	58.8	1.76	2.70	13.5	3.40	3.20
8H-1, 90	62.10	1.571			36.19	60.8	1.72	2.72	11.2	3.17	2.42
8H-2, 78	63.48	1.528			34.96	60.2	1.76	2.78	11.9	2.26	2.18
8H-4, 90	66.40	1.550			40.19	64.4	2.03	2.72	15.3	2.81	2.45
8H-5, 84	68.04	1.554			34.45	60.5	1.80	2.65	14.6	2.40	2.63
8H-6, 20	68.90	1.530			34.39	59.4	1.77	2.74		2.77	2.93
9H-2, 72	72.92	1.533			38.26	68.5	1.83	2.64	14.6	2.55	2.52
9H-4, 94	76.14	1.572			33.23	57.6	1.78	2.64	13.2	2.53	2.32
9H-6, 68	78.88	1.557			34.19	60.3	1.81	2.91	24.7	2.58	2.51
10H-2, 68	82.40	1.556			36.16	61.8	1.75	2.84	20.0	2.50	
10H-6, 63	88.30	1.756			32.95	68.9	2.14		33.7		
11X-1, 80	90.50	5.862			0.70	1.7	2.40				
11X-3, 85	93.55	1.583			32.32	57.8	1.83	2.75	53.9	2.90	
14X-2, 85	104.05	1.540			37.93	62.9	1.70	2.66	29.2	2.60	2.30
14X-4, 45	106.65	1.543			32.88	57.4	1.79	2.66	22.4	2.88	2.72
16X-1, 110	123.80	1.548			27.79	52.0	1.92	2.70	22.4		
16X-3, 115	126.85	1.650									
17X-2, 14	133.84	1.632	1.684	−3.136	32.03	56.1	1.79	2.71			
17X-4, 20	136.90	1.603	1.665	−3.794	32.65	56.3	1.77	2.66			
17X-5, 73	139.13	1.665	1.690	−1.490	31.96	55.5	1.78	2.66			
18X-2, 11	143.26	1.567			32.85	63.8	1.99	2.67			
18X-4, 37	146.57	1.564			32.59	57.8	1.82				
18X-6, 146	150.66	1.554			30.85	56.4	1.87	2.70			
19X-2, 142	154.12	1.673			26.34	51.7	2.01	2.71			
19X-4, 146	157.16	1.643			27.14	50.8	1.92	2.63			
20X-2, 69	162.89	2.133	2.131	0.094	25.88	47.8	1.89	2.56			
21X-1, 25	170.45	1.698	1.641	3.414	29.47	53.6	1.86	2.63			
22X-2, 130	182.50	1.766	1.797	−1.740	27.43	51.2	1.91	2.69			
22X-4, 111	185.31	1.711	1.730	−1.104	29.18	53.2	1.87	2.67			
22X-6, 41	187.61	1.716	1.732	−0.928	27.72	51.6	1.91	2.69			
23X-2, 110	191.80	1.654	1.680	−1.560	31.05	55.7	1.84	2.68			
23X-4, 32	194.02	3.533	3.911	−10.156	0.99	2.2	2.29				
23X-4, 73	194.43	1.775			26.04	48.5	1.91	2.67			
24X-2, 54	200.74	1.799	1.783	0.893	30.39	54.5	1.84	2.66			
24X-4, 37	203.57	1.843	1.853	−0.541	27.19	50.5	1.90	2.68			
25X-2, 22	209.92	1.752	1.760	−0.456	32.69	57.1	1.79	2.68			
25X-4, 9	212.79	1.924	1.895	1.519	32.11	56.8	1.81	2.64			
25X-4, 133	214.03	1.885			30.83	55.0	1.83	2.67			
26X-1, 12	217.82	1.667	1.670	−0.180	27.14	50.3	1.90	2.65			
26X-1, 40	218.10	1.683									
28X-CC, 10	236.80	2.374			23.34	42.9	1.88	2.45			
29X-1, 38	245.08	1.846			27.90	51.4	1.89	2.64			
30X-2, 67	256.37	1.708			25.12	47.9	1.95	2.66			
30X-3, 21	257.41	1.766									
31X-CC, 30	264.00	4.898	4.842	1.150	4.23	10.5	2.63	2.70			
32X-CC, 3	273.23	3.941	3.976	−0.884	9.04	22.3	2.52	2.73			
33X-CC, 23	282.93	5.044	4.945	1.982	2.42	6.5	2.73	2.68			
122-761C-											
2R-1, 44	160.64	1.803			28.90	53.40	1.89	2.68			
5R-1, 24	230.24	2.089	2.216	−5.900	21.84	42.80	2.01	2.73			
5R-3, 23	233.23	2.060	2.066	−0.291	21.50	42.00	2.00	2.69			
6R-1, 59	235.59	2.059	2.119	−2.872	22.21	43.30	2.00	2.71			
7R-1, 61	240.61	1.695	1.687	0.473	42.34	67.60	1.64				
7R-2, 8	241.58	2.023	2.125	−4.918	28.42	51.40	1.85	2.63			
8R-1, 25	245.25	1.919			26.57	49.30	1.90	2.66			
9R-1, 145	251.45	1.663	1.677	−0.838	15.99	32.70	2.09	2.60			
9R-1, 24	250.24	4.563			1.32	2.40	1.84	2.38			
9R-2, 8	251.58	1.714	1.689	1.469	39.40	64.40	1.67	2.59			
10R-1, 37	255.37	1.646									
10R-1, 83	255.83	1.713									
10R-1, 124	256.24	1.684									
10R-2, 4	256.54	1.655			34.10	60.40	1.82	2.78			

Table 8 (continued).

Core, section, interval (cm)	Depth (mbsf)	V_{ph} (km/s)	V_{pv} (km/s)	Anisotropy (%)	Water content (%)	Porosity (%)	Wet-bulk density (g/cm^3)	Grain density (g/cm^3)	Shear strength (kPa)	Formation factor horizontal	Formation factor vertical
10R-2, 20	256.70	1.678									
10R-2, 37	256.87				25.15	47.90	1.95	2.67			
12R-1, 70	265.20	4.069			11.16	26.40	2.43	2.76			
15R-1, 23	279.73	4.709			3.17	8.30	2.68	2.69			
23R-4, 48	342.18	3.233	3.212	0.652	6.48	15.60	2.46	2.67			
24R-2, 27	348.47	1.865	1.852	0.699	21.65	44.80	2.12	2.66			
25R-CC, 34	356.53	3.598			4.38	11.10	2.60	2.68			
26R-2, 100	368.20	2.799	3.055	−8.746	9.62	22.10	2.35	2.64			
26R-4, 145	371.65	4.345	4.452	−2.433	2.88	7.40	2.61	2.65			
30R-2, 97	401.17	1.826	1.743	4.651	25.56	50.20	2.01	2.65			
31R-2, 74	410.44	5.003	5.007	−0.080	14.73	30.60	2.12	2.70			
31R-4, 129	413.99		2.815		4.55	12.60	2.84	2.72			
32R-2, 111	420.31	4.796	5.163	−7.370	2.21	5.70	2.64	2.66			
32R-3, 114	421.84	3.377	3.000	11.824	11.34	26.20	2.37	2.74			
33R-2, 40	429.10	1.688			23.74	45.40	1.96	2.60			

Table 9. Thermal-conductivity data collected from Hole 761B.

Core, section, interval (cm)	Depth (mbsf)	Thermal/conductivity (W/m·K)
122-761B-		
1H-1, 90	0.90	0.967
1H-2, 65	2.15	1.134
1H-3, 65	3.65	1.198
2H-2, 75	6.45	1.184
2H-3, 75	7.95	1.193
2H-5, 75	10.95	1.183
2H-6, 75	12.45	1.177
3H-2, 40	15.60	1.209
3H-3, 40	17.10	1.241
3H-4, 60	18.80	1.179
3H-7, 40	23.10	1.283
6H-1, 50	42.90	1.361
6H-2, 50	44.40	1.390
6H-4, 50	47.40	1.477
6H-6, 50	50.40	1.341
7H-2, 81	54.01	1.331
7H-3, 80	55.50	1.534
7H-4, 68	56.88	1.474
7H-5, 68	58.38	1.500
8H-1, 70	61.90	1.423
8H-2, 70	63.40	1.472
8H-3, 70	64.90	1.491
8H-4, 70	66.40	1.442
9H-2, 70	72.90	1.475
9H-3, 70	74.40	1.526
9H-4, 70	75.90	1.516
9H-5, 70	77.40	1.559
9H-6, 70	78.90	1.514
10H-2, 70	82.40	1.422
10H-3, 70	83.90	1.212
10H-4, 70	85.40	1.503
10H-5, 70	86.90	1.416
11X-1, 65	90.36	1.415
11X-2, 70	91.90	1.455
11X-3, 70	93.40	1.765
14X-1, 50	102.20	1.423
14X-2, 50	103.70	1.412
14X-3, 50	105.20	1.557
14X-4, 50	106.70	2.026
17X-1, 55	132.75	1.453
17X-3, 59	135.79	1.379
17X-5, 65	138.85	1.518
17X-6, 67	140.37	1.402
18X-1, 75	142.45	1.497
18X-3, 69	145.39	1.517
18X-5, 54	148.24	1.566
18X-6, 73	149.93	1.566

caused by water invasion of the quick-connect junction on the bitter end of the logging cable. The cable was beheaded and a new termination made up by the Schlumberger engineer. The run into the hole recommenced at 0605 hr.

A bridge was encountered at approximately 260 mbsf. Several attempts were made to break through, but the obstruction remained solid. Logging up began at 0735 hr. The logging run ended at 0900 hr and the tool was brought out of the hole. It was decided that the chances of actually reaching the bottom of the hole were rather slim. As the geochemical tool can be run through the pipe we decided to use this tool. A wiper trip was started and the pipe was lowered to the bottom of the hole while the geochemical tool string was readied. The tool string was put in the pipe at 1315 hr. The neutron source for the GST failed at 1400 hr, and was changed by 1445 hr. Calibration of the GST at 100 mbsf began at 1455 hr. The tool was run to the bottom of the hole and logging up through pipe began at 1720 hr. Logging was finished at 2020 hr; the tool string was on the rig floor at 2110 hr.

Data Processing

The quality of the data was very good. The original data were smoothed using a 1-m running average calculated at 0.5-m intervals to produce the plots in this section. Smoothing of the data removes some of the abrupt spikes (relative maxima or minima). However, the resolution of the tools is on the order of 0.5–1.0 m owing to source-receiver spacing, so little true resolution is lost in the smoothing process.

Open-Hole Logging

The interval from 125 mbsf to 260 mbsf was logged in the open hole with the seismic-stratigraphic tool string. The profiles of total gamma ray count (SGR tool), deep induction resistivity (DIT-E tool), and sonic velocity (from the array seismic tool, or SDT) are presented in Figure 37. The logs are recorded primarily over an interval of pelagic ooze and chalk. The logs exhibit low gamma ray counts (10–15 API), low velocities (2.0–2.2 km/s), and low electrical resistivities (1–2 ohm-m). These values are a result of the high porosity and relative lack of cementation of the sediments. At approximately 170 mbsf, broad maxima in the gamma ray and resistivity logs indicate the position of the Cretaceous/Tertiary boundary interval. The increase in gamma-ray activity is related to the increased clay and zeolite content above the boundary. The increased resistivity above the Cretaceous/Tertiary boundary may be the result of zeolites in pore spaces that would otherwise act as a conductive link in the sediment microstructure; alternatively, it may result from resistive chert (or porcellanite) layers acting as partial insulators.

Above the base of the logged section there is an increase in gamma-ray flux and a small increase in electrical resistivity that suggest a clay-rich unit of slightly lower porosity than the pelagic sediment overlying the interval. At the very base of the interval (below 255 mbsf) gamma-ray counts and compres-

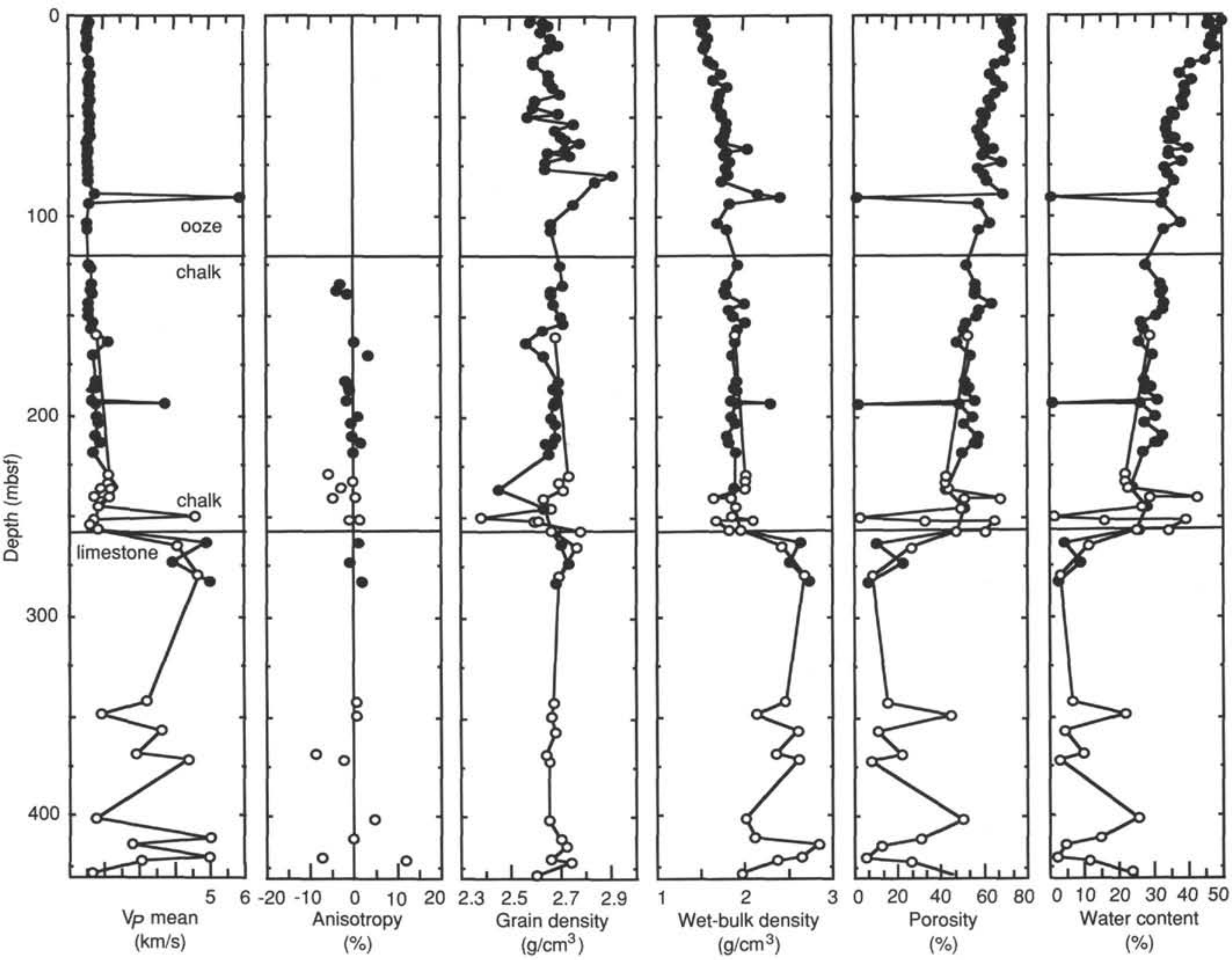

Figure 32. Physical-property data from Site 761 (mean compressional velocity from Hamilton Frame measurements, velocity anisotropy, grain density, wet-bulk density, porosity, and water content). Solid symbols = Hole 761B; open symbols = Hole 761C.

sional-wave velocity drop, which may indicate the silty sandstone that was cored in this interval (Core 122-761B-30X), while the resistivity increase at 265 mbsf probably represents the top of the shallow-water limestone unit observed at this level (Core 122-761B-31X).

Geochemical Logging Through the Drill Pipe

The Schlumberger geochemical logging string was run from 415 mbsf to approximately 75 mbsf. Owing to the poor hole condition, the tool was run through the drill pipe. The geochemical tools are not standard oilfield instruments and are still considered developmental in many applications. In addition, although they provide useful information when run through a steel drill string, the interpretation of the data is not routine and much of the following discussion is preliminary. Values of the respective elemental counts are discussed in relative abundance terms to highlight their qualitative nature.

Pipe Effects

The drill string within the borehole consists of normal drill pipe and a thickened section at the terminus called the bottom hole assembly (BHA). A schematic of the BHA alongside a profile of relative iron abundance is shown in Figure 38. The standard pipe (5.00-in. outer diameter, or OD; 4.13-in. inner diameter, or ID) at Hole 761C extended to 270 mbsf. Between 270 mbsf and 329.5 mbsf a slightly thicker-walled pipe was employed (5.5-in. OD). A 10.5-m-long section of 7.25-in. OD pipe joined the 5.5-in. section to an 8.25-in. OD segment that extended from 340 mbsf to the bottom of the pipe (415 mbsf). The presence of the BHA is seen in the iron record at 329.5 mbsf (Fig. 38) where the pipe OD increases to 7.25-in. The relative abundance of iron measured by the tool increases from near 10% to values greater than 25%. At shallower levels in the hole regular spikes, spaced approximately 10 m apart, are a response to the 7.25-in. OD pipe joints.

The geometry of the BHA in the borehole produces effects in other parameters measured by the geochemical logging string. Profiles of the relative abundances of chlorine and hydrogen are plotted in Figure 39 along with the total gamma ray log. Under open-hole conditions, chlorine and hydrogen respond primarily to the salinity of the borehole and pore fluid and to the porosity of the formation. At Site 761 it appears that the pore fluids did not differ significantly from seawater salinity, so changes in chlorine and hydrogen seen in the well log are results either of changes in the formation porosity or in the pipe and BHA geometry. Relative minima in hydrogen and

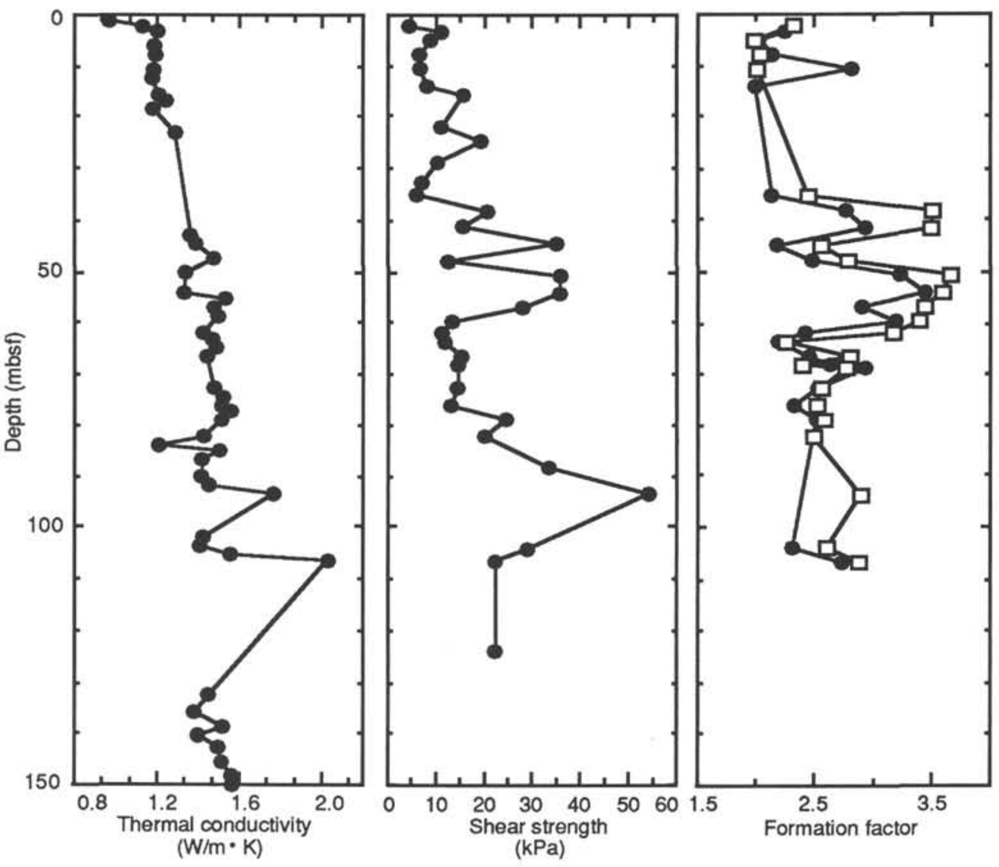

Figure 33. Physical-property data from Site 761 (thermal conductivity; shear strength; formation factor: open squares = horizontal measurements, perpendicular to the core axis and solid circles = vertical measurements, parallel to the core axis).

chlorine are seen in the upper parts of the log, where pipe joints have displaced borehole fluid with steel. These peaks coincide with the relative maxima of iron content seen in Figure 39. At approximately 260 mbsf there is a drop in both the chlorine and hydrogen relative abundances not related to any change in the size or geometry of the BHA. This is evidence for a drop in porosity in the formation below this level. This change corresponds to the appearance of shallow-water limestones and the Rhaetian/Cretaceous boundary.

Attenuation of natural gamma radiation (from the formation) is caused by the increased thickness of steel at the pipe joints. This results in relative minima in the gamma-ray log. A small local maximum at the Cretaceous/Tertiary boundary (measured through the pipe; see open-hole log discussion above) can be seen as well as a larger maximum between 230 to 260 mbsf. The record between 290 and 345 mbsf does not reflect natural radiation from the formation, but rather an interval of the drill pipe irradiated by the neutron source during a calibration procedure prior to the upward logging trip.

The effects of logging through the drill pipe with the geochemical string (e.g., changes in the relative abundances of iron, chlorine, and hydrogen in the well-logging record) are related to the displacement of water in the borehole by the steel in the pipe joints or the BHA. As pipe does not displace the formation, the abundance of elements not contained in either steel or seawater are relatively unaffected and their relative abundances can be compared without correction.

Calcium, Silicon, and Aluminum

Calcium exists in the sediments drilled at Site 761 mainly in the form of calcium carbonate, either as tests in pelagic oozes and chalks or in limestones and spar cement. This distribution is documented by the profile of relative calcium abundance in Figure 40. Calcium values remain fairly constant within the range of 0.10 to 0.15 in the oozes and the chalks from the top of the log to around 230 mbsf. A decrease in calcium is seen near the clay-rich zone and sand layer near 260 mbsf. Below the sand layer the calcium log clearly defines a long interval of high calcium abundance in which core recovery was limited to only a few meters of shallow-water limestones. The well-log data suggest that this interval is almost entirely limestone. Limestone layers with a few clay or sand stringers are also well defined by the calcium log between 348 and 405 mbsf.

The abundance of silicon in the formations penetrated at Site 761 is the result of three contributing factors: (1) biogenic silica in the form of opaline tests or reprecipitated as opal-CT in porcellanites, (2) terrigenous quartz grains, and (3) clays, which may come from a nearby source area or result from the diagenetic breakdown of volcanic ash. Aluminum in the sediments, however, probably resides predominantly in the clays, although it is present in other detrital grains such as feldspars and micas. Profiles of silicon and aluminum abundance and the ratio of Si to Al are plotted in Figure 41. There are several interesting observations to be made from these data. Both silicon and aluminum vary downhole, but their ratio remains relatively constant from the top of the logged

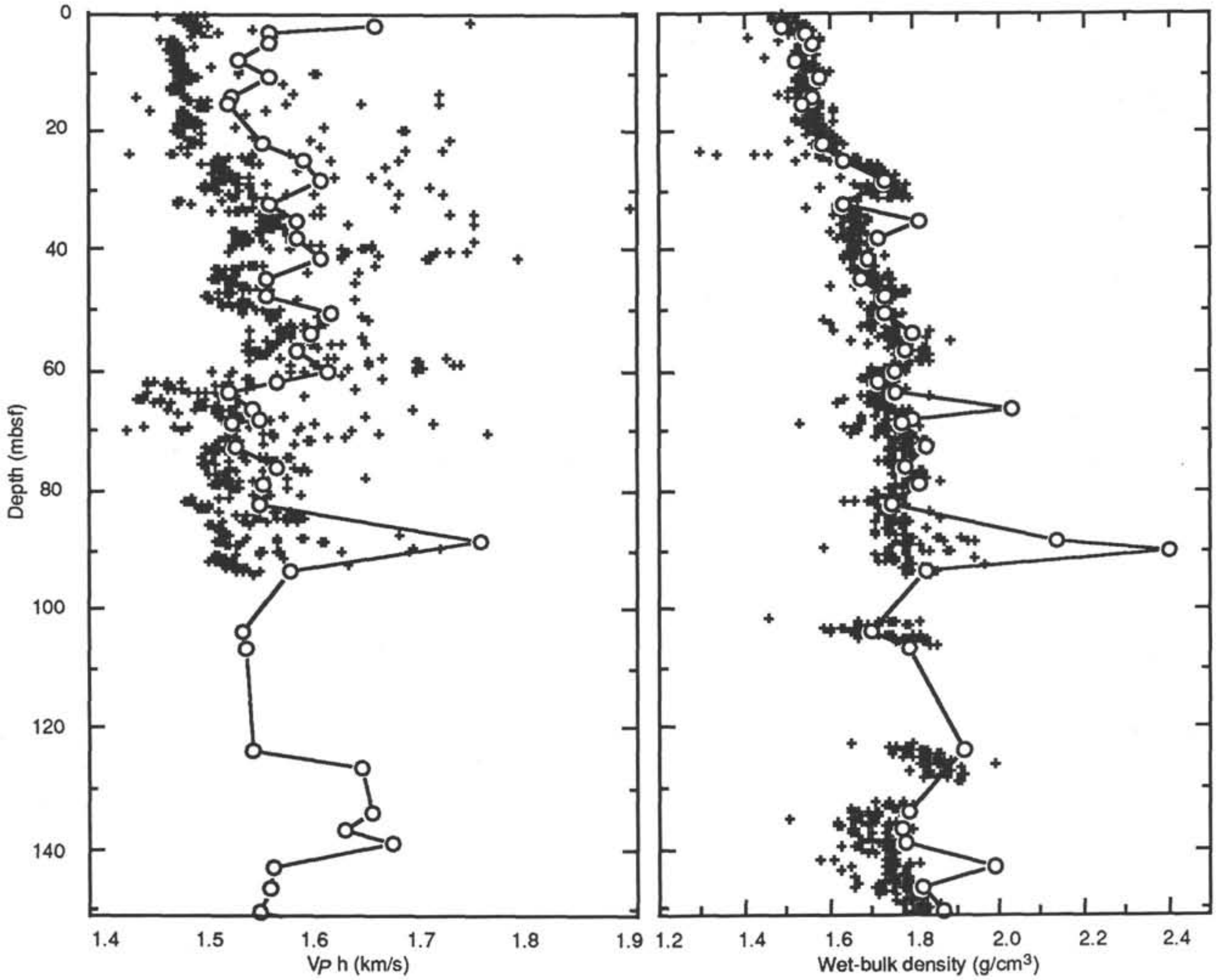

Figure 34. Physical-property data from Site 761 (velocity: crosses = *P*-wave logger data, open circles = Hamilton Frame values; wet-bulk density: crosses = GRAPE estimates, open circles = gravimetric measurements).

interval to approximately 340 mbsf. This constancy is impressive given the fact that the depth interval over which it occurs spans the pelagic oozes and chalks, the clay-rich zone around 250 mbsf, and the relatively pure carbonates between 260 and 340 mbsf. Since this ratio does not increase or decrease through the clay-rich zone, it appears that the major contributor to the silica signal above 340 mbsf is clay. The sand layer, several meters in thickness, which occurs at approximately 260 mbsf (Core 122-761B-30X) does not appear in the Si/Al record as a significant spike. This may be the result of poor tool resolution, or some other effect yet to be understood.

The mixed nature of the increase in the Si/Al ratio below 340 mbsf at Site 761 indicates that the mineralogy of silica-bearing rocks varies much more in the lower section of the hole than in the upper. Core description shows clastic input to be periodically significant in the lower section (see "Lithostratigraphy," this chapter). This suggests that peaks and troughs in the Si/Al ratio may be indicative of changes in the relative proportions of quartz and clay grains.

SUMMARY AND CONCLUSIONS

Introduction

Site 761 (proposed Site EP9E; 16°44.23'S, 115°32.10'E, water depth 2167.9 m) is located on the top of the central part of the Wombat Plateau, about 20 km north of Site 760 (Fig. 42). Hole 761B was continuously cored by APC to a depth of 89.7 mbsf, and by XCB to a total depth of 286.7 mbsf. Recovery in this hole was excellent in the uppermost 96 m, but varied from 0% to 102.4% between 96 mbsf and 286.7 m, owing to the presence of porcellanite layers (mainly between 96 and 123 m) and hard mid-Cretaceous lithologies (below 237 mbsf). Overall recovery of Hole 761B was 199.08 m, or 69.4%.

In Hole 761C we washed down to 160.2 mbsf, recored the Cretaceous/Tertiary boundary (160.2–179.2 mbsf), and then washed down to 230 mbsf to recore the interval poorly recovered in Hole 761B (between 230 and 286.7 mbsf). Below this depth the hole penetrated upper Triassic rocks, to a total depth of 436.7 mbsf. Recovery in the alternating hard and soft Triassic lithologies was very poor (usually below 20%, often below 10%). The total recovery of Hole 761C was only 72.14 m, or 32% of the 225.7 m cored. Once again, this underscores the pressing need to develop better tools for recovering alternating hard and soft lithologies. To obtain information in the poorly recovered intervals, special care was taken to condition the hole for logging. However, bridging prevented open-hole logging below 260 mbsf; we therefore decided to log through the pipe with the geochemical tool.

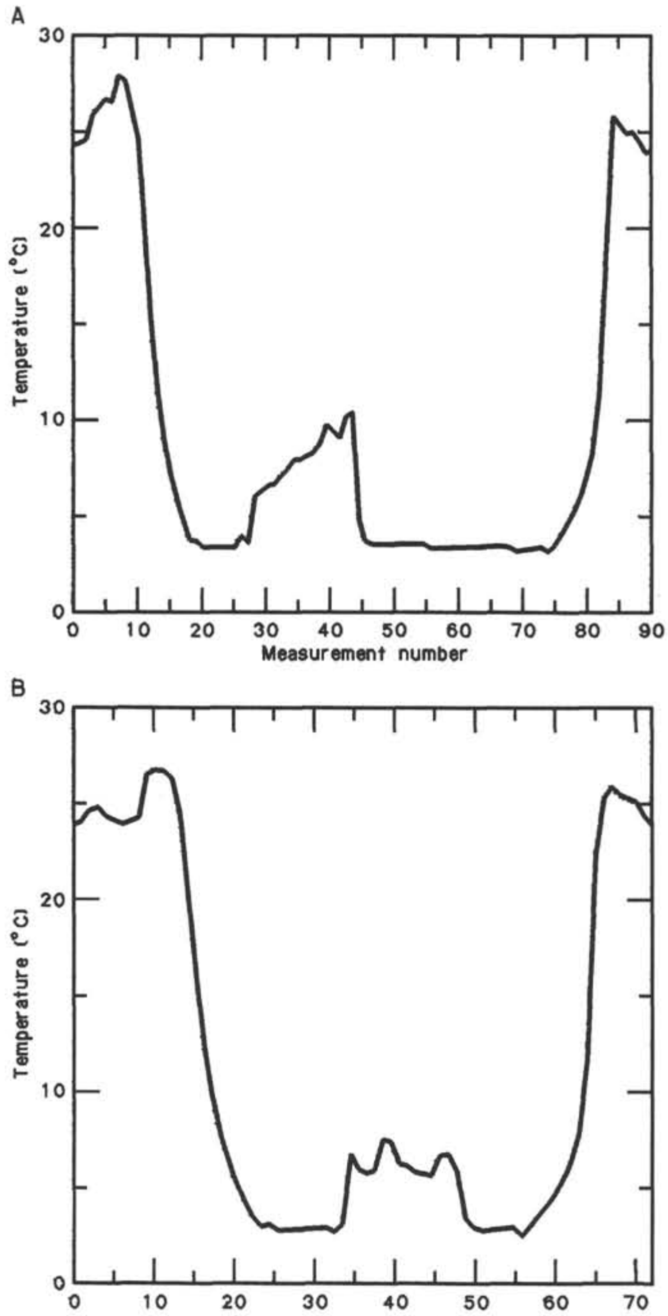

Figure 35. Temperature-versus-time records obtained with the temperature probe in Hole 761B. **A.** 32.7 mbsf. **B.** 89.7 mbsf.

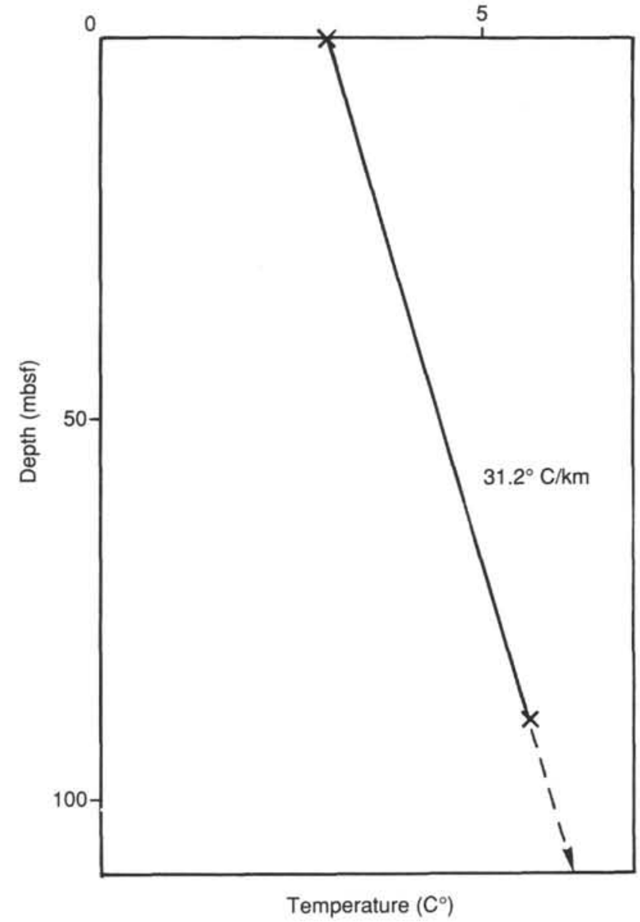

Figure 36. Temperature gradient in Hole 761B.

The objectives of Site 761 were similar to those of Site 760, with the additional objectives being (1) to retrieve a more complete Tertiary to mid-Cretaceous section and thus date the late Mesozoic-Cenozoic reflectors, and (2) to retrieve a younger Mesozoic (possibly Rhaetian and younger) stratigraphic section (Fig. 42).

Drilling at Site 761 provided us with several important discoveries, especially a possibly complete Cretaceous/Tertiary boundary interval, a condensed and low-sedimentation-rate lower Cretaceous post-rift sequence, and a nearly complete marine Rhaetian syn-rift sequence. As this site did not contain the anticipated Jurassic record below the main post-rift unconformity, we decided to address this objective at proposed Site EP9F (Site 764, northern rim of Wombat Plateau, Fig. 42).

Stratigraphy, Paleoenvironment and Sedimentary History

The stratigraphic results of Site 761 and some tentative paleoenvironmental interpretations are summarized in Figure 2C, "Summary and Highlights" chapter, this volume (in back pocket). We will discuss the most important discoveries in stratigraphic order (for a more detailed treatment, see "Lithostratigraphy," this chapter).

Norian Deltaic Sedimentation (Unit VI, 436.7–422.4 mbsf)

The Norian, at the base of Site 761, is characterized by black, more or less laminated, carbonaceous claystones with pyrite nodules and coal seams. This lithology resembles the coeval paralic sediments described from Site 760 (see "Summary and Conclusions," Site 760 chapter, this volume). We envisage a paralic (marginal marine to deltaic/coal swamp) environment with limited bottom-water circulation for this sequence.

(Early) Rhaetian Open-Shelf Limestone/Calcareous Claystone Deposition (Unit V, 422.4–338.3 mbsf)

The contact of the paralic claystone (Unit VI) with the overlying dark, laminated marine claystones and crinoidal limestones of (Subunit VB, early Rhaetian) is abrupt and marked by an intraclastic floatstone at the base. This contact appears to be a sequence boundary, documenting a sea-level

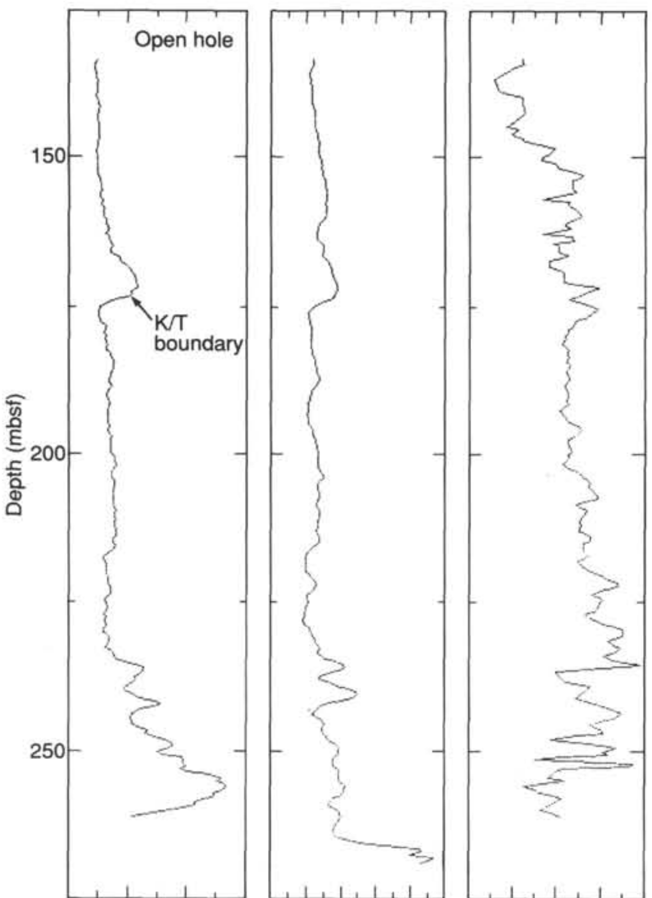

Figure 37. Open-hole logs of gamma-radiation, electrical resistivity, and compressional wave velocity recorded at Site 761 by the seismic-stratigraphic tool string. Data have been smoothed using a 1.0-m running average calculated at 0.5-m intervals.

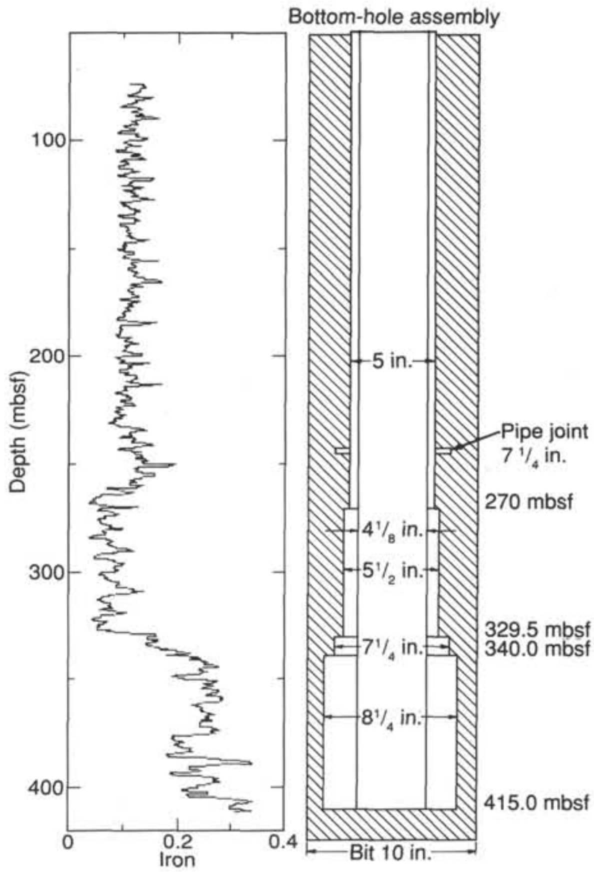

Figure 38. Relative abundance of elemental iron recorded through the drill pipe at Site 761 by the geochemical tool string. Alongside the well-log data is a schematic of the pipe and bottom-hole assembly (BHA). Data have been smoothed using a 1.0-m running average calculated at 0.5-m intervals. Vertical scales are the same.

lowstand, followed by a slow sea-level rise (transgression) that initiated the Rhaetian eustatic cycle (Haq et al., 1987). These overlying black claystones are rich in coccoliths, and hence fully marine. The claystones are also rich in ostracodes. The origin of the interbedded crinoidal limestones is not clear. They might indicate an open-marine, comparatively deep-water environment or, alternatively, a shallow-water subtidal environment. Most Alpine Jurassic crinoidal sediments are essentially of tidal origin (i.e., contain features such as giant ripples). Today, however, crinoid colonies live in the lower photic zone, and if displaced by turbidity currents or slumps, could be deposited in an even deeper setting. We observed sharp erosive lower contacts and grading in some crinoidal limestones, which might suggest a turbiditic origin. An alternative interpretation is that the crinoidal limestones are storm deposits (tempestites) formed in a shallow-water environment. This matter will be pursued in shore-based studies.

A pebbly mudstone (containing coarse quartz and one fragment of reworked ooid grainstone with crinoids) at the base of Subunit VB is a puzzling feature (Fig. 22B). Two working hypotheses concerning this lithology were developed by the sedimentologists, and will be investigated by further shore-based work.

1. Deeper-water origin by mass wasting: the sequence boundary between Units VI and V may be a hiatus, during which the Wombat Plateau experienced block faulting, followed by rapid subsidence and syn-depositional erosion of the higher blocks, with mass flows or slumps into the moderate shelf depths of the lower blocks.

2. The sequence boundary between Units IV and V may be a time gap: deposits overlying this contact, including abundant quartz (commonly observed just above a coastal onlap), may not be the very first shallow-shelf-wedge deposits of the lowstand system track, but are instead reworked quartz grains from underlying siliciclastic formations. These are represented by the pebble of ooid grainstone, which is reworked just above the sequence boundary and which does not belong to the underlying Norian sequence.

In general, sedimentation of the lower Rhaetian Subunit VB was characterized by a considerable terrigenous influx and probably greater water depths than the overlying upper Rhaetian Subunit VA. On the basis of logging results, the siliciclastic portion of Subunit VB contains upward-fining cycles that might indicate delta-plain flooding. As deposition of this subunit ceased, we assume a situation of open-marine shelf-margin conditions (i.e., the strandline having moved considerably landward during a sea-level rise).

The overlying Subunit VA is characterized by less-siliciclastic material and by shallow-subtidal water depths, proba-

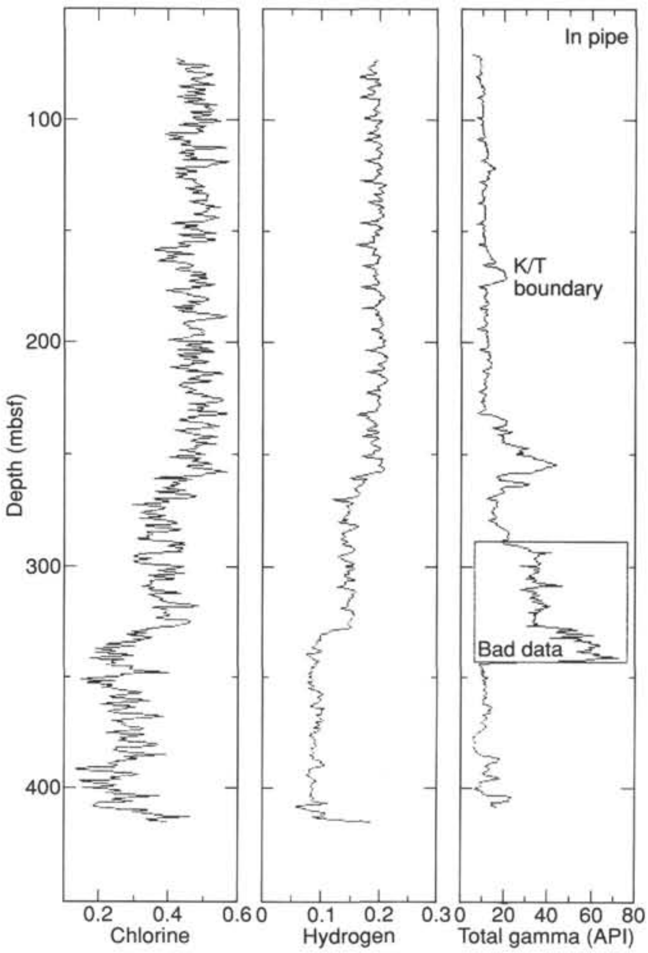

Figure 39. Well-log profiles, recorded using the geochemical tool string at Site 761. Data have been smoothed using a 1.0-m running average calculated at 0.5-m intervals. Relative abundances of chlorine and hydrogen, and the total gamma ray flux. The effect of the BHA can be seen below 330 mbsf. Bad gamma-ray data are the result of pipe irradiation during tool calibration prior to logging.

bly on the order of a few tens of meters (i.e., photic zone), judging from the presence of red algae and hermatypic corals. Two of the five lithofacies types in this unit (detailed in "Lithostratigraphy," this chapter) are rhythmically interlayered: (1) black, laminated to massive silty claystone to calcareous claystone (marlstone/limestone), and (2) calcareous, bioturbated, mollusk-rich mudstone (to wackestone).

In general, conspicuous claystone/limestone cycles can be explained by (1) cyclic changes of clay input into the basin ("dilution"), (2) changes in fertility and carbonate productivity, (3) fluctuations of carbonate dissolution, or (4) a combination of these factors (Ogg et al., 1987). At present, we favor "dilution cycles" (fluctuations of clay input). Ultimately, all mentioned causes may be linked to orbital forcing.

The limestones of Subunit VA generally contain a mollusk-coralline-algal association, whereas the crinoids and ostracodes are mostly associated with the black-claystone facies. Carbonate grainstones to packstones contain a microreefal association of red coralline algae and corals. Especially noteworthy are thalli of red algae ("rhodoliths") in life position within the mudstone. Some limestone types are dolomitized.

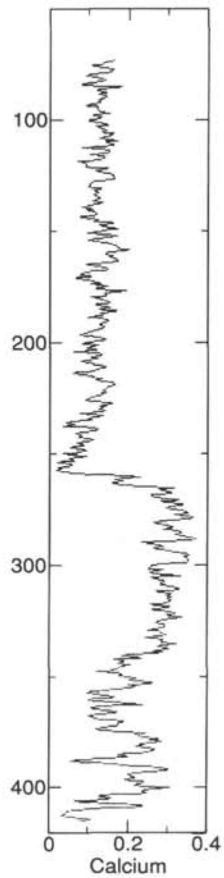

Figure 40. Profile of the relative abundance of elemental calcium, recorded with the geochemical tool string at Site 761. A massive limestone unit extends from 260 to 340 msbf.

The Rhaetian Shallow-Water Carbonate Platform (Unit IV, 338.3–259.5 mbsf)

Above 338 mbsf, Unit IV (upper Rhaetian) is made up of 78.8 m of white to very pale brown, neritic limestones that were deposited in very shallow-subtidal, intertidal, or even supratidal settings. Further studies will address the question of whether the upward shallowing between Units V and IV resulted from continued carbonate buildup (equaling or exceeding subsidence), slow sea-level drop, tectonic uplift, or a combination of these causes. Within Unit IV, an upward-shallowing (regressive) trend is recognized. This is inferred from our observation that the lower part of the unit (Cores 122-761C-23R to -17R) is dominated by wackestones and packstones with hermatypic, branching corals, etc., that indicate a protected low-energy lagoonal setting, whereas well-sorted, ooid-foraminiferal grainstones (occasionally also with peloids), algal mats, and megalodonts prevail in the upper part (Cores 122-761C-16R to -12R) and indicate a peri-reefal, intertidal setting with sporadic supratidal exposure (Fig. 42). The following important carbonate microfacies types are differentiated in this unit (see also "Lithostratigraphy," this chapter):

1. algal mats with stromatolitic lamination, birdseye structures, and *Stromatactis*-type vugs, attesting to periodic, subaerial desiccation and a tropical tidal-flat environment;

2. skeletal wackestones and packstones, partly dolomitized and rich in mollusks, green algae (dasycladaceans), echinoderm fragments, hermatypic corals, and *Megalodon*, a

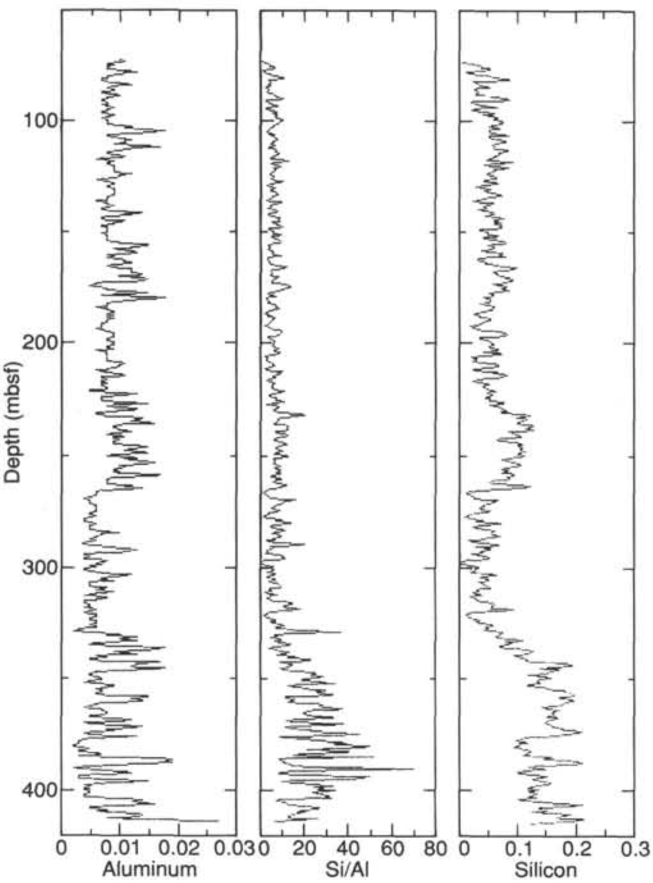

Figure 41. Profiles of the relative abundances of aluminum and silicon and the ratio of silicon to aluminum, recorded with the geochemical tool string at Site 761. Note that the Si/Al ratio remains relatively constant throughout most of the hole although there are fluctuations in the relative amounts of each.

very common, thick-shelled, large pelecypod in upper Triassic Tethys limestones around the world (e.g., in the lagoonal Lofer cycles of the Dachsteinkalk of the northern Calcareous Alps);

3. skeletal peloidal packstones to grainstones with crinoids and foraminifers (patchy dolomitization); and

4. well-sorted ooid-foraminiferal grainstones with the benthic foraminifer *Triasina hantkeni* and birdseye structures (which variably contain neomorphosed calcite or are dolomitized).

The *Megalodon* shells suggest a lagoonal setting; the hermatypic corals and sponges are associated with wacke- to packstones. Here, *Triasina hantkeni* might be more typical of a high-energy (grainstone) environment, although it also occurs in quiet-water (micritic) settings below wave base, close to a reef (Schott, 1983). Therefore, we favor a shallow-subtidal (lagoonal) setting for most of the upper Rhaetian microfacies types rather than a bank-edge (patch reef) environment. The ooids suggest a local Bahamas-type ooid shoal environment (unless they were reworked).

The association of green algae (dasycladaceans) with hermatypic corals suggests a low-latitude tropical environment of the southeast Tethys Sea ("Chlorozoan-association"), as compared to the more temperate (subtropical?) "foramol-association," described from the Carnian-Norian section at Sites 759 and 760.

The Post-Rhaetian/Pre-Berriasian Unconformity

A hiatus up to 70 m.y. long exists at the major pre-Berriasian "post-rift" unconformity at Site 761. This post-Rhaetian erosional event may have occurred under subaerial and/or submarine conditions (to be resolved by detailed shore-based studies). One possible scenario is that the post-Rhaetian (possibly post-mid Jurassic) uplift and subaerial erosion of the plateau was followed by the formation of a paleokarst morphology under subaerial conditions. Subsequently, the cracks and voids were cemented, followed by slow submergence during latest Jurassic to earliest Cretaceous times. Another scenario is post-Rhaetian drowning of the carbonate platform, followed by nondeposition (condensation), submarine dissolution, and cementation. In this case, the sunken carbonate platform experienced winnowing and/or slow deposition, followed by submarine erosion during the total period of the Jurassic. The distinct truncation of Triassic strata by the post-rift unconformity as seen in the seismic profiles (e.g., *Rig Seismic* Line 56–13) favors the first interpretation.

Origin of the Early Cretaceous Belemnite-Rich Ferruginous Sand (Unit III, 259.5–255.4 mbsf)

Directly overlying this major post-Rhaetian unconformity, we recovered a thin (approximately 4.1 m) but nonetheless critical sequence of (1) brown, unconsolidated, lithic quartzose sand grading upwards into (2) a dark, yellowish brown, poorly sorted, quartzose, lithic, clayey sandstone, rich in mollusks and belemnites, and finally (3) a light yellowish brown nannofossil clay to silty claystone. The age is not known, but is probably late Berriasian to early Valanginian as is the overlying Subunit IIC (Core 122-761C-7R), which was dated by nannofossils. According to preliminary dates from the belemnites (J. Mutterlose, pers. comm., 1989), Unit III might be Tithonian to Valanginian in age.

The depositional environment of this condensed interval requires further shore-based study. However, we tentatively interpret a deepening and upward-fining sequence from (1) littoral to nearshore sand (containing heavy minerals, volcanic rock fragments, glauconite, and mollusks, which indicate reworking during a marine transgression), to (2) a moderately deep (mid-shelf?) milieu for the belemnite-mollusk sands, to (3) an outer shelf/upper slope, open-marine, hemipelagic setting for the nannofossil claystones.

However, the iron stain of the quartz grains and the commonly observed Mn micronodules and "manganese sands" could be explained by *in situ* precipitation in a deep-water hardground environment during very low or zero sedimentation rate conditions, and the laminated to cross-bedded sands could indicate repeated reworking. Thus it is possible that the deepest sands represent a fairly deep (outer shelf?) nondepositional environment and a long time interval. Further studies must clarify whether this was a long interval of sediment-starved conditions, or fairly rapid shelf sand deposition during a transgressive period followed by nondeposition, reworking, or erosion.

Nevertheless, it is clear that at the end of the deposition of Unit III, the Wombat Plateau had subsided to moderately deep (outer shelf/upper slope) water depths with terrigenous and volcanic components (clay minerals, quartz, etc.) becoming successively more mixed with pelagic (nannofossil carbonate) constituents. The presence of volcanic rock fragments and altered glass indicates a major post-breakup volcanic event coinciding with the initiation of seafloor spreading at the nearby Argo Abyssal Plain (about 140 m.y. ago; Leg 123 Shipboard Scientific Party, 1989). Concentrated occurrences

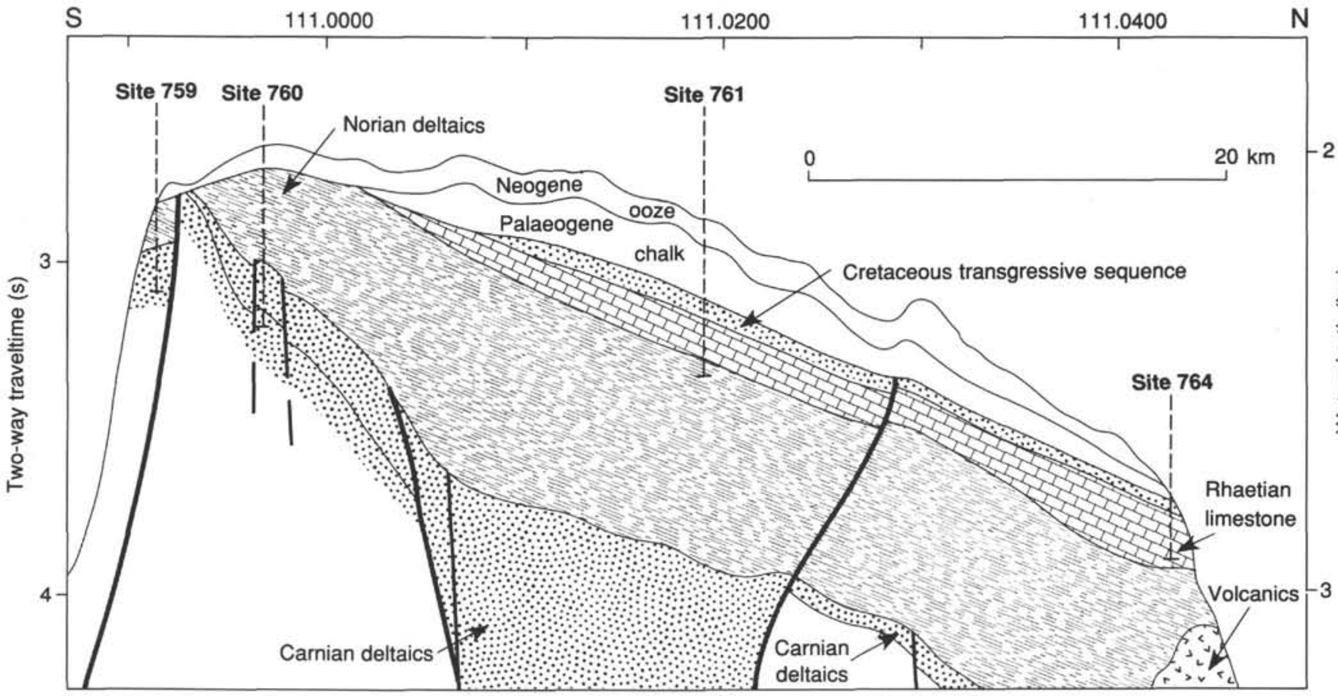

Figure 42. Structural N-S cross section of Wombat Plateau. Line drawing of compressed *Rig Seismic* seismic profile 56-13, modified by shipboard data.

of belemnites (with glauconite and phosphorite) of early Cretaceous age have been reported worldwide from many condensed sections representing major relative sea-level rise events (von Rad, 1985).

The Late Berriasian to Early Valanginian Low-Sedimentation-Rate Sequence (Subunit IIC, 255.4–240.0 mbsf)

A 15.4-m-thick, low-sedimentation-rate, early Neocomian section overlies Unit III. It consists of light to dark yellowish brown calcisphere-nannofossil chalk interbedded with several smectite (bentonite) beds that, according to the gamma-ray logs, might be several meters thick. This suggests a hemipelagic environment for these deposits originating during the subsidence of Wombat Plateau (to bathyal depths). Changes in the clay input caused rhythmic color banding over 20–30 cm intervals. The presence of thoracospheres (calcareous dinoflagellates) probably indicates a hypersaline "stressed," possibly restricted environment during the "juvenile" stage of Indian Ocean formation. Zeolite (clinoptilolite?) is also present.

Particularly interesting are six distinct layers of white, pale-brown to pink, massive, waxy "clay," which were determined to be a pure smectite mixture by XRD analysis. Some smectite layers have sharp basal and gradational upper contacts, suggesting deposition by gravitational processes. Mn micronodules were found in thin laminae within these layers.

The smectite layers are interpreted as bentonites (altered volcanic ash or ash turbidites). The age of these deposits supports this interpretation, as the onset of seafloor spreading in the Argo Abyssal Plain was also dated as late Berriasian to early Valanginian (140 m.y. ago; Leg 123 Shipboard Scientific Party, 1989). During the Neocomian both the Roe Rise volcanic epilith (west of the Wombat Plateau) and the large volcanic structure of the Wallaby Plateau (south of Exmouth Plateau) originated (von Rad and Exon, 1983), an indication of a major post-breakup phase of volcanism. Similar bentonite layers of Berriasian to Valanginian age associated with radiolarian mudstones were also discovered in the nearby Argo Abyssal Plain at Site 765 by the ODP Leg 123 Shipboard Scientific Party (1989).

The calcisphere oozes between the bentonite layers represent hemipelagic sedimentation during sea-level highstands. Calcispheres indicate a pelagic environment far from the shoreline, which apparently migrated landward. Four mudstone/calcisphere chalk cycles were observed in the total gamma-ray log (see Fig. 39).

Mid-Late Cretaceous Pelagic Chalk Deposition (Subunits IIB–IIA, 240.0–175.9 mbsf)

Subsidence of the Wombat Plateau continued during the deposition of the very pale brown nannofossil chalk of Subunit IIB. The Albian to lower Maestrichtian chalk is eupelagic (the last terrigenous influx was noticed in Core 122-761B-27X). After the Albian the plateau apparently had subsided sufficiently to avoid the influence of sea-level fluctuations. The chalk contains foraminifers and *Inoceramus* fragments. Local layers or nodules of porcellanitic chert[3] replacing a radiolarian-rich foraminiferal chalk and the presence of authigenic zeolite (clinoptilolite) suggest dissolution of skeletal opal, diagenetic silica mobilization, and reprecipitation as authigenic silicate (zeolite) or opal-CT. The porcellanites contain Albian to Cenomanian radiolarians and are intermediate in maturity (some of the opal-CT of the matrix has already been transformed into diagenetic quartz).

[3] We define "porcellanite" as a silicified rock in which opal-CT > diagenetic quartz; "chert s.s." is a silicified rock consisting mainly of diagenetic quartz; "porcellanitic chert" is a transition of the two rock types (Riech and von Rad, 1979).

The Cretaceous/Tertiary Boundary

An incomplete (but slightly disturbed) K/T boundary interval was recovered in Hole 761B (Core 122-761B-21X-4, 122 cm) and a somewhat more complete (although also slightly more disturbed) boundary was recovered in Hole 761C (Core 122-761C-3R-3, 70 cm). The boundary is marked by (displaced?) porcellanite fragments and by a sharp color and compositional change between the white youngest Maestrichtian (nannofossil Zone CC26) and the bioturbated, very pale brown clayey nannofossil chalk of the overlying Paleocene nannofossil Zone NP2. A variety of shore-based biostratigraphic, magnetostratigraphic, chemostratigraphic, and isotopic-stratigraphic studies will be performed in this carefully sampled critical interval. A broad peak on the gamma-ray and resistivity logs may have been produced by increased clay (plus zeolite?) content, and/or by the presence of porcellanite layers.

The Expanded Paleocene Chalk Sequence (Subunit ID, 175.9–122.7 mbsf)

The 53.2-m-thick Paleocene sequence of Subunit ID appears to be complete and of great importance for biostratigraphic, magnetostratigraphic, and isotope-stratigraphic analyses. The chalks contain several intervals with porcellanite nodules. The basal Paleocene section above the Cretaceous/Tertiary boundary is rich in clay and authigenic clinoptilolite.

Eocene to Quaternary Pelagic Sediments (Subunits IC–IA, 122.7–0.0 mbsf)

The lower to middle Eocene ooze sequence of Subunits IC–IB consists of white nannofossil ooze with several layers of porcellanite. The concentration of porcellanite nodules and layers is strongest in the upper Lower to lower Middle Eocene sequence, as is the case with most silicified rock occurrences of the Pacific and Atlantic Oceans (Riech and von Rad, 1979). This suggests a global paleoenvironmental signal (enhanced siliceous plankton productivity and preservation). As only small porcellanite fragments were recovered and the downhole logs did not show clearly defined silica peaks, it is difficult to ascertain the thickness of the "chert horizon" that slowed drilling to 1.5 m/hr and appears as a sharp reflector in the seismic records. However, we assume a minimum thickness of 1–3 m of "massive" porcellanite (or a number of porcellanite nodule horizons) for the interval between 90 and 100 mbsf.

The late Oligocene to Quaternary Subunits IB to IA contain eupelagic, white bioturbated nannofossil ooze with faint color banding that is better developed upsection. The preservation of nannofossils and foraminifers (which increase in abundance towards the Quaternary) is excellent. Several hiatuses were noted, especially between the middle Eocene/upper Oligocene, the upper Miocene/upper Pliocene, and Pliocene/Quaternary sections. Color bands 10–30 cm thick, with the darker layers richer in foraminifers than the lighter ones (which demonstrates that these are not dissolution cycles), might represent Milankovitch cycles.

Organic and Inorganic Geochemistry

Organic carbon contents were very low (<0.1%) in the oozes and chalks, reaching higher values (to about 1%) in the black Rhaetian limestones and calcareous silty claystones of Units IV and V. Black organic-rich claystones with 3%–5% total organic carbon (TOC) occur only in the Norian (Unit VI). This organic matter was determined to be thermally immature to marginally mature (corresponding to R_o values around 0.4%–0.6%). Methane values were generally below 1–4 ppm and ethane values were below detection, indicating that low-molecular-weight hydrocarbons were locally (thermally) generated from type III (land plant) organic material. Unlike the Carnian section of Site 760, no thermogenic gas was detected.

Inorganic geochemical investigations focused on pore-water samples from the uppermost 150 m (Unit I, Cenozoic). Below the main unconformity (260.0 mbsf), Mg^{2+} decreases, Ca^{2+} increases, and the Mg^{2+}/Ca^{2+} ratio decreases. Pore-water silica concentration increases slightly below the mudline (owing to early-diagenetic skeletal-opal dissolution), drops to 0.5 mM around 30–50 mbsf, and reaches a maximum of 1.4–1.7 mM between 100–180 mbsf (the interval of maximum silica mobilization and porcellanite formation). Silica and alkalinity have an inverse relationship between 30 and 60 mbsf.

Physical Properties

Physical-property data gave good indications of downhole diagenetic changes and helped to correlate seismic stratigraphy, downhole logging, and lithostratigraphy at Site 761. Except for cherts (2.4–5.7 km/s) sonic velocities show a steady increase with increasing downhole compaction from 1.53 km/s (Subunit IA, below the mudline) to 1.85 km/s (Subunit IIB, 240.0 mbsf). Lower-than-average sonic velocities were found between 240.0–260.0 mbsf (unlithified bioclastic sands with high-porosity smectite layers, Subunit IIC–Unit III). Velocities in the Rhaetian carbonates below 260.0 mbsf are highly variable (1.7 km/s in calcareous mudstones to 5 km/s in well-cemented bioclastic limestones) as claystones, calcareous silty claystones, and limestones are interbedded. Porosities drop from 72% in the ooze to 55% in chalk, and to less than 10% in limestone, whereas bulk densities increase from 1.49 g/cm^3 (near-surface sediments) to 1.8 g/cm^3 (chalk at 122 mbsf) and to 2.0–2.64 g/cm^3 for calcareous silty claystones/limestones around 260 mbsf.

Biostratigraphy

The upper part of the section cored at Site 761 comprises a mostly complete and expanded upper Santonian through Paleocene interval, and more condensed, but fairly complete Cenozoic. The expanded Santonian-Paleocene section should prove useful for detailed magneto-biostratigraphic and stable-isotopic studies. The presence of well-preserved radiolarians in the Paleocene makes this interval especially valuable and offers the unique opportunity for establishing a Paleocene radiolarian zonation (unzoned at present).

At Site 761 the Cretaceous/Tertiary boundary interval was cored twice (in Holes 761B and 761C) and represents a possibly complete boundary succession, suitable for more detailed work, including iridium analyses.

Belemnites, found in the upper Lower Cretaceous Unit III, might prove to be valuable fossils for determining the age and paleoenvironment of this critical interval, especially if oxygen isotope studies can work out the paleoclimate of the early Cretaceous in the southern hemisphere.

The nearly complete marine Rhaetian cored at this site is the first record of its kind in the Indian Ocean and southern hemisphere. The occurrence at Site 761 of the late Triassic index foraminifer *Triasina hantkeni* is the first record of this species in the vicinity of Australia, and is thus a promising paleontological discovery. The upper Triassic section cored here also yielded pelecypods, calcareous nannofossils, and palynomorphs.

Magnetostratigraphy

Whole-core measurements, as well as a few discrete samples analyzed on board ship, yielded paleomagnetic results of varying quality for different parts of the recovered succession. The magnetostratigraphic results were generally satisfactory and complete for the Quaternary. The relatively high sedimentation rates in the late Santonian through Paleocene interval were conducive to the identification of principal polarity features corresponding to magnetic chrons C34 through C24. Results in the remainder of the Tertiary and Mesozoic were generally unsatisfactory, and further detailed studies will be necessary to ascertain the presence of a meaningful magnetic signal.

Downhole Measurements

Because of severe bridging problems at 260 mbsf, the first and only open-hole run with the seismic stratigraphic tools was successful only above that depth. A second run with a suite of geochemical logs was made through the drill pipe between 415 and 75 mbsf. In spite of the pipe enclosure, the logs obtained were of good quality. The logs were useful in reconstructing the lithofacies of the intervals with poor sediment recovery, and the overall log response was very helpful in determining the facies trends of upward-deepening or upward-shoaling cycles for sequence-stratigraphic analysis (see "Downhole Measurements," this chapter) and the identification of transgressive and highstand systems tracts.

Seismic Stratigraphy

Reassessment of the seismic data after the completion of Sites 759, 760, and 761 shows considerable differences from the interpretations before drilling, where the ages of the major unconformities were determined from regional geology and rock samples dredged from the flanks of the Wombat Plateau. The post-drilling reinterpretation allows the deep structure in the Wombat half graben (south of the plateau) to mirror closely that on Exmouth Plateau, with major displacement at the top of a Triassic unconformity. These and other data suggest that the Wombat half graben may have already formed during the pre-Callovian rift phase that eventually led to the late Jurassic–earliest Cretaceous breakup of the north margin of the Exmouth Plateau (see details in "Seismic Stratigraphy," Site 763 chapter, this volume) and not in post-Neocomian times, as thought previously (Exon et al., 1982).

REFERENCES

Bathurst, R.G.C., 1959. The cavernous structure of some Mississippian Stromatactis reefs in Lancashire, England. *J. Geol.*, 67:506–521.

———, 1980. Stromatactis—Origin related to submarine-cemented crusts in Paleozoic mud mounds. *Geology*, 8:131–134.

Bralower, T. J., Monechi, S., and Thierstein, H. R., 1989. Calcareous nannofossil zonation of the Jurassic-Cretaceous boundary interval and correlation with the geomagnetic polarity timescale. *Mar. Micropaleontol.*, 14:153–235.

Emeis, K.-C., and Kvenvolden, K. K., 1986. Shipboard organic geochemistry on *JOIDES Resolution*. *ODP Tech. Note*, 7.

Exon, N. F., von Rad, U., and von Stackelberg, U., 1982. The geological development of the passive margins of the Exmouth Plateau off northwest Australia. *Mar. Geol.*, 47:131–152.

Foreman, H. P., 1973. Radiolaria of Leg 10 with systematics and ranges for the families Amphipyndacidae, Artostrobiidae, and Theoperidae. *In* Worzel, J. L., Bryant, W., et al., *Init. Repts. DSDP*, 10: Washington (U.S. Govt. Printing Office), 407–474.

Garland, G. D., 1979. *Introduction to Geophysics*: Philadelphia (Saunders).

Gieskes, J. M., 1981. Deep-sea drilling interstitial waters: implications for chemical alteration of the oceanic crust, Layer I and II. *Soc. Econ. Paleontol. Mineral. Spec. Publ.*, 31:149–167.

Gieskes, J. M., Elderfield, H., Lawrence, J. R., Johnson, J., Meyers, B., and Campbell, A., 1982. Geochemistry of interstitial waters and sediments, Leg 64, Gulf of California. *In* Curray, J. R., Moore, D. G., et al., *Init. Repts. DSDP*, 64: Washington (U.S. Govt. Printing Office), 675–694.

Haq, B. U., Hardenbol, J., and Vail, P. R., 1987. Chronology of fluctuating sea levels since the Triassic. *Science*, 235:1156–1167.

Helby, R., Morgan, R., and Partridge, A. D., 1987. A palynological zonation of the Australian Mesozoic. *Mem. Assoc. Australas. Palaeontol.*, 4:1–94.

Jafar, A. S., 1983. Significance of Late Triassic calcareous nannoplankton from Austria and Southern Germany. *Neues. Jahrb. Geol. Palaeontol. Abh.*, 166:218–259.

Jakubowski, M., 1987. Lower Cretaceous nannofossil zonation of the North Sea Basin. *Abh. Geol. Bundesanst. Austria*, 39:100–119.

Kastner, M., and Gieskes, J. M., 1976. Interstitial water profiles and sites of diagenetic reactions, Leg 35, DSDP, Bellinghausen Abyssal Plain. *Earth Planet. Sci. Lett.*, 33:11–20.

Lasaga, A. C., and Holland, H. D., 1976. Mathematical aspects of non-steady state diagenesis. *Geochim. Cosmochim. Acta*, 40:257–266.

Leg 123 Shipboard Scientific Party, 1989. The birth of the Indian Ocean. *Nature*, 337:506–507.

Martini, E., 1971. Standard Tertiary and Quaternary nannoplankton zonation. *In* Farinacci, A. (Ed.), *Proc. 2nd Planktonic Conf.*: Rome (Ed. Tecnoscienza), 739–785.

Monechi, S., 1984. Campanian to Pleistocene calcareous nannofossil stratigraphy from the northwest Pacific Ocean, Deep Sea Drilling Project Leg 86. *In* Heath, G. R., Burckle, L., et al., *Init. Repts. DSDP*, 86: Washington (U.S. Govt. Printing Office), 301–336.

Ogg, J. G., Haggerty, J., Sarti, M., and von Rad, U., 1987. Lower Cretaceous pelagic sediments of Deep Sea Drilling Project Site 603, western North Atlantic: a synthesis. *In* Van Hinte, J. E., Wise, S. W., Jr., et al., *Init. Repts. DSDP*, 93: Washington (U.S. Govt. Printing Office), 1305–1331.

Perch-Nielsen, K., 1977. Albian to Pleistocene calcareous nannofossils from the western South Atlantic. *In* Perch-Nielsen, K., and Supko, P. R., et al., *Init. Repts. DSDP*, 39: Washington (U.S. Govt. Printing Office), 699–823.

———, 1985a. Cenozoic calcareous nannofossils. *In* Bolli, H. M., Saunders, J. B., and Perch-Nielsen, K. (Eds.), *Plankton Stratigraphy:* Cambridge (Cambridge Univ. Press), 427–554.

———, 1985b. Mesozoic calcareous nannofossils. *In* Bolli, H. M., Saunders, J. B., and Perch-Nielsen, K. (Eds.), *Plankton Stratigraphy:* Cambridge (Cambridge Univ. Press), 329–426.

Pessagno, E. A., Jr., 1976. *Radiolarian Zonation and Stratigraphy of the Upper Cretaceous portion of the Great Valley Sequence, California Coast Ranges:* Micropaleontol. Spec. Publ., 2.

———, 1977. *Lower Cretaceous Radiolarian Biostratigraphy of the Great Valley Sequence and Franciscan Complex, California Coast Ranges*. Spec. Publ. Cushman Found. Foraminiferal Res., 15.

Riech, V., and von Rad, U., 1979. Silica diagenesis in the Atlantic Ocean: diagenetic potential and transformations. *In* Talwani, M., Hay, W., and Ryan, W.B.F. (Eds.), *Deep Drilling Results in the Atlantic Ocean: Continental Margins and Paleoenvironment:* Washington (Am. Geophys. Union), 315–340.

Roth, P. H., 1978. Cretaceous nannoplankton biostratigraphy and oceanography of the Northwestern Atlantic Ocean. *In* Benson, W. E., Sheridan, R. E., et al., *Init. Repts. DSDP*, 44: Washington (U.S. Govt. Printing Office), 731–759.

Sanfilippo, A., and Riedel, W. R., 1985. Cretaceous Radiolaria. *In* Bolli, H. M., Saunders, J. B., and Perch-Nielsen, K. (Eds.), *Plankton Stratigraphy:* Cambridge (Cambridge Univ. Press), 573–630.

Sanfilippo, A., Westberg-Smith, M. J., and Riedel, W. R., 1985. Cenozoic radiolaria. *In* Bolli, H. M., Saunders, J. B., and Perch-Nielsen, K. (Eds.), *Plankton Stratigraphy:* Cambridge (Cambridge Univ. Press), 631–712.

Schaefer, R. G., and Leythaeuser, D., 1984. C_2–C_8 hydrocarbons in sediments from Deep Sea Drilling Project Leg 75, Holes 530A, Angola Basin, and 532, Walvis Ridge. *In* Hay, W. W., Sibuet, J.-C., et al., *Init. Repts. DSDP*, 75: Washington (U.S. Govt. Printing Office), 1055–1067.

Schott, M., 1983. Sedimentation and diagenesis of a subsiding carbonate platform: Rhaetic and Liassic of the Brünnstein-Auerbach region, Bavarian Calcareous Alps. *Facies*, 9:1–60.

Schrader, H.-J., 1972. Kieselsäure-Skelette in Sedimenten des ibero-marokkanischen Kontinentalrandes und angrenzender Tiefsee-Ebenen. *Meteor-Forsch.-Ergebnisse*. C., 8:10–36.

Sclater, J. G., Parsons, B., and Jaupart, C., 1981. Oceans and continents: similarities and differences in the mechanisms of heat loss. *J. Geophys. Res.*, 86:11535–11552.
Sissingh, W., 1977. Biostratigraphy of Cretaceous calcareous nannoplankton. *Geol. Mijnbouw*, 56:37–65.
Thierstein, H. R., 1981. Late Cretaceous nannoplankton and the change at the Cretaceous-Tertiary boundary. *In* Warme, J. E., et al. (Eds.), *The Deep Sea Drilling Project: A Decade of Progress:* Soc. Econ. Paleontol. Mineral. Spec. Publ., 32:355–394.
Thierstein, H. R., and Okada, H., 1979. The Cretaceous/Tertiary boundary event in the North Atlantic. *In* Tucholke, B. E., Vogt, P. R., et al., *Init. Repts. DSDP,* 43: Washington (U.S. Govt. Printing Office), 601–616.
von Rad, U., 1985. Lithostratigraphy, diagenesis and paleoenvironment of the Cretaceous-Tertiary post-platform sediments of the Mazagan Escarpment off Central Morocco (CYAMAZ Campaign/1982). *Oceanol. Acta Sp. Vol.,* 5:161–182.
von Rad, U., and Exon, N. F., 1983. Mesozoic-Cenozoic sedimentary and volcanic evolution of the starved passive margin off northwest Australia. *AAPG Mem.,* 34:253–281.

Ms122A-107

NOTE: All core description forms ("barrel sheets") and core photographs have been printed on coated paper and bound as Section 3, near the back of the book, beginning on page 387.